iSEE: Interface Structure, Evolution and Energy-based machine learning predictor of binding affinity changes upon mutations

Cunliang Geng[a], Anna Vangone[a], Gert E. Folkers[a], Li C. Xue[a1] and Alexandre M.J.J. Bonvin[a1]

[a]Bijvoet Center for Biomolecular Research, Faculty of Science - Chemistry, Utrecht University, Padualaan 8, 3584 CH Utrecht, the Netherlands;

[1]Correspoding authors. Email: l.xue@uu.nl, a.m.j.j.bonvin@uu.nl; T: +31 30 2533641, +31 30 2533859.

Short title:

iSEE: Predicting binding affinity changes upon mutations

Keywords:

Protein-protein interactions, single point mutation, binding affinity, machine learning, full mutation scanning.

Abstract

Quantitative evaluation of binding affinity changes upon mutations is crucial for protein engineering and drug design. Machine learning-based methods are gaining increasing momentum in this field. Due to the limited number of experimental data, using a small number of sensitive predictive features is vital to the generalization and robustness of such machine learning methods. Here we introduce a fast and reliable predictor of binding affinity changes upon single point mutation, based on a random forest approach. Our method, iSEE, uses a limited number of **i**nterface **S**tructure, **E**volution and **E**nergy-based features for the prediction. iSEE achieves, using only 31 features, a high prediction performance with a Pearson correlation coefficient (PCC) of 0.80 and a root mean square error of 1.41 kcal mol^{-1} on a diverse training dataset consisting of 1102 mutations in 57 protein-protein complexes. It competes with existing state-of-the-art methods on two blind test datasets. Predictions for a new dataset of 540 mutations in 58 protein complexes from the recently published SKEMPI 2.0 database reveals that none of the current methods perform well (PCC<0.4), although their combination does improve the predictions. Feature analysis for iSEE underlines the significance of evolutionary conservations for quantitative prediction of mutation effects.

Introduction

The affinity between proteins and their binding partners is a fundamental property that governs their function in cells. Mutations in proteins can induce changes in the binding affinity for their interaction partners, altering their functioning by perturbing their communication network. Missense mutations are often linked to various human diseases[1], such as cancer. Quantitative characterization of binding affinity changes can therefore shed light on the relation between coding variations and disease phenotypes, and guide the design of effective therapeutics for genetic disorders. It can also be particularly useful for engineering protein-protein interactions with modulated binding affinity.

Various experimental methods can be used to quantitatively measure binding affinities[2,3], each with their own limitations and precision. Although they provide valuable information, experimental methods can be labor-intensive and time-consuming, and, as a consequence, lag behind the rapid advances of sequencing technologies, which are generating a huge amount of data on disease-causing mutations. This calls for the development of reliable and fast computational methods for estimating the mutation effects on binding affinity (i.e., the binding free energy change between a wild type and mutant complex, $\Delta\Delta G$).

Computational methods for $\Delta\Delta G$ prediction can be largely grouped into three main strategies: 1) Rigorous methods, such as thermodynamic integration and free energy perturbation[4,5], 2) empirical energy-based methods, based for example on classical mechanics or statistical potentials[6-10] (typically in linear forms), and 3) machine learning-based methods which can exploit a large variety of energetics and non-energetics (e.g. geometric, evolutionary) features[11-13]. The rigorous methods can be accurate but they are computationally highly demanding. Their application is, therefore, limited to mainly low-throughput and small system $\Delta\Delta G$ calculations. The empirical energy-based methods are much faster and more

broadly applied. They usually take a form of linear functions, often with only energy-based terms, and fail to exploit evolution information, which can limit their ability to capture mutation effects on binding affinity. Insufficient conformational sampling, especially for mutations in flexible regions, can limit the accuracy of energy-based methods. In contrast, machine learning-based methods are potentially less sensitive to this since they can model mutation effects using not only potentials or energies but also other relevant features, such as, sequence, structure and evolution. Machine learning approaches typically aim to model the intrinsic relationship between features of a mutation site and the response variable (e.g., the binding affinity change) by training statistical models from mutation datasets with experimentally determined ΔΔG. Due to the data-driven essence of machine learning, the availability of a large amount of reliable experimental data and the construction of features that can reflect structural and physico-chemical changes caused by mutations are crucial factors for the success for this type of methods. It is therefore not surprising that the publication of the SKEMPI database[14] (version 1.1, which was in the past six years the largest mutation ΔΔG dataset for protein-protein complexes containing 3047 mutations in 85 complexes) quickly promoted the emergence of several machine learning-based ΔΔG predictors[11-13]. However, the SKEMPI 1.1 dataset is still rather limited in size and one has to be careful not to use too many features to train a model to avoid overfitting problems. It is therefore important to design fast and reliable ΔΔG predictors that exploit only a limited number of sensitive and relevant features. Very recently, an update of SKEMPI was published, version 2.0[15], which provides a much extensive dataset and gives us the opportunity to test various predictors on data none of them has previously seen.

Residue conservation plays a central role in determining the binding affinity. It has been verified that the binding energy is not evenly distributed among the interfacial residues. Instead, some residues (hot-spots) contribute most to the binding affinity[16-18]. Such residues

are often highly conserved. Interface conversation has been used in several of the best performing ΔΔG predictors[13,19]. However, since the conservation measure they used is structure-based, relying on the availability of structural homologs[13,19], the application and prediction of these ΔΔG predictors are largely limited by the availability and the number of such homologs. By contrast, conservation from Position Specific Scoring Matrix (PSSM) is sequence-based and thus better applicable. The PSSM value is a log likelihood ratio between the observed probability of one type of amino acid appearing in a specific position in the multiple sequence alignment (MSA) and the expected probability of that amino acid type appearing in a random sequence[20]. Thus, each position of a protein can be represented as a 20 by 1 PSSM profile (or vector), which captures the conservation property of each amino acid type at a specific position.

Here we present a machine learning-based method named iSEE (interface Structure, Evolution and Energy-based ΔΔG predictor), which combines HADDOCK[21], structure and energy terms of wildtype and mutant complexes as well as PSSM conservation profiles before and after mutations (**Figure 1**). HADDOCK[21] is our in-house docking program, which has been consistently ranking among the top predictors and scorers in CAPRI, a community-wide experiment for the prediction of biomolecular interactions[22]. Its simple but sensible scoring function has contributed much to its success[23]. It includes intermolecular van der Waals (Evdw) and Coulomb electrostatics (Eelec) energies, an empirical desolvation energy term (Edesolv)[24] and buried surface area (BSA), which is only used in intermediate scoring steps and not in the final scoring function. iSEE is based on a random forest model[25] for ΔΔG prediction, trained on a subset of 1102 single point mutations from 57 complexes from SKEMPI 1.1. It uses a small number of features (31) to lower the overfitting risk and competes with both empirical potentials- and machine learning-based state-of-the-art methods on an existing independent test dataset (the Benedix *et al.* NM dataset[8]) and a large

test dataset from the recently released SKEMPI 2.0 database. The recent release of SKEMPI 2.0 allows us for the first time to test various ΔΔG predictors on a large new blind dataset with more than 500 mutations. Analysis of the importance of the features used in iSEE highlights the significance of evolutionary information in predicting the effect of mutations on the binding affinity of protein complexes.

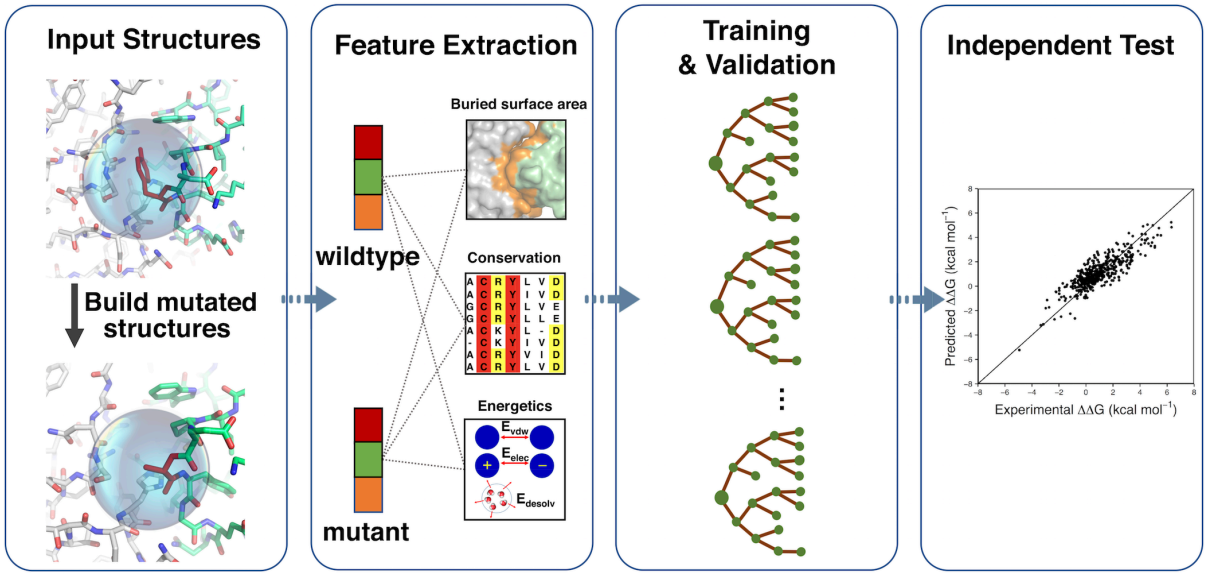

Figure 1. The workflow of iSEE predictor. Only the 3D structure of wildtype complex and mutation information are necessary input for iSEE. We first model the mutated structure using HADDOCK (the water refinement web service). Then we extract features related to the evolutionary conservation and to changes in structure and energetics caused by the mutation. A random forest algorithm is then optimized and cross validated on a training dataset, resulting in our final ΔΔG predictor iSEE. Finally, iSEE is evaluated on two blind test datasets and compared with other current leading ΔΔG predictors.

Methods

Training and test datasets. Three datasets of experimental ΔΔG with available crystal structures of protein complexes were used in this study. Only single point mutations in the interface of the protein-protein complexes were considered, and only for dimeric complexes

for ease of computations, but our prediction scheme can be easily extended to multimers. The interface residues were defined following Levy's method[26] as those located in the core, rim and support regions.

The training dataset was extracted from the DACUM database (https://github.com/haddocking/DACUM)[27], our ΔΔG database derived from the SKEMPI 1.1 database[14]. DACUM contains 1872 single point mutations in 81 protein complexes. After applying the above-mentioned filter criteria, 1102 single point mutations in 57 protein complexes were selected.

We compiled two independent datasets, not used for training, to evaluate and compare our predictor with state-of-the-art ΔΔG predictors.

We selected a subset from the Benedix *et al.* NM dataset[8] for which predictions of various ΔΔG predictors have already been reported[7,9]. The original NM dataset has both single point and multiple point mutations in protein dimer or multimer complexes. We applied the same filtering criteria as above. Moreover, to avoid any overlap between the training dataset and the test dataset, mutations existing in the training dataset were filtered out from the original NM dataset. This procedure resulted in 19 mutations in one complex (PDB ID: **1IAR**). For this heterodimer complex, only ΔΔG values for mutations on chain A were contained in our training dataset, while all ΔΔG data in the NM dataset are for mutations on chain B. Thus, the NM dataset is distinct from our training dataset at the level of mutation position. In the remaining of our paper, we will refer to those data as "the NM dataset".

Finally, we selected new data from the recently released SKEMPI 2.0 database. After applying the above-mentioned filter criteria, 540 mutations in 58 protein complexes were selected. We will refer to this dataset as "the S540 dataset" in the remaining paper.

Predictive features. We compiled a list of 31 features including intermolecular energy terms and buried surface area (BSA) from HADDOCK[21] and conservation values from PSSM.

To obtain the structural and energetic features, both wild type and mutant structures were refined using the protocol implemented in the refinement interface of the HADDOCK server[28]. The mutations were introduced by simply changing the identity of the residue in the coordinate file and letting HADDOCK rebuild the missing side-chain atoms and refine the interface in explicit solvent using the TIP3P water model and the Optimized Potentials for Liquid Simulations (OPLS) force field[29] with an 8.5Å cutoff for the non-bonded interactions. The HADDOCK terms for wildtype and mutant complex were extracted from the top ranked HADDOCK model. The HADDOCK-derived features are:

- Evdw, the intermolecular van der Waals energy described by a 12-6 Lennard-Jones potential.
- Eelec, the intermolecular electrostatic energy described by a Coulomb potential.
- Edesolv, an empirical desolvation energy term[24].
- BSA, the buried surface area calculated by taking the difference between the sum of the solvent accessible surface area (SASA) for each individual protein and the SASA of the protein complex using 1.4Å water probe radius.

The four HADDOCK terms of wildtype complex and the differences of the HADDOCK terms between mutant and wildtype complexes were used as HADDOCK-based predictive features, which are named as Evdw_wt, Eelec_wt, Edesolv_wt, BSA_wt, Evdw_diff, Eelec_diff, Edesolv_diff and BSA_diff.

The PSSM was calculated through PSI-BLAST of BLAST 2.3.0[30] using a local version of the software and databases with the following parameters: BLOSUM62 was used as scoring matrix by default, and PAM30 was used when BLOSUM62 failed for short sequences; the number of iterations was 3 and the e-value threshold was set to 0.0001; the BLAST database was the nr database (non-redundant BLAST curated protein sequence database, version on Aug. 22nd 2016). Default values were used for all the other parameters. For each mutation position of a query protein, 4 types of conservation features were extracted from the PSSM file:

- the PSSM profile for this position, which is a 20 by 1 vector (PSSM_AA).
- the information content for this position (PSSM_IC).
- the individual PSSM value for the wildtype residue at this position (PSSM_wt).
- the difference between the individual PSSM values for mutant residue and wildtype residue at this position (PSSM_diff).

Training procedures and evaluation metrics. We used the random forest algorithm[31] from the R Caret package[32] to train our ΔΔG predictor. We optimized the parameters of random forest over 10 times 10-fold cross-validations on the training dataset: the number of trees to grow, defined by the "ntree" parameter, was varied from 10 to 100 in steps of 10, and the number of variables randomly sampled as candidates at each split, defined the "mtry" parameter, was sampled from 1 to 20. The prediction performance was evaluated by root mean square error (RMSE) and Pearson's correlation coefficient (PCC).

Comparison with other ΔΔG predictors. The performance of the iSEE ΔΔG predictor was compared with several state-of-the-art ΔΔG predictors on the independent NM and SKEMPI 2.0 S540 test datasets. For the NM dataset, the predicted ΔΔG values of pred1[9], pred2[9],

CC/PBSA[8], BeAtMuSiC[10] and FoldX[6] were directly extracted from Li et al[9] and those of ZeMu from Dourado's paper[7]. Predictions of mCSM[11] and BindProfX[19] for the test datasets were directly obtained from their respective webservers. The default parameters of BindProfX were used except the "Score to use" which was set to "interface profile and physics potential" (the authors reported it to work best for single point mutations[19]). A local version of FoldX (4.0) was used for the S540 dataset.

Classification of mutations. Mutation were classified based on three scenarios: the location of the mutation, the type of mutated amino acid and the change in the size of the amino acid side-chain.

Based on the type of secondary structure a mutation is located, it was classified as a loop or non-loop mutation. We used DSSP[33,34] (v2.0.4) for secondary structure assignment. DSSP code S, B and blank were considered as loop, otherwise non-loop.

Based on the type of mutated amino acid, a mutation was called "toALA" mutation when a residue was mutated to alanine, otherwise "toNonALA" mutation.

The change of amino acid size was defined as the difference of volumes (ΔV) between mutant and wildtype amino acids. The volumes of the 20 amino acids were taken from literature[35]. A mutation was classified as "neutral" if $|\Delta V| \leq 10$ Å^3, as small to large ("toLarge") if $\Delta V > 10$ Å^3, and as large to small ("toSmall") if $\Delta V < -10$ Å^3.

Feature importance analysis. We used the algorithm from the R package randomForest[31] to evaluate feature importance. The feature importance is measured by the decrease of mean squared error when splitting on a feature, averaged over all trees. The importance measure of a group of features was calculated by taking the sum of weighted importance of each feature in that group with the weight for each feature defined as the number of times the feature was

chosen as split variable over all trees divided by the total of all group member features. The PSSM profile scores for the 20 amino acids was treated as a group (PSSM_AA). The best model trained on the entire training dataset with parameters ntree = 80 and mtry = 7 was used to analyze the feature importance.

Data and model availability. All PDB files including the HADDOCK-refined models, and PSSM files used in this work are available from the SBGrid Data repository[36] (doi:10.15785/SBGRID/520). The iSEE predictor and features used for training and test are freely available on GitHub from https://github.com/haddocking/iSee.

Results

Training and validation of iSEE on a large diverse single point mutation dataset. We trained iSEE on a relatively large and diverse dataset consisting of experimental ΔΔG values for 1102 single point mutations in the interface of 57 dimer complexes. Among those, 656 mutations are in loops, 767 are non-ALA mutations, 376 correspond to small to large substitutions and 590 from large to small size. For each mutation, we extracted 31 energetics and conservation features (see Methods). A random forest (RF) model was trained and evaluated using 10-fold cross-validation(CV). The data are randomly divided into 10 parts, 9 of which are used for training and the left-out one for evaluating the performance of the trained RF model. This process was repeated 10 times to reduce the randomness of the data partition. From this training, a RF model with 80 trees and 7 randomly selected variables for each node achieved the best average root mean square error (RMSE) value **(Figure S1** in Supporting Information**)**. The resulting best performing ΔΔG predictor, called iSEE, was compared with state-of-the-art ΔΔG predictors (see below).

iSEE's prediction performance shows an average RMSE of 1.41±0.14 kcal mol^{-1} and a Pearson's correlation coefficient (PCC) of 0.80±0.06 over the cross-validated sets **(Figure 2A)**. The predictor performs as well for ALA and non-ALA mutations, mutations inside and outside loops, and mutations corresponding to different changes in side-chain sizes (**Figure 2B-2D**). This indicates that our approach is not very sensitive to possible conformational changes coming from loop flexibility and is robust for different types of mutations. We further evaluated the applicability of iSEE to different types of protein complexes. Our results show that iSEE has a strong generalizability for predicting ΔΔG trends for mutations within complexes (**Figure S2 and S3**).

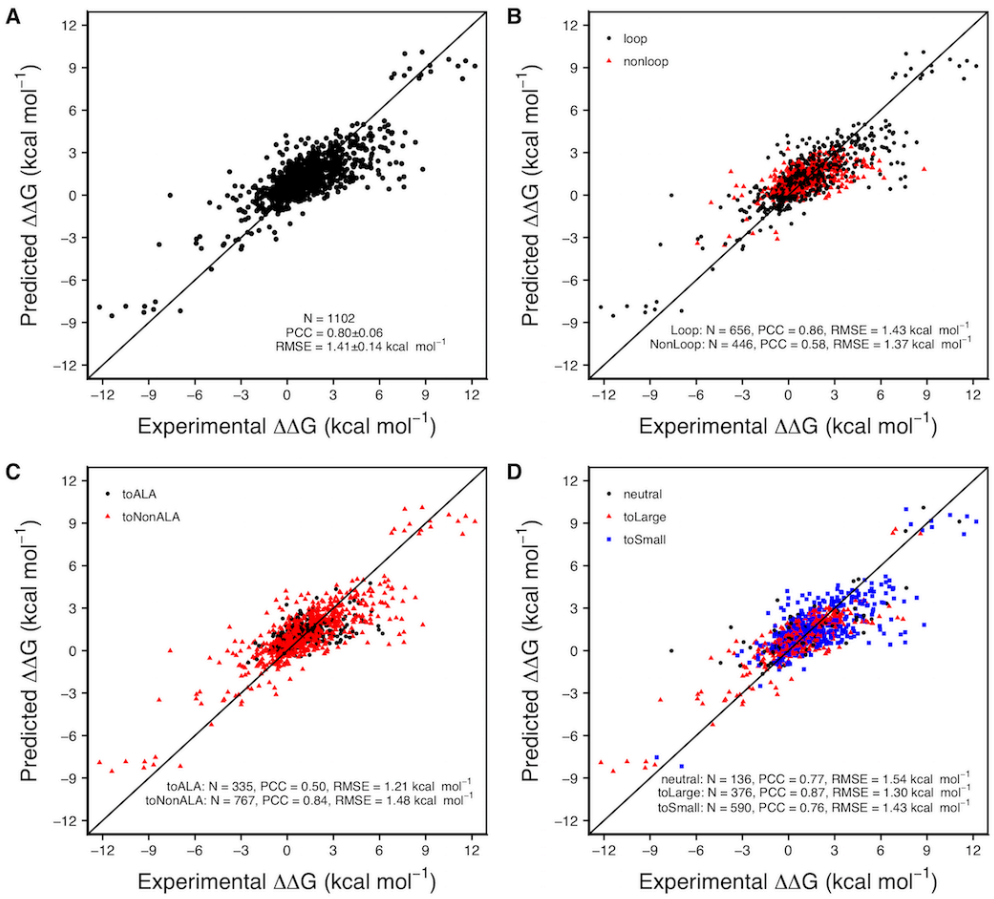

Figure 2. Correlations between predicted and experimental ΔΔG values for the training dataset consisting of 1102 single point mutations from the SKEMPI[14]/DACUM[27] database. Ten times 10-fold cross-validation (CV) was applied during training, and the average of the CV predicted ΔΔG values

are shown here for all mutations (A) and mutations classified as loop or non-loop (B), type of mutated amino acid (C), and change in amino acid size (D). The diagonal indicates an ideal prediction. PCC is the Pearson's correlation coefficient and RMSE represents root mean squared error.

iSEE competes with state-of-the-art ΔΔG predictors. We evaluated the performance of our iSEE ΔΔG predictor on the blind Benedix *et al.* NM dataset[8] (see Methods) and compared it to several other state-of-the-art ΔΔG predictors based on empirical potentials or machine learning methods, which have been tested by Li et al.[9] on the same data set. We only selected data from the NM data set for mutations that were not represented in the training data, which left 19 single point mutations for one complex (heterodimer, PDB ID: **1IAR**).

iSEE was compared to the following predictors:

- FoldX, which models free energy as a linear combination of multiple energy terms with weights optimized on a set of experimental ΔΔG values[6].
- ZeMu, which can model conformational changes upon mutation using molecular dynamics simulations but relies on FoldX to predict ΔΔG[7].
- CC/PBSA[8], pred1[9] and pred2[9], which generate an ensemble of structures and apply a Molecular Mechanics - Poisson-Boltzmann Surface Area (MM-PBSA) approach to calculate the binding free energy.
- BeAtMuSiC, which is based on a linear combination of coarse grained statistical potentials[10].

- mCSM[11], a machine learning based approach, using distance-specific atom-contacts (calculated from the wild-type structures only) and pharmacophore changes of the mutation site as features of Gaussian processes to predict ΔΔG.

- BindProfX[19], which is mainly based on evolutionary interface profile constructed from structural homologs, and combines the interface profile score with FoldX through a simple linear function to predict ΔΔG.

iSEE compares favorably with the eight other predictors considered here over the independent NM test set with a RMSE of 1.37 kcal mol^{-1} and a PCC of 0.73 (**Figure 3**), belonging to the top four predictors with PCCs over 0.70: BindProfX (0.81), iSEE (0.73), FoldX (0.72) and ZeMu (0.70). The ΔΔG predictions of the top four predictors are statistically significant with p values lower than 0.001, while other predictors have larger p values ranging from 0.006 to 0.523. Note that since CC/PBSA did use the NM data for training[8], its performance might be over-estimated.

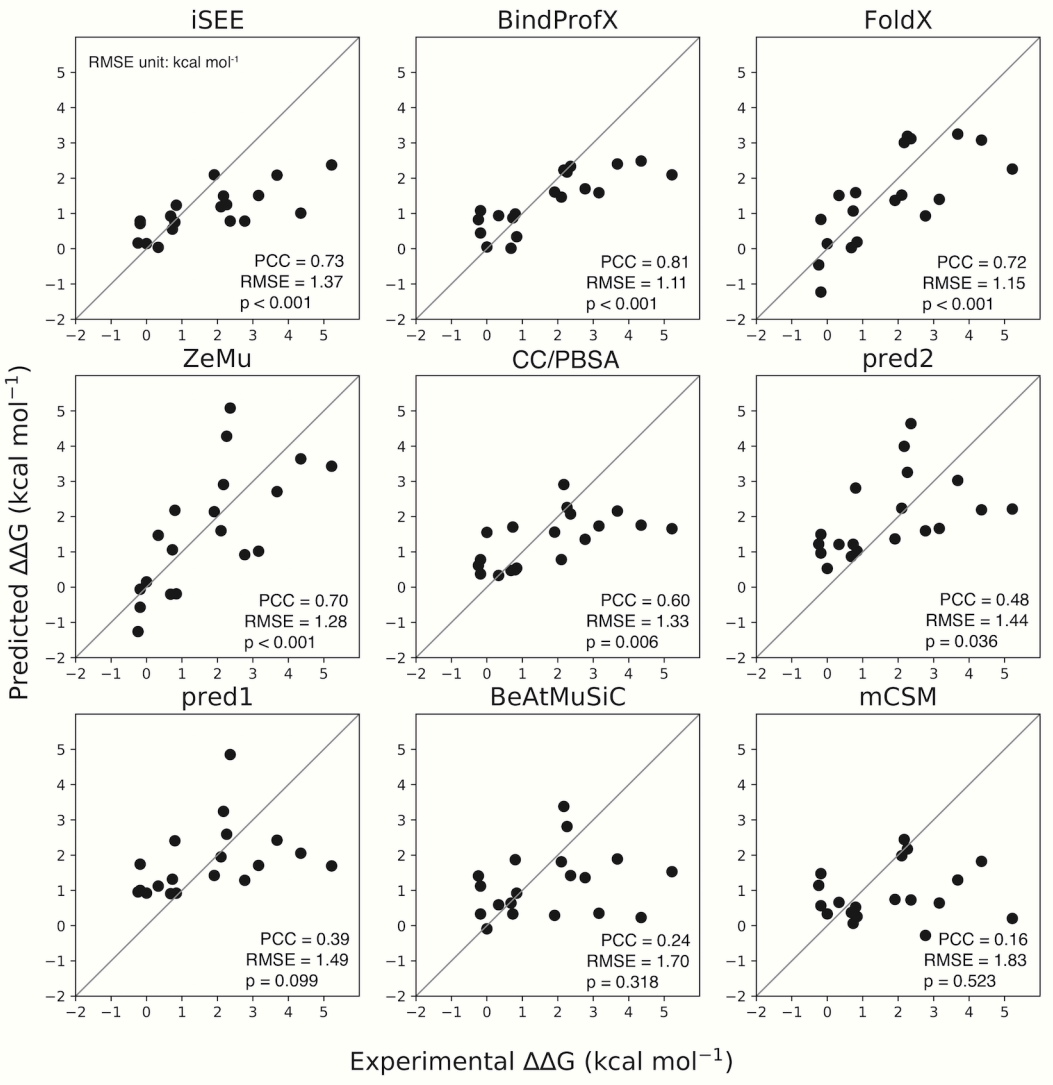

Figure 3. Predicted versus experimental ΔΔG for various ΔΔG predictors tested on a subset of the Benedix *et al.* NM dataset[8] consisting of 19 mutations for one complex, non-overlapping with our training set. This subset was not used in any of the predictors, except for CC/PBSA. PCC is the Pearson's correlation coefficient, p is two tailed p value of PCC, and RMSE represents root mean squared error.

There is still plenty of room to further improve ΔΔG predictors. We benchmarked iSEE and three other ΔΔG predictors (FoldX, mCSM and BindProfX) on a much larger blind test dataset (the S540 dataset) constructed from the recently released SKEMPI 2.0 update. This

dataset contains 540 mutations in 58 protein complexes that have not been seen by any predictor tested here. None of the four ΔΔG predictors performs well on this large blind test set (**Figure 4**). BindProfX performs best with an RMSE of 1.24 kcal mol^{-1} and PCC of 0.38 while iSEE achieves an RMSE of 1.32 kcal mol^{-1} and PCC of 0.27.

To see if a combination of those ΔΔG predictors could improve the prediction performance, we simply averaged their predictions. The resulting combined predictor outperforms all the individual predictors with improved RMSE (1.19 kcal mol^{-1}) and PCC (0.45) (**Figure 4**).

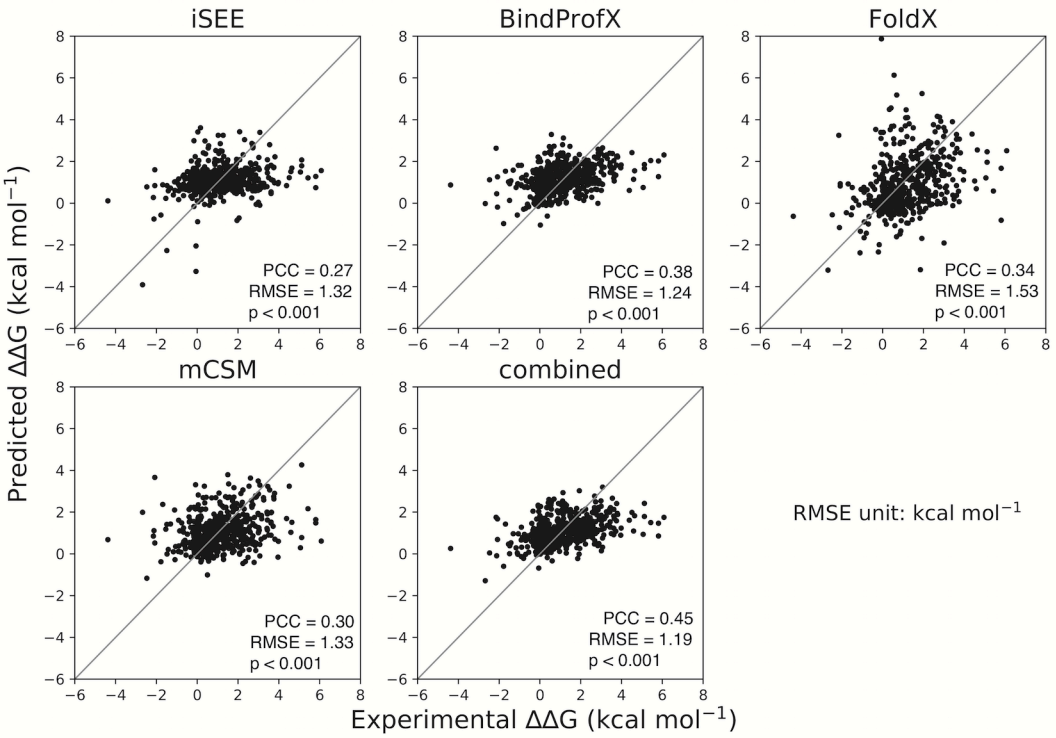

Figure 4. Correlations between predicted and experimental ΔΔG for various ΔΔG predictors tested on 540 mutations of SKEMPI 2.0. PCC is the Pearson's correlation coefficient, p is two tailed p value of PCC, and RMSE represents root mean squared error.

Feature importance. We analyzed the importance of iSEE features for the prediction performance. This was done by calculating the averaged decrease of mean squared error for

splitting on a given feature over all trees in the random forest model (see Methods). The results (**Figure 5**) reveal that the PSSM value of the wildtype amino acid (PSSM_wt) and the difference of PSSM values between mutant and wildtype residues (PSSM_diff) are the two most important features. They capture the evolutionary conservation of a specific amino acid at the mutation position and its change after mutation, respectively. PSSM has been proven to provide crucial information in various related topics, such as binding site predictions[37] and hot-spot predictions[38]. The alignment depth does not seem to have much impact on the prediction performance (**Figure S4**). However, with most entries having over 300 sequences in their alignment a more systematic study should be performed to come to clear conclusions on this. The next most important feature is an energetic term, namely the change in intermolecular electrostatic energy calculated by HADDOCK between the mutant and wildtype complexes (Eelec_diff), followed by the PSSM information content (PSSM_IC). The latter captures the evolutionary conservation over all 20 types of amino acids that can potentially appear at the mutation position. The high importance of the PSSM_wt, PSSM_diff and PSSM_IC features indicate that evolutionary conservation is essential to quantitatively describe the effect of mutations on binding affinity.

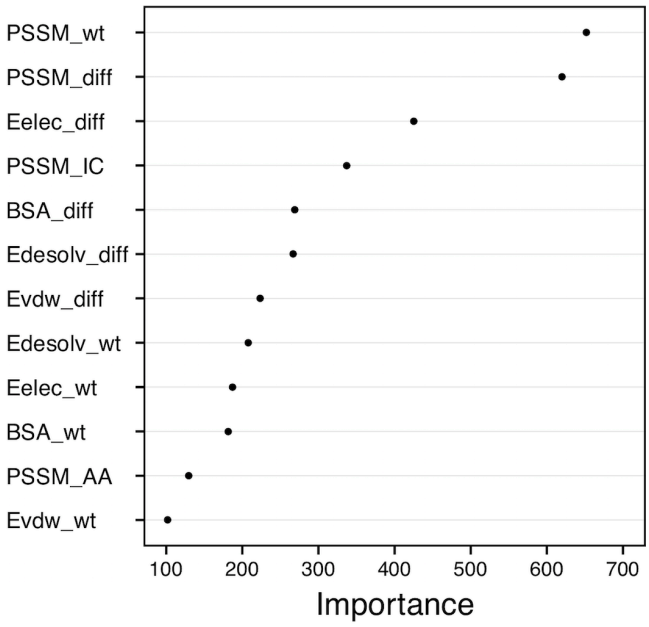

Figure 5. iSEE feature importance analysis. The importance value is measured as the decrease of mean squared prediction error when splitting on a given feature, averaged over all trees. The higher its value, the more important is the corresponding feature. The PSSM profile scores for the 20 amino acids are presented as a group in "PSSM_AA".

Discussion

We have developed a machine learning based ΔΔG predictor, iSEE, for quantitative prediction of the effects of single point mutations at the interface of a protein-protein complex. By combining structural, evolutionary and energetic features and training on a large and diverse dataset, our iSEE predictor not only demonstrated a consistent and high performance on various types of mutations during training, but also competed with state-of-the-art methods (based on empirical potential or machine learning models) on independent blind test datasets.

Compared with other machine learning methods, our predictor uses a rather small number of features, 31 in total which minimize the risk of overfitting (mCSM, for example, could use over 100 features). Evolutionary features, which benefit from the wealth of sequence data, are particularly sensitive to describe the impact of mutations on binding affinity as demonstrated by our feature importance analyses. The evolutionary conservation at both the amino acid type level (PSSM_wt and PSSM_diff) and mutation position level (PSSM_IC) were dominant amongst all iSEE features. Next to evolutionary features, energetic terms calculated with HADDOCK contribute to a quantitatively prediction of ΔΔGs, in particular the change of intermolecular electrostatic energy (Eelec_diff).

Unlike mCSM for which only wild-type structures are needed as input, iSEE does require the structures of both wildtype and mutant complexes. Models of the mutant complexes were

obtained using the HADDOCK refinement server[28]. The robust prediction results for mutations in loop vs. non-loop and mutations with different residue size changes indicates that this approach—the short refinement in explicit solvent performed by HADDOCK—can handle a small degree of conformational changes and remove steric clashes. To explore whether using an ensemble of structural models instead of a single model would improve the prediction performance, we also trained and tested iSEE using the average features calculated from the top 4 models returned by the HADDOCK refinement server. iSEE seems rather robust with respect to small conformational differences that might affect the energetic terms since using values from the top-ranked model or averages over the best 4 does not have any significant impact on its performance (**Table S1**). More systematic analyses are however needed to draw solid conclusions on this point.

With the recent release of SKEMPI 2.0, it becomes possible to benchmark current ΔΔG predictors on a large and novel blind dataset. Our benchmarking results on a set of 540 mutations show that all state-of-the-art ΔΔG predictors do not perform well with PCCs lower than 0.4. This indicates there is still a plenty of room for further improvements. Interestingly, averaging the predictions from the different ΔΔG predictors generated an improved prediction performance, indicating the various ΔΔG predictors might use complementary features. This should be useful for further development and improvement of ΔΔG predictors.

Acknowledgement

This work was supported by the European H2020 e-Infrastructure grant BioExcel (grant no. 675728). CG acknowledges financial support from the China Scholarship Council (grant no. 201406220132). AV acknowledges financial support from the European Union's H2020 Marie Skłodowska-Curie Individual Fellowships (grant no. BAP-659025). LX acknowledges

financial support from the Dutch Foundation for Scientific Research (Veni grant 722.014.005). We thank Dr. I.S. Moreira, P. Koukos and F. Ambrosetti for fruitful discussions and help about datasets and hot-spots. We also acknowledge the use of software from the SBGrid consortium[33] for various analysis tasks. This work has no conflict of interest.

References

1. Wang X, Wei X, Thijssen B, Das J, Lipkin SM, Yu H. Three-dimensional reconstruction of protein networks provides insight into human genetic disease. Nature Biotechnology. 2012;30(2):159–164.

2. Zhou M, Li Q, Wang R. Current Experimental Methods for Characterizing Protein–Protein Interactions. ChemMedChem. 2016;11(8):738–756.

3. Kastritis PL, Bonvin AMJJ. On the binding affinity of macromolecular interactions: daring to ask why proteins interact. Journal of The Royal Society Interface. 2012;10(79):20120835–20120835.

4. Steinbrecher T, Abel R, Clark A, Friesner R. Free Energy Perturbation Calculations of the Thermodynamics of Protein Side-Chain Mutations. Journal of Molecular Biology. 2017;429(7):923–929.

5. Perthold JW, Oostenbrink C. Simulation of Reversible Protein-Protein Binding and Calculation of Binding Free Energies Using Perturbed Distance Restraints. Journal of Chemical Theory and Computation. 2017;13(11):5697–5708.

6. Guerois R, Nielsen JE, Serrano L. Predicting Changes in the Stability of Proteins and Protein Complexes: A Study of More Than 1000 Mutations. Journal of Molecular Biology. 2002;320(2):369–387.

7. Dourado DFAR, Flores SC. A multiscale approach to predicting affinity changes in protein-protein interfaces. Proteins: Structure, Function, and Bioinformatics. 2014;82(10):2681–2690.

8. Benedix A, Becker CM, de Groot BL, Caflisch A, Böckmann RA. Predicting free energy changes using structural ensembles. Nature Methods. 2009;6(1):3–4.

9. Li M, Petukh M, Alexov E, Panchenko AR. Predicting the Impact of Missense Mutations on Protein–Protein Binding Affinity. Journal of Chemical Theory and Computation. 2014;10(4):1770–1780.

10. Dehouck Y, Kwasigroch JM, Rooman M, Gilis D. BeAtMuSiC: prediction of changes in protein–protein binding affinity on mutations. Nucleic Acids Research. 2013;41(W1):W333–W339.

11. Pires DEV, Ascher DB, Blundell TL. mCSM: predicting the effects of mutations in proteins using graph-based signatures. Bioinformatics. 2013;30(3):335–342.

12. Berliner N, Teyra J, Çolak R, Garcia Lopez S, Kim PM. Combining Structural Modeling with Ensemble Machine Learning to Accurately Predict Protein Fold Stability and Binding Affinity Effects upon Mutation Kurgan L, editor. PLoS ONE. 2014;9(9):e107353.

13. Brender JR, Zhang Y. Predicting the Effect of Mutations on Protein-Protein Binding Interactions through Structure-Based Interface Profiles Jernigan RL, editor. PLOS Comput Biol. 2015;11(10):e1004494.

14. Moal IH, Fernández-Recio J. SKEMPI: a Structural Kinetic and Energetic database of Mutant Protein Interactions and its use in empirical models. Bioinformatics. 2012;28(20):2600–2607.

15. Jankauskaite J, Jiménez-García B, Dapkūnas J, Fernández-Recio J, Moal IH. SKEMPI 2.0: An updated benchmark of changes in protein-protein binding energy, kinetics and thermodynamics upon mutation. Bioinformatics. 2018 Jul 18.

16. Moreira IS, Fernandes PA, Ramos MJ. Hot spots—A review of the protein–protein interface determinant amino-acid residues. Proteins: Structure, Function, and Bioinformatics. 2007;68(4):803–812.

17. DeLano WL. Unraveling hot spots in binding interfaces: progress and challenges. Current Opinion in Structural Biology. 2002;12(1):14–20.

18. Martins SA, Perez MAS, Moreira IS, Sousa SF, Ramos MJ, Fernandes PA. Computational Alanine Scanning Mutagenesis: MM-PBSA vs TI. Journal of Chemical Theory and Computation. 2013;9(3):1311–1319.

19. Xiong P, Zhang C, Zheng W, Zhang Y. BindProfX: Assessing Mutation-Induced Binding Affinity Change by Protein Interface Profiles with Pseudo-Counts. Journal of Molecular Biology. 2017;429(3):426–434.

20. Hertz GZ, Stormo GD. Identifying DNA and protein patterns with statistically significant alignments of multiple sequences. Bioinformatics. 1999;15(7):563–577.

21. Cyril Dominguez, Rolf Boelens A, Bonvin AMJJ. HADDOCK: A Protein−Protein Docking Approach Based on Biochemical or Biophysical Information. Journal of the American Chemical Society. 2003;125(7):1731–1737.

22. Janin J, Henrick K, Moult J, Eyck LT, Sternberg MJE, Vajda S, Vakser I, Wodak SJ. CAPRI: A Critical Assessment of PRedicted Interactions. Proteins: Structure, Function, and Bioinformatics. 2003;52(1):2–9.

23. Vangone A, Rodrigues JPGLM, Xue LC, van Zundert GCP, Geng C, Kurkcuoglu Z, Nellen M, Narasimhan S, Karaca E, van Dijk M, et al. Sense and simplicity in HADDOCK scoring: Lessons from CASP-CAPRI round 1. Proteins: Structure, Function, and Bioinformatics. 2017;85(3):417–423.

24. Fernández-Recio J, Totrov M, Abagyan R. Identification of Protein–Protein Interaction Sites from Docking Energy Landscapes. Journal of Molecular Biology. 2004;335(3):843–

865.

25. Breiman L. Random Forests. Machine Learning. 2001;45(1):5–32.

26. Levy ED. A Simple Definition of Structural Regions in Proteins and Its Use in Analyzing Interface Evolution. Journal of Molecular Biology. 2010;403(4):660–670.

27. Geng C, Vangone A, Bonvin AMJJ. Exploring the interplay between experimental methods and the performance of predictors of binding affinity change upon mutations in protein complexes. Protein Engineering, Design and Selection. 2016;29(8):291–299.

28. van Zundert GCP, Rodrigues JPGLM, Trellet M, Schmitz C, Kastritis PL, Karaca E, Melquiond ASJ, van Dijk M, de Vries SJ, Bonvin AMJJ. The HADDOCK2.2 Web Server: User-Friendly Integrative Modeling of Biomolecular Complexes. Journal of Molecular Biology. 2016;428(4):720–725.

29. Jorgensen WL, Tirado-Rives J. The OPLS [optimized potentials for liquid simulations] potential functions for proteins, energy minimizations for crystals of cyclic peptides and crambin. Journal of the American Chemical Society. 1988;110(6):1657–1666.

30. Altschul SF, Madden TL, Schäffer AA, Zhang J, Zhang Z, Miller W, Lipman DJ. Gapped BLAST and PSI-BLAST: a new generation of protein database search programs. Nucleic Acids Research. 1997;25(17):3389.

31. Liaw A, Wiener M. Classification and regression by randomForest. R news. 2002.

32. Kuhn M. Building Predictive Models in R Using the caret Package. Journal of Statistical Software. 2008;28(1):1–26.

33. Morin A, Ben Eisenbraun, Key J, Sanschagrin PC, Timony MA, Ottaviano M, Sliz P. Cutting Edge: Collaboration gets the most out of software. eLife. 2013;2:e01456.

34. Kabsch W, Sander C. Dictionary of protein secondary structure: Pattern recognition of hydrogen-bonded and geometrical features. Biopolymers. 1983;22(12):2577–2637.

35. Harpaz Y, Gerstein M, Chothia C. Volume changes on protein folding. Structure. 1994;2(7):641–649.

36. Meyer PA, Socias S, Key J, Ransey E, Tjon EC, Buschiazzo A, Lei M, Botka C, Withrow J, Neau D, et al. Data publication with the structural biology data grid supports live analysis. Nature Communications. 2016;7:ncomms10882.

37. Walia RR, Xue LC, Wilkins K, El-Manzalawy Y, Dobbs D, Honavar V. RNABindRPlus: A Predictor that Combines Machine Learning and Sequence Homology-Based Methods to Improve the Reliability of Predicted RNA-Binding Residues in Proteins Kurgan L, editor. PLoS ONE. 2014;9(5):e97725.

38. Moreira IS, Koukos PI, Melo R, Almeida JG, Preto AJ, Schaarschmidt J, Trellet M, Gümüş ZH, Costa J, Bonvin AMJJ. SpotOn: High Accuracy Identification of Protein-Protein Interface Hot-Spots. Scientific Reports. 2017;7(1):8007.

Supporting material

for

iSEE: Interface Structure, Evolution and Energy-based machine learning predictor of binding affinity changes upon mutations

Cunliang Geng[a], Anna Vangone[a], Gert E. Folkers[a], Li C. Xue[a1] and Alexandre M.J.J. Bonvin[a1]

[a]Bijvoet Center for Biomolecular Research, Faculty of Science - Chemistry, Utrecht University, Padualaan 8, 3584 CH Utrecht, the Netherlands;

[1]Correspoding authors. Email: l.xue@uu.nl, a.m.j.j.bonvin@uu.nl; T: +31 30 2533641, +31 30 2533859.

Table of Contents

SI Results

Evaluation of iSEE's applicability to different protein complexes

The original cross-validation described in the main text splits the dataset based on mutations and not complexes. A consequence of this is that related mutations could appear for a given complex in both the training and test sets, which might lead to an overestimation of the performance. To check for this, we selected 13 complexes from the training dataset with more than 20 mutations per complex. We then compared the prediction performance of iSEE on leave-one-complex-out cross-validation and leave-one-mutation-out cross-validation. For the leave-one-complex-out CV, all mutations that belong to a specific complex were hold out as independent test data, and the model was trained on mutations from all the remaining complexes. For the leave-one-mutation-out CV, each mutation in a complex was, in turn, hold out as a test data and the remaining mutations of that complex and the mutations of all other complexes were used for training.

The prediction performance on each complex between leave-one-complex-out CV and leave-one-mutation-out CV is compared in **Figure S2A**. Both cross-validation schemes show similar performances as clearly seen from the similar PCC values (with a p-value of 0.127 of Wilcoxon signed rank test). This indicates that iSEE has a strong generalizability on predicting the trend of ΔΔG values among a group of mutations. The Wilcoxon test applied on RMSE values gives, however, a p-value of 0.008, indicating a small significant difference in prediction error for each complex between the two cross-validation schemes.

We can also see that the PCC values are not uniform over various complexes, covering a large range from -0.01 to 0.97. iSEE shows varying prediction performance on different complexes. This observation is not correlated to the binding affinity of the wildtype complex (PCC = 0.09, data not shown). However, the low PCC values mainly resulted from the complexes that have a narrow range of ΔΔG values (≤l0.5l kcal mol^{-1}) (**Figure S2B and S3**), which are close to the experimentally measured ΔΔG error of about 0.5 kcal mol^{-1}[1].

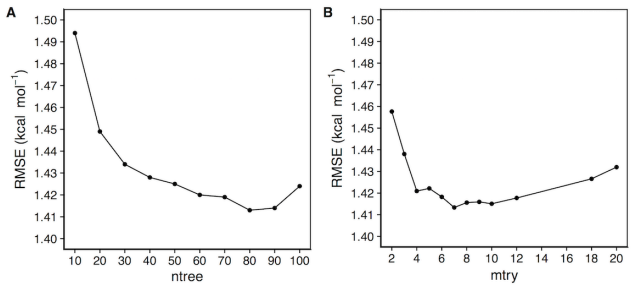

Figure S1. Cross-validation performance for different ntree and mtry settings. Given a specific ntree value, the random forest model is optimized on different mtry values by cross-validation on the training dataset. The best average RMSE for each ntree value is shown in (A). The lowest RMSE was obtained for ntree **=** 80. The RMSE values for different mtry values for ntree = 80 are shown in (B)**.** The best RMSE was obtained for mtry = 7. The final iSEE predictor uses the parameters of ntree = 80 and mtry = 7.

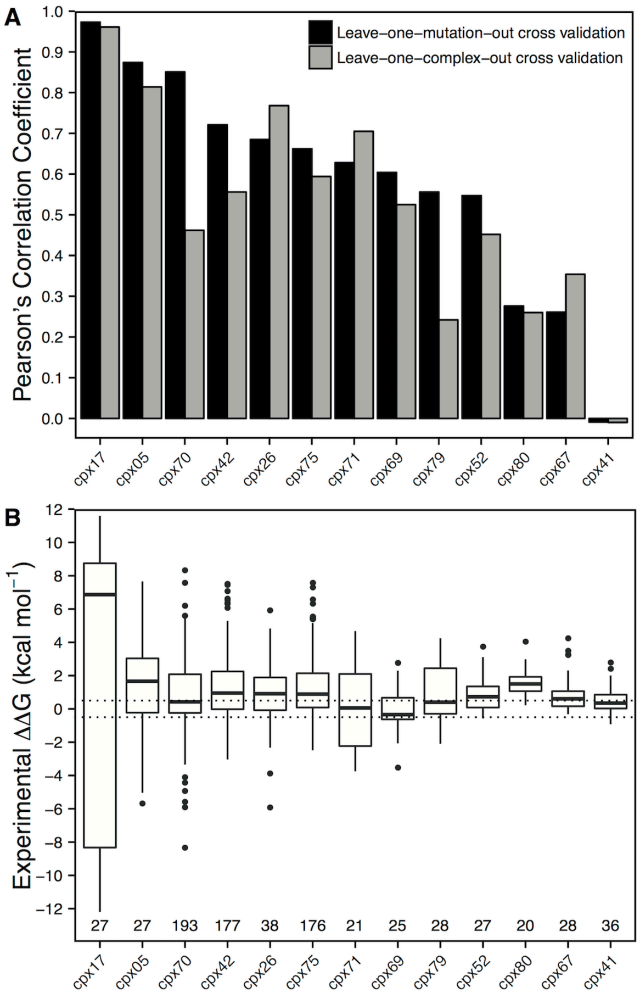

Figure S2. Evaluation of iSEE generalizability at the protein complex level. **(A)** Comparison of Pearson's correlation coefficients for each complex between leave-one-mutation-out cross-validations and leave-one-complex-out cross-validations. **(B)** Distribution of experimental ΔΔG values and number of mutations for each complex. Dotted lines denote ΔΔG of +0.5 and -0.5 kcal mol^{-1}. The complexes were ordered from left to right in order from high to low Pearson's correlation coefficients of leave-one-mutation-out cross-validations.

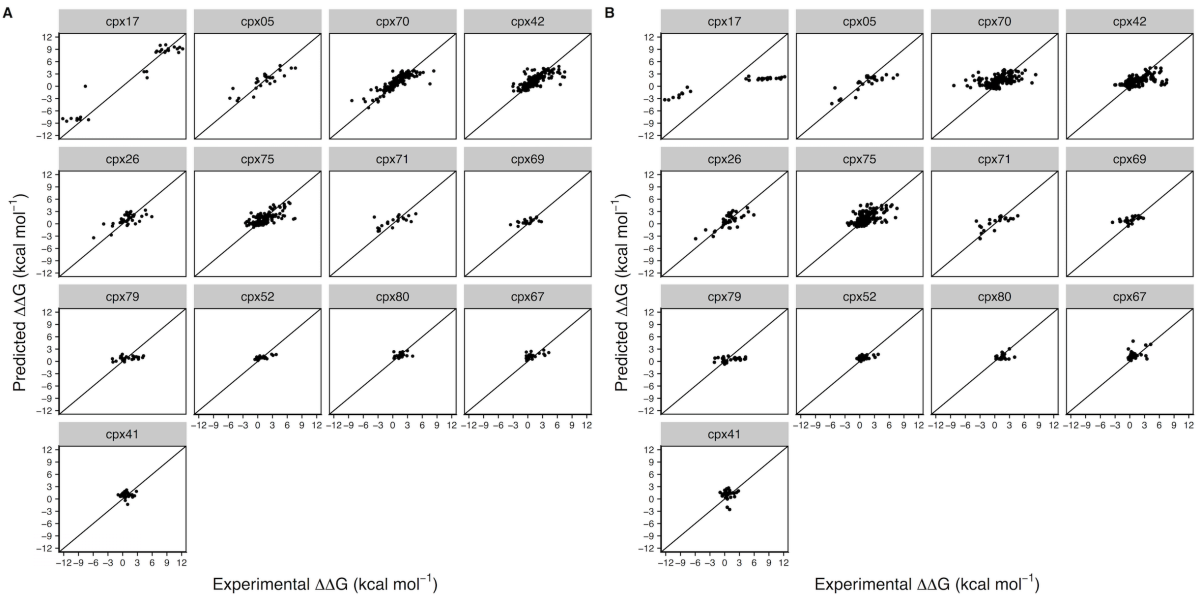

Figure S3. Correlations between predicted and experimental ΔΔG for each type of complex performing **(A)** leave-one-mutation-out and **(B)** leave-one-complex-out cross-validation. The complex types are ordered from left to right based on decreasing Pearson's correlation coefficients of leave-one-mutation-out cross-validations.

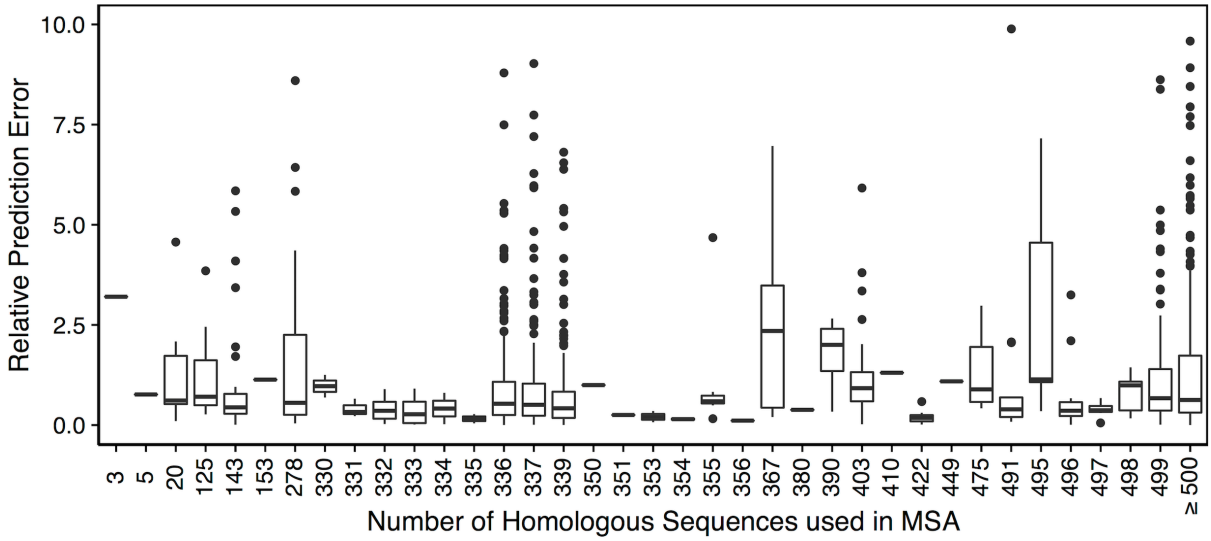

Figure S4. iSEE prediction's performance as a function of the multiple sequence alignment depth used for constructing the PSSM. The performance is reported here as the relative prediction error: | (ΔΔGpred - ΔΔGexp) / ΔΔGexp | from cross-validations using the SKEMPI dataset. For clarity, the y axis scale excludes 25 mutations with relative prediction errors larger than 10. Further, 12 mutations with ΔΔGexp equal to zero are not shown here because we cannot calculate relative prediction errors for them.

Table S1. Performance of iSEE using different number of structural models from the HADDOCK refinement. The structure and energy features of iSEE were calculated using only the top (best ranked) structural model (iSEE_top1) and the average of features over the top four models (iSEE_top4).

	Method	RMSE (kcal mol^{-1})	PCC
Training and Cross validation	iSEE_top1	1.41±0.14	0.80±0.06
	iSEE_top4	1.42±0.13	0.80±0.05
Test on NM dataset	iSEE_top1	1.37	0.73
	iSEE_top4	1.20	0.77
Test on S540 dataset	iSEE_top1	1.32	0.27
	iSEE_top4	1.39	0.23

Table S2. iSEE features.

Feature Type	Feature Name		Comments
Structure	BSA_wt		Buried surface area of the wildtype complex
	BSA_diff		= BSA_mut – BSA_wt
Energy	Evdw_wt		Intermolecular van de Waals energy of the wildtype complex
	Eelec_wt		Intermolecular electrostatic energy of the wildtype complex
	Edesolv_wt		Desolvation energy of the wildtype complex
	Evdw_diff		= Evdw_mut – Evdw_wt
	Eelec_diff		= Eelec_mut – Eelec_wt
	Edesolv_diff		= Edesolv_mut – Edesolv_wt
Evolution	PSSM_wt		PSSM value for the wildtype amino acid type at the mutation position
	PSSM_diff		= PSSM_mut – PSSM_wt
	PSSM_IC		Information content at the mutation position
	PSSM_AA	A, R, N, D, C, Q, E, G, H, I, L, K, M, F, P, S, T, W, Y, V	PSSM profile for 20 amino acid types at the mutation position

Table S3. iSEE training dataset with experimental ΔΔG and average predictions of cross-validations. "SS" stands for the secondary structure (loop or nonloop), "muttype" for the type of mutated amino acid (toALA or toNonALA), "mutvol" for the change of amino acid size (toSmall, neutral, or toLarge), and "complex" for the index of complex types.

mutationID	ΔΔGexp	ΔΔGpred	SS	muttype	mutvol	complex
1A22_A_SER51ALA	0.35	0.44	nonloop	toALA	neutral	cpx41
1A22_A_PHE165ALA	0.41	1.83	nonloop	toALA	toSmall	cpx41
1A22_A_SER62ALA	0.16	0.68	loop	toALA	neutral	cpx41
1A22_A_ILE168ALA	0.81	1.42	nonloop	toALA	toSmall	cpx41
1A22_A_GLN22ALA	-0.22	0.66	nonloop	toALA	toSmall	cpx41
1A22_A_ASN63ALA	0.31	1.39	loop	toALA	toSmall	cpx41
1A22_A_ARG172ALA	0.54	0.37	nonloop	toALA	toSmall	cpx41
1A22_A_PHE180ALA	0.19	1.27	loop	toALA	toSmall	cpx41
1A22_A_GLU56ALA	0.41	0.65	nonloop	toALA	toSmall	cpx41
1A22_A_THR164ALA	1.91	1.04	nonloop	toALA	toSmall	cpx41
1A22_A_ARG167ALA	2.42	0.77	nonloop	toALA	toSmall	cpx41
1A22_A_HIS18ALA	-0.49	0.71	nonloop	toALA	toSmall	cpx41
1A22_A_GLN68ALA	0.59	0.41	nonloop	toALA	toSmall	cpx41
1A22_A_PRO48ALA	0.41	0.84	nonloop	toALA	toSmall	cpx41
1A22_A_LYS161ALA	2.01	0.46	nonloop	toALA	toSmall	cpx41
1A22_A_LEU45ALA	1.22	0.62	nonloop	toALA	toSmall	cpx41
1A22_A_GLU65ALA	-0.47	0.61	nonloop	toALA	toSmall	cpx41
1A22_A_ASP160ALA	0.79	2.19	nonloop	toALA	toSmall	cpx41
1A22_A_CYS171ALA	1.01	1.56	nonloop	toALA	toSmall	cpx41
1A22_A_HIS21ALA	0.16	1.54	nonloop	toALA	toSmall	cpx41
1A22_A_LYS157ALA	-0.16	1.04	nonloop	toALA	toSmall	cpx41
1A22_A_GLU163ALA	-0.92	1.01	nonloop	toALA	toSmall	cpx41
1A22_A_ASP26ALA	-0.21	1.09	nonloop	toALA	toSmall	cpx41
1A22_A_TYR153ALA	0.35	0.50	nonloop	toALA	toSmall	cpx41
1A22_A_GLN46ALA	0.11	0.97	nonloop	toALA	toSmall	cpx41
1A22_A_PRO61ALA	1.21	1.21	loop	toALA	toSmall	cpx41
1A22_A_ARG64ALA	1.64	0.99	nonloop	toALA	toSmall	cpx41
1A22_A_ARG156ALA	0.28	1.48	nonloop	toALA	toSmall	cpx41
1A22_A_TYR42ALA	0.20	0.73	nonloop	toALA	toSmall	cpx41
1A22_B_ARG11MET	1.00	-1.32	loop	toNonALA	toSmall	cpx41
1A22_B_SER174ALA	0.03	0.83	loop	toALA	neutral	cpx41
1A22_B_ARG11LEU	0.52	-0.36	loop	toNonALA	toSmall	cpx41
1A22_B_SER58ALA	-0.51	0.84	nonloop	toALA	neutral	cpx41
1A22_B_CYS81ALA	0.00	1.08	nonloop	toALA	toSmall	cpx41
1A22_B_TRP63PHE	2.78	1.85	nonloop	toNonALA	toSmall	cpx41
1A22_B_CYS67ALA	0.00	1.41	nonloop	toALA	toSmall	cpx41
1A4Y_A_TRP261ALA	0.10	1.36	nonloop	toALA	toSmall	cpx67
1A4Y_A_TRP375ALA	1.03	1.47	nonloop	toALA	toSmall	cpx67
1A4Y_A_GLU344ALA	0.18	1.23	nonloop	toALA	toSmall	cpx67
1A4Y_A_TYR434PHE	0.56	1.65	nonloop	toNonALA	neutral	cpx67
1A4Y_A_TRP263ALA	1.17	1.36	nonloop	toALA	toSmall	cpx67
1A4Y_A_TYR434ALA	3.26	1.80	nonloop	toALA	toSmall	cpx67
1A4Y_A_ASP435ALA	3.48	1.45	nonloop	toALA	toSmall	cpx67
1A4Y_A_TRP318ALA	1.50	1.15	nonloop	toALA	toSmall	cpx67
1A4Y_A_ARG457ALA	-0.22	0.16	nonloop	toALA	toSmall	cpx67
1A4Y_A_TYR437ALA	0.84	1.10	loop	toALA	toSmall	cpx67
1A4Y_A_SER289ALA	0.04	0.89	nonloop	toALA	neutral	cpx67
1A4Y_A_GLU401ALA	0.88	1.13	nonloop	toALA	toSmall	cpx67
1A4Y_A_LYS320ALA	-0.31	1.34	loop	toALA	toSmall	cpx67
1A4Y_A_ILE459ALA	0.68	1.21	nonloop	toALA	toSmall	cpx67
1A4Y_A_TYR437PHE	0.25	1.09	loop	toNonALA	neutral	cpx67
1A4Y_B_HIS84ALA	0.17	0.81	loop	toALA	toSmall	cpx67
1A4Y_B_LYS40GLY	3.24	2.76	loop	toNonALA	toSmall	cpx67
1A4Y_B_ARG5ALA	2.31	1.98	nonloop	toALA	toSmall	cpx67
1A4Y_B_HIS13ALA	-0.30	2.26	nonloop	toALA	toSmall	cpx67
1A4Y_B_GLU108ALA	-0.32	0.77	nonloop	toALA	toSmall	cpx67
1A4Y_B_ARG31ALA	0.25	1.01	nonloop	toALA	toSmall	cpx67
1A4Y_B_TRP89ALA	0.24	1.44	loop	toALA	toSmall	cpx67

1A4Y_B_LYS40GLN	4.25	2.15	loop	toNonALA	toSmall	cpx67
1A4Y_B_ARG32ALA	0.91	1.20	nonloop	toALA	toSmall	cpx67
1A4Y_B_GLN12ALA	0.30	1.62	nonloop	toALA	toSmall	cpx67
1A4Y_B_HIS114ALA	0.66	2.46	nonloop	toALA	toSmall	cpx67
1A4Y_B_ASN68ALA	0.12	0.69	loop	toALA	toSmall	cpx67
1A4Y_B_HIS8ALA	0.90	0.55	nonloop	toALA	toSmall	cpx67
1ACB_B_LEU38SER	4.95	4.99	loop	toNonALA	toSmall	cpx12
1ACB_B_LEU38PRO	6.85	3.68	loop	toNonALA	toSmall	cpx12
1ACB_B_LEU38GLY	6.03	4.67	loop	toNonALA	toSmall	cpx12
1ACB_B_LEU38GLU	6.55	4.52	loop	toNonALA	toSmall	cpx12
1ACB_B_LEU38ILE	4.23	4.91	loop	toNonALA	neutral	cpx12
1ACB_B_LEU38ASP	6.77	4.34	loop	toNonALA	toSmall	cpx12
1AK4_B_PRO93ALA	0.68	1.59	nonloop	toALA	toSmall	cpx29
1AK4_B_HIS87ARG	1.64	0.87	loop	toNonALA	toLarge	cpx29
1AK4_B_HIS87ALA	1.01	1.25	loop	toALA	toSmall	cpx29
1AK4_B_ALA88VAL	0.77	1.06	loop	toNonALA	toLarge	cpx29
1AK4_B_PRO85ALA	1.09	1.32	loop	toALA	toSmall	cpx29
1AK4_B_ALA92VAL	0.36	1.12	loop	toNonALA	toLarge	cpx29
1AK4_B_ILE91ALA	0.24	0.87	loop	toALA	toSmall	cpx29
1AK4_B_ALA88GLY	2.65	0.57	loop	toNonALA	toSmall	cpx29
1AK4_B_GLY89VAL	3.03	1.74	loop	toNonALA	toLarge	cpx29
1AK4_B_ALA92GLY	0.58	1.23	loop	toNonALA	toSmall	cpx29
1AK4_B_VAL86ALA	0.99	0.96	loop	toALA	toSmall	cpx29
1AK4_B_HIS87GLN	0.97	1.16	loop	toNonALA	neutral	cpx29
1AK4_B_PRO90ALA	2.17	1.03	loop	toALA	toSmall	cpx29
1AK4_B_ILE91VAL	0.00	0.58	loop	toNonALA	toSmall	cpx29
1AK4_B_GLY89ALA	2.08	1.93	loop	toALA	toLarge	cpx29
1B2S_A_ALA27LYS	-3.86	-2.94	nonloop	toNonALA	toLarge	cpx05
1B2S_B_ALA43THR	-0.34	-0.48	nonloop	toNonALA	toLarge	cpx05
1B2U_A_ALA27LYS	-5.04	-0.54	nonloop	toNonALA	toLarge	cpx05
1B2U_B_ALA36ASP	-4.17	-3.55	nonloop	toNonALA	toLarge	cpx05
1B3S_A_ALA102HIS	-5.68	-2.93	loop	toNonALA	toLarge	cpx05
1B3S_B_PHE30TYR	0.60	0.15	nonloop	toNonALA	neutral	cpx05
1BRS_A_GLU58ALA	-0.33	0.86	loop	toALA	toSmall	cpx05
1BRS_A_GLU71CYS	2.53	2.04	nonloop	toNonALA	toSmall	cpx05
1BRS_A_HIS100GLY	6.82	4.42	loop	toNonALA	toSmall	cpx05
1BRS_A_ARG57LYS	2.49	0.63	loop	toNonALA	toSmall	cpx05
1BRS_A_HIS100ASP	4.55	3.91	loop	toNonALA	toSmall	cpx05
1BRS_A_GLU71TRP	1.66	2.30	nonloop	toNonALA	toLarge	cpx05
1BRS_A_HIS100LEU	7.66	4.42	loop	toNonALA	neutral	cpx05
1BRS_A_ARG81GLN	5.42	2.54	loop	toNonALA	toSmall	cpx05
1BRS_A_GLU71PHE	2.23	2.21	nonloop	toNonALA	toLarge	cpx05
1BRS_A_TRP33PHE	1.41	2.96	loop	toNonALA	toSmall	cpx05
1BRS_A_GLU71TYR	2.41	2.20	nonloop	toNonALA	toLarge	cpx05
1BRS_A_GLU71SER	3.01	2.07	nonloop	toNonALA	toSmall	cpx05
1BRS_A_HIS100GLN	4.55	5.04	loop	toNonALA	neutral	cpx05
1BRS_A_GLU71GLN	1.45	2.53	nonloop	toNonALA	neutral	cpx05
1BRS_A_ASN56ALA	3.06	2.14	loop	toALA	toSmall	cpx05
1BRS_B_TYR29ALA	3.47	1.19	nonloop	toALA	toSmall	cpx05
1BRS_B_THR42ALA	1.86	1.26	nonloop	toALA	toSmall	cpx05
1BRS_B_TRP38PHE	1.64	2.65	nonloop	toNonALA	toSmall	cpx05
1BRS_B_TRP44PHE	0.06	1.19	nonloop	toNonALA	toSmall	cpx05
1BRS_B_TYR29PHE	-0.13	1.82	nonloop	toNonALA	neutral	cpx05
1CSE_B_LEU38ASP	4.35	2.95	loop	toNonALA	toSmall	cpx74
1CSE_B_LEU38GLY	2.25	3.54	loop	toNonALA	toSmall	cpx74
1CSE_B_LEU38ILE	2.94	2.97	loop	toNonALA	neutral	cpx74
1CSE_B_LEU38GLU	2.35	3.45	loop	toNonALA	toSmall	cpx74
1CSE_B_LEU38SER	1.17	3.63	loop	toNonALA	toSmall	cpx74
1CSE_B_LEU38PRO	6.67	2.20	loop	toNonALA	toSmall	cpx74
1CSO_B_ILE13LEU	-4.42	-0.87	loop	toNonALA	neutral	cpx70
1CT0_B_SER13LEU	-4.10	-3.45	loop	toNonALA	toLarge	cpx70
1CT2_B_THR13LEU	-3.16	-3.12	loop	toNonALA	toLarge	cpx70
1CT4_B_VAL13LEU	-3.00	-3.82	loop	toNonALA	toLarge	cpx70
1E96_A_ASN26HIS	1.09	1.61	loop	toNonALA	toLarge	cpx64
1E96_A_ILE33ASN	2.01	1.89	loop	toNonALA	toSmall	cpx64
1EAW_A_THR144ALA	0.09	0.57	loop	toALA	toSmall	cpx55
1EAW_A_ASP214ALA	2.23	1.08	nonloop	toALA	toSmall	cpx55
1EAW_A_PHE92ALA	0.89	1.15	nonloop	toALA	toSmall	cpx55
1EAW_A_TYR141ALA	0.50	-0.36	nonloop	toALA	toSmall	cpx55

1EAW_A_PHE89ALA	0.73	0.50	loop	toALA	toSmall	cpx55
1EAW_A_ASP91ALA	0.65	0.77	nonloop	toALA	toSmall	cpx55
1EAW_A_ARG48ALA	0.59	0.87	nonloop	toALA	toSmall	cpx55
1EAW_A_ILE45ALA	-0.19	0.72	loop	toALA	toSmall	cpx55
1EAW_A_PHE50ALA	-0.43	0.50	loop	toALA	toSmall	cpx55
1EAW_A_TYR52ALA	-0.08	1.15	loop	toALA	toSmall	cpx55
1EAW_A_GLN169ALA	-0.13	0.62	nonloop	toALA	toSmall	cpx55
1EAW_A_ILE26ALA	-0.82	1.29	nonloop	toALA	toSmall	cpx55
1EAW_A_ASP47ALA	1.50	0.77	loop	toALA	toSmall	cpx55
1EAW_A_HIS138ALA	-0.02	0.38	loop	toALA	toSmall	cpx55
1EAW_A_GLN23ALA	-0.52	1.16	nonloop	toALA	toSmall	cpx55
1EFN_A_THR13HIS	1.24	0.91	loop	toNonALA	toLarge	cpx35
1EFN_A_ILE12ALA	1.45	-0.31	loop	toALA	toSmall	cpx35
1EMV_A_ILE51ALA	0.85	2.16	nonloop	toALA	toSmall	cpx26
1EMV_A_THR36ALA	0.90	-0.40	nonloop	toALA	toSmall	cpx26
1EMV_A_SER26ALA	0.17	0.98	loop	toALA	neutral	cpx26
1EMV_A_THR25ALA	0.73	0.59	loop	toALA	toSmall	cpx26
1EMV_A_VAL35ALA	1.66	1.49	nonloop	toALA	toSmall	cpx26
1EMV_A_SER46ALA	0.01	0.35	loop	toALA	neutral	cpx26
1EMV_A_GLU28ALA	1.42	2.75	nonloop	toALA	toSmall	cpx26
1EMV_A_VAL32ALA	2.58	0.00	nonloop	toALA	toSmall	cpx26
1EMV_A_ASN22ALA	0.14	0.68	nonloop	toALA	toSmall	cpx26
1EMV_A_ASP49ALA	5.92	1.74	nonloop	toALA	toSmall	cpx26
1EMV_A_SER27ALA	0.96	0.80	loop	toALA	neutral	cpx26
1EMV_A_TYR53ALA	4.63	3.34	loop	toALA	toSmall	cpx26
1EMV_A_GLU39ALA	2.08	2.08	nonloop	toALA	toSmall	cpx26
1EMV_A_SER48ALA	2.19	1.83	nonloop	toALA	neutral	cpx26
1EMV_A_TYR52ALA	4.83	2.28	nonloop	toALA	toSmall	cpx26
1EMV_A_HIS44ALA	0.83	2.82	loop	toALA	toSmall	cpx26
1EMV_A_CYS21ALA	0.92	2.14	nonloop	toALA	toSmall	cpx26
1EMV_A_PRO54ALA	1.24	1.72	loop	toALA	toSmall	cpx26
1EMV_A_PRO45ALA	0.44	2.17	loop	toALA	toSmall	cpx26
1EMV_A_LEU31ALA	3.42	0.60	nonloop	toALA	toSmall	cpx26
1EMV_A_GLY47ALA	1.49	2.42	nonloop	toALA	toLarge	cpx26
1EMV_B_ASN75ALA	2.33	2.22	nonloop	toALA	toSmall	cpx26
1EMV_B_GLN92ALA	-0.28	1.22	loop	toALA	toSmall	cpx26
1EMV_B_SER78ALA	-0.54	0.27	nonloop	toALA	neutral	cpx26
1EMV_B_PHE86ALA	3.88	1.82	loop	toALA	toSmall	cpx26
1EMV_B_SER77ALA	-0.23	0.55	nonloop	toALA	neutral	cpx26
1EMV_B_LYS97ALA	1.96	0.86	loop	toALA	toSmall	cpx26
1EMV_B_THR87ALA	0.16	0.84	loop	toALA	toSmall	cpx26
1EMV_B_VAL98ALA	1.09	-0.07	loop	toALA	toSmall	cpx26
1EMV_B_ARG54ALA	1.67	2.99	nonloop	toALA	toSmall	cpx26
1EMV_B_SER84ALA	-0.11	0.81	loop	toALA	neutral	cpx26
1EMV_B_ASN72ALA	1.16	1.06	loop	toALA	toSmall	cpx26
1EMV_B_SER74ALA	-0.24	0.34	nonloop	toALA	neutral	cpx26
1F47_A_LYS14ALA	-0.04	3.25	nonloop	toALA	toSmall	cpx34
1F47_A_TYR5ALA	0.87	2.71	loop	toALA	toSmall	cpx34
1F47_A_ASP7GLY	1.14	1.78	loop	toNonALA	toSmall	cpx34
1F47_A_PHE11ALA	2.44	1.95	nonloop	toALA	toSmall	cpx34
1F47_A_ASP7ALA	1.73	1.58	loop	toALA	toSmall	cpx34
1F47_A_ILE8ALA	2.52	1.76	nonloop	toALA	toSmall	cpx34
1F47_A_LEU12ALA	2.29	1.43	nonloop	toALA	toSmall	cpx34
1F47_A_ASP7SER	2.06	1.39	loop	toNonALA	toSmall	cpx34
1F47_A_ASP4ALA	0.69	2.52	loop	toALA	toSmall	cpx34
1F47_A_PRO9ALA	-0.06	1.02	nonloop	toALA	toSmall	cpx34
1F47_A_GLN15ALA	-0.05	1.70	nonloop	toALA	toSmall	cpx34
1F47_A_LEU6ALA	0.93	2.57	loop	toALA	toSmall	cpx34
1FC2_A_TYR10TRP	0.41	0.88	nonloop	toNonALA	toLarge	cpx63
1FCC_B_GLU42ALA	0.39	0.63	nonloop	toALA	toSmall	cpx48
1FCC_B_TRP43ALA	3.77	2.41	nonloop	toALA	toSmall	cpx48
1FCC_B_ASP40ALA	0.27	1.32	loop	toALA	toSmall	cpx48
1FCC_B_LYS31ALA	3.48	0.76	nonloop	toALA	toSmall	cpx48
1FCC_B_THR25ALA	0.24	0.83	nonloop	toALA	toSmall	cpx48
1FCC_B_LYS28ALA	1.26	0.92	nonloop	toALA	toSmall	cpx48
1FCC_B_ASN35ALA	2.36	0.69	nonloop	toALA	toSmall	cpx48
1FFW_A_TYR105TRP	0.71	1.69	nonloop	toNonALA	toLarge	cpx24
1FFW_A_ALA89VAL	0.09	0.96	loop	toNonALA	toLarge	cpx24
1FFW_B_ASP49ALA	0.10	0.91	nonloop	toALA	toSmall	cpx24

1FFW_B_ASP44ALA	-0.07	0.75	loop	toALA	toSmall	cpx24
1FFW_B_CYS55ALA	0.20	1.37	nonloop	toALA	toSmall	cpx24
1FFW_B_GLU20ALA	0.64	1.02	nonloop	toALA	toSmall	cpx24
1FFW_B_HIS23ALA	0.03	0.65	nonloop	toALA	toSmall	cpx24
1FFW_B_GLU13ALA	0.72	1.61	nonloop	toALA	toSmall	cpx24
1FFW_B_ILE58ALA	0.43	1.00	loop	toALA	toSmall	cpx24
1FFW_B_PHE56ALA	3.64	1.43	nonloop	toALA	toSmall	cpx24
1FR2_A_ALA39GLU	-2.08	-0.54	nonloop	toNonALA	toLarge	cpx26
1GC1_B_GLN33ALA	0.11	0.48	loop	toALA	toSmall	cpx37
1GC1_B_LYS46ALA	1.43	1.14	nonloop	toALA	toSmall	cpx37
1GC1_B_SER60ALA	-0.09	0.53	nonloop	toALA	neutral	cpx37
1GC1_B_LYS35ALA	0.32	0.97	nonloop	toALA	toSmall	cpx37
1GC1_B_GLN40ALA	-0.41	1.07	nonloop	toALA	toSmall	cpx37
1GC1_B_ASN32ALA	0.18	0.70	nonloop	toALA	toSmall	cpx37
1GC1_B_THR45ALA	-0.15	0.37	nonloop	toALA	toSmall	cpx37
1GC1_B_SER42ALA	0.00	0.74	nonloop	toALA	neutral	cpx37
1GC1_B_ARG59ALA	1.18	0.54	nonloop	toALA	toSmall	cpx37
1GC1_B_LEU44ALA	1.06	0.72	nonloop	toALA	toSmall	cpx37
1GC1_B_GLN25ALA	0.03	0.19	loop	toALA	toSmall	cpx37
1GC1_B_LYS29ALA	0.54	1.80	nonloop	toALA	toSmall	cpx37
1GC1_B_ASP63ALA	-0.32	0.44	nonloop	toALA	toSmall	cpx37
1GC1_B_ASN52ALA	0.71	0.51	nonloop	toALA	toSmall	cpx37
1GC1_B_GLU85ALA	1.32	0.87	nonloop	toALA	toSmall	cpx37
1GC1_B_HIS27ALA	0.28	1.24	nonloop	toALA	toSmall	cpx37
1GC1_B_GLN64ALA	0.44	0.25	nonloop	toALA	toSmall	cpx37
1GC1_B_SER23ALA	0.29	0.81	loop	toALA	neutral	cpx37
1GL0_B_MET28LYS	-0.57	1.25	loop	toNonALA	neutral	cpx14
1GL1_B_LEU29VAL	4.26	1.01	loop	toNonALA	toSmall	cpx13
1H9D_B_VAL3ALA	1.28	0.82	loop	toALA	toSmall	cpx04
1H9D_B_LEU93ALA	0.86	1.15	nonloop	toALA	toSmall	cpx04
1H9D_B_ARG2ALA	1.06	1.46	loop	toALA	toSmall	cpx04
1H9D_B_GLN66ALA	1.25	0.87	loop	toALA	toSmall	cpx04
1H9D_B_GLY60ALA	1.90	0.98	loop	toALA	toLarge	cpx04
1H9D_B_ASN94ALA	2.11	0.69	nonloop	toALA	toSmall	cpx04
1HE8_A_LYS80VAL	0.47	0.65	nonloop	toNonALA	toSmall	cpx62
1IAR_A_ARG53GLN	0.84	0.98	nonloop	toNonALA	toSmall	cpx52
1IAR_A_GLN8ALA	-0.02	0.56	nonloop	toALA	toSmall	cpx52
1IAR_A_PHE82ASP	-0.58	0.47	nonloop	toNonALA	toSmall	cpx52
1IAR_A_TRP91ASP	1.31	1.16	nonloop	toNonALA	toSmall	cpx52
1IAR_A_GLN78ALA	0.13	0.67	nonloop	toALA	toSmall	cpx52
1IAR_A_THR6ASP	1.39	0.75	nonloop	toNonALA	neutral	cpx52
1IAR_A_ARG85GLU	1.22	1.27	nonloop	toNonALA	toSmall	cpx52
1IAR_A_ARG88ALA	3.75	1.66	nonloop	toALA	toSmall	cpx52
1IAR_A_TRP91ALA	0.73	0.92	nonloop	toALA	toSmall	cpx52
1IAR_A_GLN78GLU	0.25	0.51	nonloop	toNonALA	neutral	cpx52
1IAR_A_ILE5ARG	0.80	0.85	nonloop	toNonALA	toLarge	cpx52
1IAR_A_LYS84ALA	0.35	1.12	nonloop	toALA	toSmall	cpx52
1IAR_A_LYS12GLU	0.14	0.56	nonloop	toNonALA	toSmall	cpx52
1IAR_A_ILE5ALA	1.17	1.06	nonloop	toALA	toSmall	cpx52
1IAR_A_LYS84ASP	1.88	0.63	nonloop	toNonALA	toSmall	cpx52
1IAR_A_GLN8ARG	0.04	0.21	nonloop	toNonALA	toLarge	cpx52
1IAR_A_THR13ALA	0.98	0.90	nonloop	toALA	toSmall	cpx52
1IAR_A_PHE82ALA	-0.09	0.47	nonloop	toALA	toSmall	cpx52
1IAR_A_LYS12SER	-0.02	0.94	nonloop	toNonALA	toSmall	cpx52
1IAR_A_ARG85ALA	0.43	1.34	nonloop	toALA	toSmall	cpx52
1IAR_A_THR6ALA	-0.10	0.79	nonloop	toALA	toSmall	cpx52
1IAR_A_ARG81ALA	0.48	1.22	nonloop	toALA	toSmall	cpx52
1IAR_A_ARG81GLU	1.46	0.86	nonloop	toNonALA	toSmall	cpx52
1IAR_A_ASN89ALA	1.56	0.97	nonloop	toALA	toSmall	cpx52
1IAR_A_THR13ASP	-0.22	1.06	nonloop	toNonALA	neutral	cpx52
1IAR_A_GLU9GLN	3.11	1.48	nonloop	toNonALA	neutral	cpx52
1IAR_A_ARG88GLN	2.83	1.75	nonloop	toNonALA	toSmall	cpx52
1JCK_B_TYR90ALA	2.59	1.77	loop	toALA	toSmall	cpx07
1JCK_B_LYS103ALA	0.68	1.27	loop	toALA	toSmall	cpx07
1JCK_B_PHE176ALA	2.13	1.02	loop	toALA	toSmall	cpx07
1JCK_B_TYR26ALA	1.77	1.36	nonloop	toALA	toSmall	cpx07
1JCK_B_THR20ALA	1.65	1.33	loop	toALA	toSmall	cpx07
1JCK_B_VAL91ALA	2.23	1.16	nonloop	toALA	toSmall	cpx07
1JCK_B_ASN60ALA	1.64	1.50	loop	toALA	toSmall	cpx07

1JTG_A_GLN74ALA	0.43	0.71	nonloop	toALA	toSmall	cpx79
1JTG_A_VAL78ALA	1.91	0.47	loop	toALA	toSmall	cpx79
1JTG_A_MET104ALA	0.74	1.13	nonloop	toALA	toSmall	cpx79
1JTG_A_VAL190ALA	-0.41	1.25	loop	toALA	toSmall	cpx79
1JTG_A_GLY212SER	-0.27	1.00	nonloop	toNonALA	toLarge	cpx79
1JTG_A_GLU79LYS	4.23	1.33	loop	toNonALA	toLarge	cpx79
1JTG_A_SER209ALA	1.24	0.79	nonloop	toALA	neutral	cpx79
1JTG_A_PRO82ALA	-0.38	1.25	nonloop	toALA	toSmall	cpx79
1JTG_A_GLU143ALA	-0.07	1.74	nonloop	toALA	toSmall	cpx79
1JTG_A_TYR80ALA	-0.17	0.94	loop	toALA	toSmall	cpx79
1JTG_A_ASN75ALA	-0.46	0.84	nonloop	toALA	toSmall	cpx79
1JTG_A_GLU85ALA	4.06	0.93	nonloop	toALA	toSmall	cpx79
1JTG_B_THR140LYS	-0.01	0.24	loop	toNonALA	toLarge	cpx79
1JTG_B_TRP112ALA	3.01	1.05	nonloop	toALA	toSmall	cpx79
1JTG_B_TYR143ALA	0.38	0.39	loop	toALA	toSmall	cpx79
1JTG_B_TYR50ALA	-0.41	0.96	nonloop	toALA	toSmall	cpx79
1JTG_B_ASP163ALA	-1.34	0.07	loop	toALA	toSmall	cpx79
1JTG_B_HIS148ALA	2.75	1.12	nonloop	toALA	toSmall	cpx79
1JTG_B_ARG160ALA	2.22	0.65	nonloop	toALA	toSmall	cpx79
1JTG_B_ASP163LYS	-1.98	-0.15	loop	toNonALA	toLarge	cpx79
1JTG_B_SER113ALA	-0.17	0.83	nonloop	toALA	neutral	cpx79
1JTG_B_TRP150ALA	4.25	1.36	nonloop	toALA	toSmall	cpx79
1JTG_B_SER71ALA	0.36	-0.12	nonloop	toALA	neutral	cpx79
1JTG_B_TRP162ALA	2.34	1.13	nonloop	toALA	toSmall	cpx79
1JTG_B_TYR53ALA	2.08	1.35	nonloop	toALA	toSmall	cpx79
1JTG_B_PHE36ALA	3.20	0.54	nonloop	toALA	toSmall	cpx79
1JTG_B_HIS41ALA	3.25	1.01	nonloop	toALA	toSmall	cpx79
1KAC_A_SER87TYR	-1.25	-0.06	loop	toNonALA	toLarge	cpx02
1KAC_A_PRO15SER	-0.79	0.58	loop	toNonALA	toSmall	cpx02
1KTZ_A_ARG64ALA	2.88	1.37	nonloop	toALA	toSmall	cpx80
1KTZ_A_ARG64LYS	2.20	1.63	nonloop	toNonALA	toSmall	cpx80
1KTZ_A_ARG13ALA	1.48	1.40	nonloop	toALA	toSmall	cpx80
1KTZ_A_VAL62ILE	0.24	0.76	nonloop	toNonALA	toLarge	cpx80
1KTZ_A_ARG13LYS	1.15	1.14	nonloop	toNonALA	toSmall	cpx80
1KTZ_B_ILE29ALA	1.37	1.48	nonloop	toALA	toSmall	cpx80
1KTZ_B_THR27ALA	1.51	1.03	nonloop	toALA	toSmall	cpx80
1KTZ_B_SER25ALA	0.33	1.00	loop	toALA	neutral	cpx80
1KTZ_B_GLU95GLN	1.63	1.84	nonloop	toNonALA	neutral	cpx80
1KTZ_B_ASP94ALA	0.81	1.38	nonloop	toALA	toSmall	cpx80
1KTZ_B_ASP8ASN	2.00	2.37	nonloop	toNonALA	toLarge	cpx80
1KTZ_B_LEU3ALA	1.82	1.42	nonloop	toALA	toSmall	cpx80
1KTZ_B_VAL53ALA	0.42	1.27	nonloop	toALA	toSmall	cpx80
1KTZ_B_SER28ALA	0.22	2.35	nonloop	toALA	neutral	cpx80
1KTZ_B_SER28LEU	4.04	1.27	nonloop	toNonALA	toLarge	cpx80
1KTZ_B_GLU31ALA	1.22	0.74	loop	toALA	toSmall	cpx80
1KTZ_B_GLU95ALA	1.49	2.21	nonloop	toALA	toSmall	cpx80
1KTZ_B_PHE6ALA	2.98	2.59	loop	toALA	toSmall	cpx80
1KTZ_B_ILE26ALA	1.90	1.10	loop	toALA	toSmall	cpx80
1KTZ_B_ASP8ALA	1.52	1.89	nonloop	toALA	toSmall	cpx80
1LFD_A_LYS39ALA	1.18	1.24	nonloop	toALA	toSmall	cpx65
1LFD_A_ARG7ALA	1.14	1.17	nonloop	toALA	toSmall	cpx65
1LFD_A_LYS19ALA	1.33	1.04	nonloop	toALA	toSmall	cpx65
1LFD_A_ASP38LYS	-1.09	0.43	nonloop	toNonALA	toLarge	cpx65
1LFD_A_ASP43ALA	-0.28	1.25	loop	toALA	toSmall	cpx65
1LFD_A_ASN14LYS	0.40	0.83	loop	toNonALA	toLarge	cpx65
1LFD_A_ASP38ALA	-0.58	0.64	nonloop	toALA	toSmall	cpx65
1LFD_A_MET17LYS	-0.92	1.43	nonloop	toNonALA	neutral	cpx65
1LFD_A_ASN41LYS	-1.17	1.30	nonloop	toNonALA	toLarge	cpx65
1M9E_B_ALA76HIS	-1.01	-0.02	loop	toNonALA	toLarge	cpx29
1MAH_A_PHE287TYR	0.79	1.67	loop	toNonALA	neutral	cpx01
1MAH_A_TYR69ASN	5.22	0.54	loop	toNonALA	toSmall	cpx01
1MAH_A_PHE287ILE	2.06	1.02	loop	toNonALA	toSmall	cpx01
1MAH_A_PHE285LEU	1.25	1.18	loop	toNonALA	toSmall	cpx01
1MAH_A_ASP71ASN	1.88	1.68	loop	toNonALA	toLarge	cpx01
1MAH_A_TYR121GLN	3.00	1.23	nonloop	toNonALA	toSmall	cpx01
1MAH_A_TRP276ARG	8.81	1.82	nonloop	toNonALA	toSmall	cpx01
1P69_A_SER15PRO	0.79	0.73	loop	toNonALA	toLarge	cpx02
1P6A_A_TYR87SER	1.25	1.25	loop	toNonALA	toSmall	cpx02
1PPF_B_ASN36HIS	-0.53	0.79	nonloop	toNonALA	toLarge	cpx42

1PPF_B_ALA15GLY	1.12	0.45	nonloop	toNonALA	toSmall	cpx42
1PPF_B_LEU18VAL	-0.49	3.02	loop	toNonALA	toSmall	cpx42
1PPF_B_GLU19GLN	0.65	1.22	loop	toNonALA	neutral	cpx42
1PPF_B_ASN36ILE	0.86	0.15	nonloop	toNonALA	toLarge	cpx42
1PPF_B_LYS13VAL	0.86	0.84	loop	toNonALA	toSmall	cpx42
1PPF_B_ARG21PRO	6.61	0.43	loop	toNonALA	toSmall	cpx42
1PPF_B_THR17PRO	3.03	2.48	nonloop	toNonALA	neutral	cpx42
1PPF_B_LYS13GLY	1.23	0.69	loop	toNonALA	toSmall	cpx42
1PPF_B_GLU19CYS	1.38	1.76	loop	toNonALA	toSmall	cpx42
1PPF_B_LEU18PHE	5.10	3.29	loop	toNonALA	toLarge	cpx42
1PPF_B_GLY32PRO	0.26	2.27	loop	toNonALA	toLarge	cpx42
1PPF_B_ASN36MET	1.08	-0.08	nonloop	toNonALA	toLarge	cpx42
1PPF_B_ASN36VAL	0.34	0.46	nonloop	toNonALA	toLarge	cpx42
1PPF_B_LEU18HIS	6.38	3.33	loop	toNonALA	neutral	cpx42
1PPF_B_THR17GLN	1.94	2.54	nonloop	toNonALA	toLarge	cpx42
1PPF_B_ALA15MET	-0.40	0.07	nonloop	toNonALA	toLarge	cpx42
1PPF_B_LYS13ARG	-0.63	0.55	loop	toNonALA	toLarge	cpx42
1PPF_B_GLU19TYR	1.23	1.53	loop	toNonALA	toLarge	cpx42
1PPF_B_THR17MET	2.47	2.29	nonloop	toNonALA	toLarge	cpx42
1PPF_B_ARG21CYS	-0.08	0.64	loop	toNonALA	toSmall	cpx42
1PPF_B_TYR20ASN	3.59	3.73	loop	toNonALA	toSmall	cpx42
1PPF_B_ALA15THR	0.95	0.63	nonloop	toNonALA	toLarge	cpx42
1PPF_B_ASN36SER	-1.33	0.47	nonloop	toNonALA	toSmall	cpx42
1PPF_B_ALA15SER	0.75	0.57	nonloop	toNonALA	neutral	cpx42
1PPF_B_TYR20CYS	3.40	4.16	loop	toNonALA	toSmall	cpx42
1PPF_B_GLU19GLY	2.09	1.54	loop	toNonALA	toSmall	cpx42
1PPF_B_ASN36TRP	1.70	0.36	nonloop	toNonALA	toLarge	cpx42
1PPF_B_LEU18ARG	7.08	2.31	loop	toNonALA	toLarge	cpx42
1PPF_B_GLY32ARG	4.78	2.02	loop	toNonALA	toLarge	cpx42
1PPF_B_LEU18ILE	-0.72	3.56	loop	toNonALA	neutral	cpx42
1PPF_B_GLY32ILE	4.31	1.99	loop	toNonALA	toLarge	cpx42
1PPF_B_PRO14ALA	-0.12	-0.89	loop	toALA	toSmall	cpx42
1PPF_B_ASN36GLU	-1.00	-0.38	nonloop	toNonALA	toLarge	cpx42
1PPF_B_LYS13ASP	0.62	0.52	loop	toNonALA	toSmall	cpx42
1PPF_B_GLU19ASN	1.20	1.09	loop	toNonALA	toSmall	cpx42
1PPF_B_PRO14PHE	-1.83	-0.90	loop	toNonALA	toLarge	cpx42
1PPF_B_LYS13ASN	0.65	0.66	loop	toNonALA	toSmall	cpx42
1PPF_B_TYR20PRO	5.29	4.20	loop	toNonALA	toSmall	cpx42
1PPF_B_THR17GLY	3.55	3.24	nonloop	toNonALA	toSmall	cpx42
1PPF_B_ARG21HIS	-0.49	-0.04	loop	toNonALA	toSmall	cpx42
1PPF_B_GLU19ASP	0.57	1.43	loop	toNonALA	toSmall	cpx42
1PPF_B_ALA15PHE	-0.07	-0.39	nonloop	toNonALA	toLarge	cpx42
1PPF_B_ALA15ASN	0.90	0.39	nonloop	toNonALA	toLarge	cpx42
1PPF_B_GLU19ALA	1.19	1.74	loop	toALA	toSmall	cpx42
1PPF_B_ASN36CYS	0.60	-0.12	nonloop	toNonALA	toSmall	cpx42
1PPF_B_GLU19PHE	1.35	1.50	loop	toNonALA	toLarge	cpx42
1PPF_B_GLU19LYS	2.09	1.17	loop	toNonALA	toLarge	cpx42
1PPF_B_TYR20VAL	4.13	3.82	loop	toNonALA	toSmall	cpx42
1PPF_B_TYR20SER	3.59	3.21	loop	toNonALA	toSmall	cpx42
1PPF_B_LYS13HIS	1.00	0.56	loop	toNonALA	toSmall	cpx42
1PPF_B_ARG21GLN	-0.02	0.06	loop	toNonALA	toSmall	cpx42
1PPF_B_THR17ASP	4.86	2.39	nonloop	toNonALA	neutral	cpx42
1PPF_B_ASN36PHE	1.82	0.11	nonloop	toNonALA	toLarge	cpx42
1PPF_B_TYR20ILE	3.88	4.06	loop	toNonALA	toSmall	cpx42
1PPF_B_ALA15ARG	-0.26	0.54	nonloop	toNonALA	toLarge	cpx42
1PPF_B_ARG21VAL	-0.35	0.51	loop	toNonALA	toSmall	cpx42
1PPF_B_ARG21ALA	0.21	0.59	loop	toALA	toSmall	cpx42
1PPF_B_GLY32TYR	1.19	1.88	loop	toNonALA	toLarge	cpx42
1PPF_B_ASN36PRO	-2.92	0.60	nonloop	toNonALA	neutral	cpx42
1PPF_B_TYR20GLY	4.13	4.27	loop	toNonALA	toSmall	cpx42
1PPF_B_LEU18PRO	6.06	3.41	loop	toNonALA	toSmall	cpx42
1PPF_B_GLY32MET	2.16	2.13	loop	toNonALA	toLarge	cpx42
1PPF_B_GLY32LEU	3.09	2.38	loop	toNonALA	toLarge	cpx42
1PPF_B_LYS13CYS	0.95	0.82	loop	toNonALA	toSmall	cpx42
1PPF_B_PRO14VAL	-1.50	-1.01	loop	toNonALA	toLarge	cpx42
1PPF_B_ASN36TYR	1.65	0.28	nonloop	toNonALA	toLarge	cpx42
1PPF_B_GLY32ASN	1.59	2.26	loop	toNonALA	toLarge	cpx42
1PPF_B_ALA15PRO	1.97	0.13	nonloop	toNonALA	toLarge	cpx42
1PPF_B_TYR20LYS	4.43	3.76	loop	toNonALA	toSmall	cpx42

1PPF_B_GLY32GLU	1.44	2.52	loop	toNonALA	toLarge	cpx42
1PPF_B_TYR20THR	4.99	3.99	loop	toNonALA	toSmall	cpx42
1PPF_B_THR17TRP	2.16	2.31	nonloop	toNonALA	toLarge	cpx42
1PPF_B_LYS13MET	0.21	0.87	loop	toNonALA	neutral	cpx42
1PPF_B_LYS13TRP	0.82	0.63	loop	toNonALA	toLarge	cpx42
1PPF_B_LYS13ALA	0.75	0.70	loop	toALA	toSmall	cpx42
1PPF_B_ARG21THR	-0.02	0.02	loop	toNonALA	toSmall	cpx42
1PPF_B_LYS13GLU	1.12	0.50	loop	toNonALA	toSmall	cpx42
1PPF_B_LYS13SER	0.45	0.78	loop	toNonALA	toSmall	cpx42
1PPF_B_ARG21PHE	-0.97	-0.18	loop	toNonALA	neutral	cpx42
1PPF_B_THR17CYS	2.06	3.07	nonloop	toNonALA	toSmall	cpx42
1PPF_B_PRO14LEU	-2.88	-1.14	loop	toNonALA	toLarge	cpx42
1PPF_B_LYS13PHE	0.95	0.78	loop	toNonALA	toLarge	cpx42
1PPF_B_GLY32ASP	2.46	1.92	loop	toNonALA	toLarge	cpx42
1PPF_B_ARG21GLU	0.45	-0.10	loop	toNonALA	toSmall	cpx42
1PPF_B_ASN36LYS	2.59	-0.09	nonloop	toNonALA	toLarge	cpx42
1PPF_B_ARG21LEU	-0.85	0.41	loop	toNonALA	toSmall	cpx42
1PPF_B_GLU19SER	1.82	1.23	loop	toNonALA	toSmall	cpx42
1PPF_B_LEU18TYR	6.54	3.12	loop	toNonALA	toLarge	cpx42
1PPF_B_ARG21ASP	0.21	0.11	loop	toNonALA	toSmall	cpx42
1PPF_B_PRO14ASP	-0.49	-1.09	loop	toNonALA	neutral	cpx42
1PPF_B_THR17TYR	2.45	2.19	nonloop	toNonALA	toLarge	cpx42
1PPF_B_PRO14THR	-0.26	-1.05	loop	toNonALA	neutral	cpx42
1PPF_B_GLU19TRP	1.51	1.74	loop	toNonALA	toLarge	cpx42
1PPF_B_ARG21GLY	0.57	2.07	loop	toNonALA	toSmall	cpx42
1PPF_B_ALA15TYR	-0.18	-0.21	nonloop	toNonALA	toLarge	cpx42
1PPF_B_ALA15LYS	1.11	0.09	nonloop	toNonALA	toLarge	cpx42
1PPF_B_GLY32HIS	1.48	2.05	loop	toNonALA	toLarge	cpx42
1PPF_B_GLY32TRP	1.62	2.20	loop	toNonALA	toLarge	cpx42
1PPF_B_LYS13TYR	0.50	0.36	loop	toNonALA	toLarge	cpx42
1PPF_B_TYR20ARG	4.31	2.98	loop	toNonALA	neutral	cpx42
1PPF_B_TYR20TRP	0.23	1.35	loop	toNonALA	toLarge	cpx42
1PPF_B_LYS13PRO	1.25	0.74	loop	toNonALA	toSmall	cpx42
1PPF_B_PRO14GLY	0.09	-0.95	loop	toNonALA	toSmall	cpx42
1PPF_B_TYR20MET	2.77	3.21	loop	toNonALA	toSmall	cpx42
1PPF_B_ARG21LYS	0.60	0.16	loop	toNonALA	toSmall	cpx42
1PPF_B_TYR20PHE	0.48	2.21	loop	toNonALA	neutral	cpx42
1PPF_B_TYR20ALA	3.17	4.35	loop	toALA	toSmall	cpx42
1PPF_B_LEU18CYS	-0.09	4.21	loop	toNonALA	toSmall	cpx42
1PPF_B_LEU18ASN	5.15	3.21	loop	toNonALA	toSmall	cpx42
1PPF_B_LYS13LEU	0.40	0.77	loop	toNonALA	neutral	cpx42
1PPF_B_THR17ASN	2.66	2.94	nonloop	toNonALA	neutral	cpx42
1PPF_B_GLU19VAL	1.14	1.33	loop	toNonALA	neutral	cpx42
1PPF_B_ALA15GLU	0.10	1.66	nonloop	toNonALA	toLarge	cpx42
1PPF_B_TYR20GLN	4.63	3.50	loop	toNonALA	toSmall	cpx42
1PPF_B_ASN36GLY	-0.56	0.18	nonloop	toNonALA	toSmall	cpx42
1PPF_B_PRO14MET	-1.55	-1.19	loop	toNonALA	toLarge	cpx42
1PPF_B_THR17ILE	1.47	2.58	nonloop	toNonALA	toLarge	cpx42
1PPF_B_THR17LEU	2.25	2.38	nonloop	toNonALA	toLarge	cpx42
1PPF_B_PRO14HIS	-1.74	-0.77	loop	toNonALA	toLarge	cpx42
1PPF_B_GLU19ARG	1.45	1.39	loop	toNonALA	toLarge	cpx42
1PPF_B_ARG21TYR	0.22	-0.21	loop	toNonALA	neutral	cpx42
1PPF_B_PRO14ILE	-1.63	-0.84	loop	toNonALA	toLarge	cpx42
1PPF_B_ARG21MET	-0.75	0.05	loop	toNonALA	toSmall	cpx42
1PPF_B_ALA15TRP	-0.63	0.29	nonloop	toNonALA	toLarge	cpx42
1PPF_B_PRO14LYS	-0.44	-0.81	loop	toNonALA	toLarge	cpx42
1PPF_B_LEU18SER	3.05	3.47	loop	toNonALA	toSmall	cpx42
1PPF_B_GLY32SER	0.90	1.83	loop	toNonALA	toLarge	cpx42
1PPF_B_LYS13THR	0.16	0.59	loop	toNonALA	toSmall	cpx42
1PPF_B_LEU18ASP	7.51	3.47	loop	toNonALA	toSmall	cpx42
1PPF_B_GLY32GLN	2.76	2.19	loop	toNonALA	toLarge	cpx42
1PPF_B_ALA15CYS	-0.66	0.85	nonloop	toNonALA	toLarge	cpx42
1PPF_B_GLU19HIS	0.68	1.29	loop	toNonALA	toLarge	cpx42
1PPF_B_PRO14ASN	-0.63	-0.79	loop	toNonALA	neutral	cpx42
1PPF_B_ALA15ILE	0.33	0.80	nonloop	toNonALA	toLarge	cpx42
1PPF_B_TYR20GLU	6.33	4.83	loop	toNonALA	toSmall	cpx42
1PPF_B_PRO14TYR	-0.95	-0.63	loop	toNonALA	toLarge	cpx42
1PPF_B_ASN36GLN	0.38	0.35	nonloop	toNonALA	toLarge	cpx42
1PPF_B_ALA15GLN	0.25	0.31	nonloop	toNonALA	toLarge	cpx42

1PPF_B_ALA15LEU	0.02	0.43	nonloop	toNonALA	toLarge	cpx42
1PPF_B_PRO14GLN	-0.80	-0.97	loop	toNonALA	toLarge	cpx42
1PPF_B_THR17HIS	1.67	2.37	nonloop	toNonALA	toLarge	cpx42
1PPF_B_PRO14GLU	-1.41	-1.35	loop	toNonALA	toLarge	cpx42
1PPF_B_THR17LYS	3.34	2.19	nonloop	toNonALA	toLarge	cpx42
1PPF_B_ALA15HIS	0.55	0.41	nonloop	toNonALA	toLarge	cpx42
1PPF_B_ARG21ILE	-0.80	0.29	loop	toNonALA	toSmall	cpx42
1PPF_B_THR17PHE	1.69	2.42	nonloop	toNonALA	toLarge	cpx42
1PPF_B_PRO14CYS	-1.98	-0.36	loop	toNonALA	toSmall	cpx42
1PPF_B_TYR20ASP	6.33	4.05	loop	toNonALA	toSmall	cpx42
1PPF_B_LEU18GLY	3.29	3.54	loop	toNonALA	toSmall	cpx42
1PPF_B_ASN36LEU	2.61	0.07	nonloop	toNonALA	toLarge	cpx42
1PPF_B_GLU19LEU	1.06	1.30	loop	toNonALA	toLarge	cpx42
1PPF_B_LYS13GLN	0.25	0.47	loop	toNonALA	toSmall	cpx42
1PPF_B_ARG21SER	0.41	-0.05	loop	toNonALA	toSmall	cpx42
1PPF_B_ARG21TRP	-0.53	0.05	loop	toNonALA	toLarge	cpx42
1PPF_B_ASN36ARG	1.84	0.83	nonloop	toNonALA	toLarge	cpx42
1PPF_B_GLU19ILE	0.71	1.32	loop	toNonALA	toLarge	cpx42
1PPF_B_LEU18TRP	7.44	2.22	loop	toNonALA	toLarge	cpx42
1PPF_B_PRO14TRP	-1.98	-1.11	loop	toNonALA	toLarge	cpx42
1PPF_B_ARG21ASN	0.33	0.75	loop	toNonALA	toSmall	cpx42
1PPF_B_LEU18THR	0.90	3.90	loop	toNonALA	toSmall	cpx42
1PPF_B_THR17ARG	3.40	2.40	nonloop	toNonALA	toLarge	cpx42
1PPF_B_GLU19MET	1.13	1.28	loop	toNonALA	toLarge	cpx42
1PPF_B_GLY32PHE	1.46	1.92	loop	toNonALA	toLarge	cpx42
1PPF_B_PRO14SER	-0.56	-0.98	loop	toNonALA	toSmall	cpx42
1PPF_B_GLU19PRO	3.17	1.47	loop	toNonALA	toSmall	cpx42
1PPF_B_ASN36THR	0.55	-0.15	nonloop	toNonALA	neutral	cpx42
1PPF_B_ASN36ASP	-3.04	-0.04	nonloop	toNonALA	toSmall	cpx42
1PPF_B_GLY32LYS	3.26	2.40	loop	toNonALA	toLarge	cpx42
1PPF_B_GLY32CYS	1.16	2.33	loop	toNonALA	toLarge	cpx42
1PPF_B_PRO14ARG	-0.14	-0.95	loop	toNonALA	toLarge	cpx42
1PPF_B_GLU19THR	1.48	1.07	loop	toNonALA	toSmall	cpx42
1PPF_B_LYS13ILE	0.62	0.56	loop	toNonALA	neutral	cpx42
1PPF_B_ASN36ALA	-1.62	0.39	nonloop	toALA	toSmall	cpx42
1PPF_B_TYR20LEU	1.36	4.01	loop	toNonALA	toSmall	cpx42
1PPF_B_ALA15ASP	1.12	0.50	nonloop	toNonALA	toLarge	cpx42
1PPF_B_GLY32THR	2.77	2.06	loop	toNonALA	toLarge	cpx42
1R0R_B_ASN31VAL	0.66	0.32	nonloop	toNonALA	toLarge	cpx75
1R0R_B_ASN31ALA	-0.03	0.42	nonloop	toALA	toSmall	cpx75
1R0R_B_GLU14ALA	2.06	1.40	loop	toALA	toSmall	cpx75
1R0R_B_GLU14CYS	2.34	2.44	loop	toNonALA	toSmall	cpx75
1R0R_B_LYS8ASP	-0.59	-0.39	loop	toNonALA	toSmall	cpx75
1R0R_B_PRO9LEU	1.17	0.02	loop	toNonALA	toLarge	cpx75
1R0R_B_GLY27ASP	2.85	1.29	loop	toNonALA	toLarge	cpx75
1R0R_B_TYR15MET	3.10	3.48	loop	toNonALA	toSmall	cpx75
1R0R_B_THR12LEU	0.66	2.20	nonloop	toNonALA	toLarge	cpx75
1R0R_B_LEU13HIS	0.56	1.88	loop	toNonALA	neutral	cpx75
1R0R_B_LEU13ASN	1.48	1.91	loop	toNonALA	toSmall	cpx75
1R0R_B_ARG16CYS	0.11	1.11	loop	toNonALA	toSmall	cpx75
1R0R_B_LYS8PRO	1.33	-0.01	loop	toNonALA	toSmall	cpx75
1R0R_B_ARG16HIS	0.52	0.41	loop	toNonALA	toSmall	cpx75
1R0R_B_ARG16TYR	0.81	0.56	loop	toNonALA	neutral	cpx75
1R0R_B_ARG16THR	0.34	0.36	loop	toNonALA	toSmall	cpx75
1R0R_B_ALA10CYS	-0.48	1.63	nonloop	toNonALA	toLarge	cpx75
1R0R_B_GLU14SER	3.13	1.71	loop	toNonALA	toSmall	cpx75
1R0R_B_GLU14ASN	2.09	1.82	loop	toNonALA	toSmall	cpx75
1R0R_B_GLY27CYS	1.40	1.69	loop	toNonALA	toLarge	cpx75
1R0R_B_LYS8TYR	-0.69	-0.35	loop	toNonALA	toLarge	cpx75
1R0R_B_PRO9VAL	1.31	0.13	loop	toNonALA	toLarge	cpx75
1R0R_B_PRO9GLU	-2.21	0.54	loop	toNonALA	toLarge	cpx75
1R0R_B_GLU14LYS	2.67	1.94	loop	toNonALA	toLarge	cpx75
1R0R_B_ALA10GLN	1.79	1.58	nonloop	toNonALA	toLarge	cpx75
1R0R_B_LYS8ARG	0.13	-0.42	loop	toNonALA	toLarge	cpx75
1R0R_B_LYS8THR	0.88	-0.29	loop	toNonALA	toSmall	cpx75
1R0R_B_ARG16ILE	0.20	0.32	loop	toNonALA	toSmall	cpx75
1R0R_B_PRO9HIS	-0.21	-0.20	loop	toNonALA	toLarge	cpx75
1R0R_B_ALA10GLY	1.10	1.44	nonloop	toNonALA	toSmall	cpx75
1R0R_B_THR12PHE	-0.07	1.93	nonloop	toNonALA	toLarge	cpx75

1R0R_B_LEU13PHE	0.61	1.64	loop	toNonALA	toLarge	cpx75
1R0R_B_GLY27TRP	1.38	2.50	loop	toNonALA	toLarge	cpx75
1R0R_B_ASN31THR	0.56	0.19	nonloop	toNonALA	neutral	cpx75
1R0R_B_GLU14TRP	1.82	2.12	loop	toNonALA	toLarge	cpx75
1R0R_B_TYR15ALA	5.40	4.76	loop	toALA	toSmall	cpx75
1R0R_B_THR12GLY	3.10	2.17	nonloop	toNonALA	toSmall	cpx75
1R0R_B_ARG16GLN	0.18	0.37	loop	toNonALA	toSmall	cpx75
1R0R_B_THR12ASP	2.85	1.75	nonloop	toNonALA	neutral	cpx75
1R0R_B_ARG16ALA	-0.10	0.30	loop	toALA	toSmall	cpx75
1R0R_B_GLU14MET	1.55	1.94	loop	toNonALA	toLarge	cpx75
1R0R_B_LEU13PRO	7.58	1.29	loop	toNonALA	toSmall	cpx75
1R0R_B_PRO9SER	0.13	0.04	loop	toNonALA	toSmall	cpx75
1R0R_B_LEU13SER	1.55	2.01	loop	toNonALA	toSmall	cpx75
1R0R_B_GLY27SER	0.90	1.72	loop	toNonALA	toLarge	cpx75
1R0R_B_LYS8TRP	-1.09	-0.09	loop	toNonALA	toLarge	cpx75
1R0R_B_GLY27TYR	0.48	2.09	loop	toNonALA	toLarge	cpx75
1R0R_B_TYR15LEU	2.54	4.02	loop	toNonALA	toSmall	cpx75
1R0R_B_ARG16ASP	-0.18	0.28	loop	toNonALA	toSmall	cpx75
1R0R_B_THR12CYS	0.80	1.93	nonloop	toNonALA	toSmall	cpx75
1R0R_B_PRO9GLN	-1.40	0.12	loop	toNonALA	toLarge	cpx75
1R0R_B_GLU14VAL	0.09	2.26	loop	toNonALA	neutral	cpx75
1R0R_B_ASN31ARG	1.44	0.69	nonloop	toNonALA	toLarge	cpx75
1R0R_B_ALA10GLU	4.51	2.50	nonloop	toNonALA	toLarge	cpx75
1R0R_B_GLY27ARG	3.42	2.09	loop	toNonALA	toLarge	cpx75
1R0R_B_LYS8VAL	0.41	-0.33	loop	toNonALA	toSmall	cpx75
1R0R_B_ALA10PHE	-2.21	-0.47	nonloop	toNonALA	toLarge	cpx75
1R0R_B_GLU14ASP	0.26	2.17	loop	toNonALA	toSmall	cpx75
1R0R_B_ALA10MET	-1.72	0.23	nonloop	toNonALA	toLarge	cpx75
1R0R_B_LEU13CYS	-1.33	2.65	loop	toNonALA	toSmall	cpx75
1R0R_B_TYR15LYS	5.44	3.86	loop	toNonALA	toSmall	cpx75
1R0R_B_THR12MET	1.31	1.73	nonloop	toNonALA	toLarge	cpx75
1R0R_B_ASN31PRO	1.46	0.37	nonloop	toNonALA	neutral	cpx75
1R0R_B_THR12PRO	4.88	1.27	nonloop	toNonALA	neutral	cpx75
1R0R_B_ALA10SER	1.72	0.68	nonloop	toNonALA	neutral	cpx75
1R0R_B_ALA10ASN	2.07	1.01	nonloop	toNonALA	toLarge	cpx75
1R0R_B_GLY27HIS	2.16	2.05	loop	toNonALA	toLarge	cpx75
1R0R_B_LYS8ILE	1.11	-0.30	loop	toNonALA	neutral	cpx75
1R0R_B_ARG16ASN	-0.05	0.22	loop	toNonALA	toSmall	cpx75
1R0R_B_ARG16MET	0.44	0.22	loop	toNonALA	toSmall	cpx75
1R0R_B_PRO9ASN	-0.91	0.46	loop	toNonALA	neutral	cpx75
1R0R_B_LYS8ALA	-0.60	0.02	loop	toALA	toSmall	cpx75
1R0R_B_LEU13VAL	2.13	2.41	loop	toNonALA	toSmall	cpx75
1R0R_B_ASN31GLY	0.28	0.55	nonloop	toNonALA	toSmall	cpx75
1R0R_B_ALA10THR	1.25	0.81	nonloop	toNonALA	toLarge	cpx75
1R0R_B_ASN31PHE	-0.18	0.35	nonloop	toNonALA	toLarge	cpx75
1R0R_B_LYS8GLY	-0.83	0.01	loop	toNonALA	toSmall	cpx75
1R0R_B_ALA10ARG	5.45	1.91	nonloop	toNonALA	toLarge	cpx75
1R0R_B_PRO9TYR	0.85	-0.06	loop	toNonALA	toLarge	cpx75
1R0R_B_THR12ARG	3.30	2.08	nonloop	toNonALA	toLarge	cpx75
1R0R_B_TYR15PRO	6.56	4.96	loop	toNonALA	toSmall	cpx75
1R0R_B_ARG16LEU	0.23	0.39	loop	toNonALA	toSmall	cpx75
1R0R_B_ASN31HIS	0.28	0.15	nonloop	toNonALA	toLarge	cpx75
1R0R_B_ALA10HIS	1.75	0.82	nonloop	toNonALA	toLarge	cpx75
1R0R_B_LEU13TYR	0.44	1.31	loop	toNonALA	toLarge	cpx75
1R0R_B_LEU13THR	0.16	2.12	loop	toNonALA	toSmall	cpx75
1R0R_B_GLU14PHE	3.57	1.83	loop	toNonALA	toLarge	cpx75
1R0R_B_ALA10LEU	-1.73	1.05	nonloop	toNonALA	toLarge	cpx75
1R0R_B_GLY27ILE	1.95	1.65	loop	toNonALA	toLarge	cpx75
1R0R_B_PRO9ARG	1.09	0.18	loop	toNonALA	toLarge	cpx75
1R0R_B_ALA10LYS	3.03	1.66	nonloop	toNonALA	toLarge	cpx75
1R0R_B_LYS8LEU	-0.32	-0.19	loop	toNonALA	neutral	cpx75
1R0R_B_ALA10TYR	-0.83	-0.84	nonloop	toNonALA	toLarge	cpx75
1R0R_B_LEU13TRP	1.50	1.54	loop	toNonALA	toLarge	cpx75
1R0R_B_GLU14THR	4.19	1.58	loop	toNonALA	toSmall	cpx75
1R0R_B_ASN31LEU	1.53	0.37	nonloop	toNonALA	toLarge	cpx75
1R0R_B_GLY27LEU	2.38	1.90	loop	toNonALA	toLarge	cpx75
1R0R_B_ASN31SER	0.48	0.18	nonloop	toNonALA	toSmall	cpx75
1R0R_B_GLU14ILE	0.73	1.70	loop	toNonALA	toLarge	cpx75
1R0R_B_GLY27GLU	1.95	2.07	loop	toNonALA	toLarge	cpx75

1R0R_B_ARG16SER	-0.02	0.40	loop	toNonALA	toSmall	cpx75
1R0R_B_ARG16TRP	0.93	0.53	loop	toNonALA	toLarge	cpx75
1R0R_B_ARG16PHE	0.44	0.30	loop	toNonALA	neutral	cpx75
1R0R_B_TYR15PHE	0.61	2.53	loop	toNonALA	neutral	cpx75
1R0R_B_TYR15THR	5.40	4.38	loop	toNonALA	toSmall	cpx75
1R0R_B_THR12ILE	0.26	1.36	nonloop	toNonALA	toLarge	cpx75
1R0R_B_GLU14HIS	1.69	1.80	loop	toNonALA	toLarge	cpx75
1R0R_B_ASN31MET	0.31	0.30	nonloop	toNonALA	toLarge	cpx75
1R0R_B_LYS8CYS	-0.61	-0.40	loop	toNonALA	toSmall	cpx75
1R0R_B_GLY27PHE	0.11	1.82	loop	toNonALA	toLarge	cpx75
1R0R_B_PRO9THR	1.18	0.08	loop	toNonALA	neutral	cpx75
1R0R_B_PRO9ALA	-0.63	-0.09	loop	toALA	toSmall	cpx75
1R0R_B_THR12ASN	0.02	1.62	nonloop	toNonALA	neutral	cpx75
1R0R_B_THR12LYS	1.91	2.13	nonloop	toNonALA	toLarge	cpx75
1R0R_B_TYR15GLU	4.55	4.03	loop	toNonALA	toSmall	cpx75
1R0R_B_LEU13ILE	3.21	1.88	loop	toNonALA	neutral	cpx75
1R0R_B_ALA10ILE	-1.77	-0.26	nonloop	toNonALA	toLarge	cpx75
1R0R_B_TYR15ASN	5.54	4.17	loop	toNonALA	toSmall	cpx75
1R0R_B_TYR15TRP	-0.36	1.54	loop	toNonALA	toLarge	cpx75
1R0R_B_ASN31ASP	0.56	0.44	nonloop	toNonALA	toSmall	cpx75
1R0R_B_GLY27GLN	2.00	2.05	loop	toNonALA	toLarge	cpx75
1R0R_B_TYR15ARG	4.41	4.26	loop	toNonALA	neutral	cpx75
1R0R_B_GLU14GLN	1.26	1.73	loop	toNonALA	neutral	cpx75
1R0R_B_GLY27PRO	1.07	1.69	loop	toNonALA	toLarge	cpx75
1R0R_B_ASN31TRP	0.06	0.65	nonloop	toNonALA	toLarge	cpx75
1R0R_B_ASN31GLN	-0.27	0.49	nonloop	toNonALA	toLarge	cpx75
1R0R_B_THR12HIS	0.52	1.68	nonloop	toNonALA	toLarge	cpx75
1R0R_B_LYS8GLU	-0.11	0.11	loop	toNonALA	toSmall	cpx75
1R0R_B_GLU14PRO	3.71	2.27	loop	toNonALA	toSmall	cpx75
1R0R_B_PRO9ASP	-2.49	0.22	loop	toNonALA	neutral	cpx75
1R0R_B_LYS8GLN	-0.52	-0.42	loop	toNonALA	toSmall	cpx75
1R0R_B_GLU14TYR	1.86	1.93	loop	toNonALA	toLarge	cpx75
1R0R_B_GLU14GLY	2.67	2.03	loop	toNonALA	toSmall	cpx75
1R0R_B_TYR15CYS	3.21	4.61	loop	toNonALA	toSmall	cpx75
1R0R_B_LYS8MET	-0.55	-0.34	loop	toNonALA	neutral	cpx75
1R0R_B_LYS8SER	-0.30	-0.11	loop	toNonALA	toSmall	cpx75
1R0R_B_ASN31LYS	1.13	0.86	nonloop	toNonALA	toLarge	cpx75
1R0R_B_ASN31ILE	0.31	0.30	nonloop	toNonALA	toLarge	cpx75
1R0R_B_ASN31GLU	-0.20	0.37	nonloop	toNonALA	toLarge	cpx75
1R0R_B_LEU13GLY	2.32	2.87	loop	toNonALA	toSmall	cpx75
1R0R_B_ALA10TRP	0.20	0.62	nonloop	toNonALA	toLarge	cpx75
1R0R_B_PRO9CYS	-0.97	0.15	loop	toNonALA	toSmall	cpx75
1R0R_B_LYS8ASN	-0.39	-0.30	loop	toNonALA	toSmall	cpx75
1R0R_B_LEU13ARG	2.89	0.81	loop	toNonALA	toLarge	cpx75
1R0R_B_LYS8HIS	-0.59	0.17	loop	toNonALA	toSmall	cpx75
1R0R_B_THR12GLN	2.19	2.24	nonloop	toNonALA	toLarge	cpx75
1R0R_B_PRO9MET	-0.03	0.31	loop	toNonALA	toLarge	cpx75
1R0R_B_TYR15VAL	3.46	4.10	loop	toNonALA	toSmall	cpx75
1R0R_B_GLU14ARG	2.07	1.99	loop	toNonALA	toLarge	cpx75
1R0R_B_LEU13ASP	4.48	2.44	loop	toNonALA	toSmall	cpx75
1R0R_B_PRO9LYS	0.34	-0.25	loop	toNonALA	toLarge	cpx75
1R0R_B_ARG16GLY	2.06	0.36	loop	toNonALA	toSmall	cpx75
1R0R_B_TYR15SER	5.09	3.18	loop	toNonALA	toSmall	cpx75
1R0R_B_PRO9ILE	1.72	0.01	loop	toNonALA	toLarge	cpx75
1R0R_B_TYR15GLY	6.31	5.24	loop	toNonALA	toSmall	cpx75
1R0R_B_GLY27THR	1.66	2.06	loop	toNonALA	toLarge	cpx75
1R0R_B_PRO9PHE	1.36	0.09	loop	toNonALA	toLarge	cpx75
1R0R_B_ALA10PRO	3.30	0.23	nonloop	toNonALA	toLarge	cpx75
1R0R_B_GLY27ASN	1.26	1.74	loop	toNonALA	toLarge	cpx75
1R0R_B_LYS8PHE	-0.78	-0.13	loop	toNonALA	toLarge	cpx75
1R0R_B_ASN31TYR	0.18	0.47	nonloop	toNonALA	toLarge	cpx75
1R0R_B_ARG16GLU	0.34	0.45	loop	toNonALA	toSmall	cpx75
1R0R_B_THR12TRP	2.89	1.00	nonloop	toNonALA	toLarge	cpx75
1R0R_B_PRO9GLY	-0.34	-0.43	loop	toNonALA	toSmall	cpx75
1R0R_B_GLY27LYS	2.89	1.98	loop	toNonALA	toLarge	cpx75
1R0R_B_ARG16LYS	-0.10	0.31	loop	toNonALA	toSmall	cpx75
1R0R_B_ALA10ASP	5.16	1.98	nonloop	toNonALA	toLarge	cpx75
1R0R_B_TYR15GLN	4.44	4.23	loop	toNonALA	toSmall	cpx75
1R0R_B_PRO9TRP	0.48	-0.10	loop	toNonALA	toLarge	cpx75

1R0R_B_GLY27MET	2.13	2.13	loop	toNonALA	toLarge	cpx75
1R0R_B_ASN31CYS	0.56	0.58	nonloop	toNonALA	toSmall	cpx75
1R0R_B_ARG16VAL	0.11	0.74	loop	toNonALA	toSmall	cpx75
1R0R_B_GLU14LEU	0.56	2.06	loop	toNonALA	toLarge	cpx75
1R0R_B_ARG16PRO	7.29	1.14	loop	toNonALA	toSmall	cpx75
1R0R_B_TYR15ILE	2.82	3.70	loop	toNonALA	toSmall	cpx75
1R0R_B_THR12TYR	-0.87	1.76	nonloop	toNonALA	toLarge	cpx75
1S0W_B_ALA142PHE	-2.10	0.65	loop	toNonALA	toLarge	cpx79
1S1Q_A_PHE86ALA	0.76	1.68	nonloop	toALA	toSmall	cpx82
1S1Q_A_ASN43ALA	1.21	1.63	nonloop	toALA	toSmall	cpx82
1S1Q_A_TRP73ALA	0.28	2.25	nonloop	toALA	toSmall	cpx82
1S1Q_A_PHE42ALA	0.20	1.31	loop	toALA	toSmall	cpx82
1S1Q_A_ASP44ALA	0.95	1.97	nonloop	toALA	toSmall	cpx82
1S1Q_A_VAL41ALA	0.66	1.37	nonloop	toALA	toSmall	cpx82
1SBB_B_VAL26TYR	-1.45	-0.03	nonloop	toNonALA	toLarge	cpx06
1SBB_B_LEU20THR	-0.09	0.45	loop	toNonALA	toSmall	cpx06
1SBB_B_TYR91VAL	0.08	1.31	nonloop	toNonALA	toSmall	cpx06
1SBN_B_ARG38LYS	-0.31	2.85	loop	toNonALA	toSmall	cpx72
1SGD_B_ASP13LEU	-5.59	-3.76	loop	toNonALA	toLarge	cpx70
1SGE_B_GLU13LEU	-5.90	-3.09	loop	toNonALA	toLarge	cpx70
1SGN_B_ASN13LEU	-3.35	-3.20	loop	toNonALA	toLarge	cpx70
1SGP_B_ALA13LEU	-2.95	-3.61	loop	toNonALA	toLarge	cpx70
1SGQ_B_GLY13LEU	-4.93	-5.23	loop	toNonALA	toLarge	cpx70
1SGY_B_TYR13LEU	-1.65	-0.15	loop	toNonALA	toSmall	cpx70
1SIB_B_LYS46ARG	-0.73	-3.11	nonloop	toNonALA	toLarge	cpx72
1TM1_B_MET40ALA	1.03	1.73	loop	toALA	toSmall	cpx71
1TM1_B_MET40PHE	1.03	0.66	loop	toNonALA	toLarge	cpx71
1TM1_B_THR39ASP	2.10	1.43	nonloop	toNonALA	neutral	cpx71
1TM1_B_ARG48CYS	3.23	1.99	nonloop	toNonALA	toSmall	cpx71
1TM1_B_MET40LYS	1.09	0.90	loop	toNonALA	neutral	cpx71
1TM1_B_TYR42GLY	4.68	2.43	loop	toNonALA	toSmall	cpx71
1TM1_B_GLU41SER	2.75	0.91	loop	toNonALA	toSmall	cpx71
1TM1_B_MET40TYR	0.06	0.96	loop	toNonALA	toLarge	cpx71
1TM1_B_THR39PRO	3.75	0.53	nonloop	toNonALA	neutral	cpx71
1TM1_B_ARG43ALA	1.26	2.19	loop	toALA	toSmall	cpx71
1TM1_B_MET40GLY	2.23	1.23	loop	toNonALA	toSmall	cpx71
1TM3_B_LYS40MET	-1.09	0.20	loop	toNonALA	neutral	cpx71
1TM4_B_GLY40MET	-2.23	-0.45	loop	toNonALA	toLarge	cpx71
1TM5_B_ALA40MET	-1.03	0.09	loop	toNonALA	toLarge	cpx71
1TM7_B_TYR40MET	-0.06	-0.97	loop	toNonALA	toSmall	cpx71
1TMG_B_PHE40MET	-1.03	0.41	loop	toNonALA	toSmall	cpx71
1TO1_B_ALA42TYR	-2.98	-1.80	loop	toNonALA	toLarge	cpx71
1UUZ_A_HIS62ASP	3.38	1.71	nonloop	toNonALA	toSmall	cpx50
1UUZ_A_HIS62ASN	1.52	2.05	nonloop	toNonALA	toSmall	cpx50
1UUZ_A_HIS62ALA	1.77	1.90	nonloop	toALA	toSmall	cpx50
1UUZ_A_CYS64ALA	0.65	2.34	nonloop	toALA	toSmall	cpx50
1UUZ_A_HIS62GLN	1.52	1.84	nonloop	toNonALA	neutral	cpx50
1X1X_B_ALA76GLU	-0.82	-2.64	nonloop	toNonALA	toLarge	cpx05
1XD3_B_ARG42LEU	-0.88	1.75	nonloop	toNonALA	toSmall	cpx84
1XD3_B_ILE44ALA	0.27	0.88	nonloop	toALA	toSmall	cpx84
1XD3_B_LYS11ARG	1.43	0.33	loop	toNonALA	toLarge	cpx84
1XD3_B_LEU8ALA	2.74	1.42	nonloop	toALA	toSmall	cpx84
1XD3_B_ASP39ALA	-0.42	0.66	nonloop	toALA	toSmall	cpx84
1XD3_B_LYS6ALA	1.38	0.64	nonloop	toALA	toSmall	cpx84
1XD3_B_ARG72LEU	1.33	0.78	loop	toNonALA	toSmall	cpx84
1XD3_B_LYS27ARG	0.27	0.55	nonloop	toNonALA	toLarge	cpx84
1XD3_B_HIS68ASN	0.00	0.66	nonloop	toNonALA	toSmall	cpx84
1XD3_B_LYS27ALA	-0.06	0.81	nonloop	toALA	toSmall	cpx84
1XD3_B_ARG74LEU	2.43	0.72	loop	toNonALA	toSmall	cpx84
1XD3_B_LYS6ARG	0.31	0.66	nonloop	toNonALA	toLarge	cpx84
1Y1K_B_ALA39THR	-2.73	-1.73	nonloop	toNonALA	toLarge	cpx71
1Y33_B_PRO39THR	-3.75	1.66	nonloop	toNonALA	neutral	cpx71
1Y34_B_ALA41GLU	-3.05	-1.02	loop	toNonALA	toLarge	cpx71
1Y3B_B_SER41GLU	-2.75	-1.21	loop	toNonALA	toLarge	cpx71
1Z7X_A_TRP263ALA	2.21	1.58	loop	toALA	toSmall	cpx68
1Z7X_A_TYR434ALA	5.95	1.47	loop	toALA	toSmall	cpx68
1Z7X_A_GLU287ALA	1.32	2.58	nonloop	toALA	toSmall	cpx68
1Z7X_A_SER289ALA	0.81	0.77	nonloop	toALA	neutral	cpx68
1Z7X_A_ILE459ALA	0.34	1.72	nonloop	toALA	toSmall	cpx68

1Z7X_A_ARG457ALA	0.85	0.39	nonloop	toALA	toSmall	cpx68
1Z7X_A_TYR437PHE	2.17	1.21	loop	toNonALA	neutral	cpx68
1Z7X_A_TYR437ALA	2.62	1.35	loop	toALA	toSmall	cpx68
1Z7X_A_TRP261ALA	1.34	1.42	nonloop	toALA	toSmall	cpx68
1Z7X_A_GLU206ALA	1.02	1.03	nonloop	toALA	toSmall	cpx68
1Z7X_A_TRP318ALA	0.99	1.55	nonloop	toALA	toSmall	cpx68
1Z7X_A_TYR434PHE	0.12	2.40	loop	toNonALA	neutral	cpx68
1Z7X_A_TRP375ALA	1.67	1.09	nonloop	toALA	toSmall	cpx68
1Z7X_A_ASP435ALA	3.66	2.22	loop	toALA	toSmall	cpx68
1Z7X_A_GLU344ALA	1.56	1.31	nonloop	toALA	toSmall	cpx68
1Z7X_A_LYS320ALA	1.32	1.61	nonloop	toALA	toSmall	cpx68
1Z7X_A_GLU401ALA	1.31	1.84	nonloop	toALA	toSmall	cpx68
2A9K_B_GLY55ASP	2.41	-0.22	nonloop	toNonALA	toLarge	cpx66
2AJF_B_THR159SER	1.82	0.24	loop	toNonALA	toSmall	cpx40
2AJF_B_ASN151LYS	2.01	1.06	nonloop	toNonALA	toLarge	cpx40
2B0Z_B_ILE87PHE	-2.53	-1.60	loop	toNonALA	toLarge	cpx30
2B10_B_SER87PHE	-1.16	-2.26	loop	toNonALA	toLarge	cpx30
2B11_B_TRP87PHE	-0.75	-0.94	loop	toNonALA	toSmall	cpx30
2B12_B_TYR87PHE	-1.57	-0.07	loop	toNonALA	neutral	cpx30
2B42_A_HIS357LYS	2.54	1.28	loop	toNonALA	toLarge	cpx78
2B42_A_HIS357ALA	1.62	1.57	loop	toALA	toSmall	cpx78
2B42_A_HIS357GLN	1.06	1.65	loop	toNonALA	neutral	cpx78
2BTF_B_GLY120PHE	1.72	2.05	nonloop	toNonALA	toLarge	cpx16
2BTF_B_LYS125ALA	0.46	1.15	nonloop	toALA	toSmall	cpx16
2BTF_B_PHE59ALA	1.60	1.06	nonloop	toALA	toSmall	cpx16
2BTF_B_VAL60GLU	0.98	0.51	nonloop	toNonALA	neutral	cpx16
2FTL_B_LYS15ASP	11.40	8.22	loop	toNonALA	toSmall	cpx17
2FTL_B_GLY36ALA	4.89	3.57	loop	toALA	toLarge	cpx17
2FTL_B_LYS15SER	7.64	9.99	loop	toNonALA	toSmall	cpx17
2FTL_B_LYS15GLY	12.20	9.11	loop	toNonALA	toSmall	cpx17
2FTL_B_LYS15ASN	7.95	8.93	loop	toNonALA	toSmall	cpx17
2FTL_B_LYS15HIS	8.69	8.50	loop	toNonALA	toSmall	cpx17
2FTL_B_LYS15GLU	9.32	8.73	loop	toNonALA	toSmall	cpx17
2FTL_B_LYS15GLN	9.27	9.15	loop	toNonALA	toSmall	cpx17
2FTL_B_ILE18ALA	4.97	2.06	nonloop	toALA	toSmall	cpx17
2FTL_B_LYS15MET	7.61	8.45	loop	toNonALA	neutral	cpx17
2FTL_B_LYS15TYR	6.78	8.29	loop	toNonALA	toLarge	cpx17
2FTL_B_LYS15PHE	6.95	8.56	loop	toNonALA	toLarge	cpx17
2FTL_B_LYS15ILE	11.10	9.12	loop	toNonALA	neutral	cpx17
2FTL_B_LYS15LEU	8.77	10.10	loop	toNonALA	neutral	cpx17
2FTL_B_GLY12ALA	4.35	3.53	loop	toALA	toLarge	cpx17
2FTL_B_LYS15THR	10.50	9.58	loop	toNonALA	toSmall	cpx17
2FTL_B_LYS15VAL	11.60	9.48	loop	toNonALA	toSmall	cpx17
2FTL_B_LYS15TRP	8.57	8.25	loop	toNonALA	toLarge	cpx17
2G2U_A_ASP79LYS	-0.45	0.70	loop	toNonALA	toLarge	cpx69
2G2U_B_ARG160ALA	0.67	0.88	nonloop	toALA	toSmall	cpx69
2G2U_B_GLY48ALA	-0.43	0.32	loop	toALA	toLarge	cpx69
2G2U_B_PHE142ALA	0.28	0.02	loop	toALA	toSmall	cpx69
2G2U_B_GLU31ALA	0.65	0.51	nonloop	toALA	toSmall	cpx69
2G2U_B_TRP112ALA	0.96	0.86	nonloop	toALA	toSmall	cpx69
2G2U_B_HIS148ALA	1.12	0.99	nonloop	toALA	toSmall	cpx69
2G2U_B_SER39ALA	-0.96	0.19	loop	toALA	neutral	cpx69
2G2U_B_GLU73MET	-3.53	-0.21	nonloop	toNonALA	toLarge	cpx69
2G2U_B_HIS41ALA	1.72	1.42	nonloop	toALA	toSmall	cpx69
2G2U_B_TYR143ALA	-1.85	0.35	loop	toALA	toSmall	cpx69
2G2U_B_LYS74ALA	-0.22	0.61	loop	toALA	toSmall	cpx69
2G2U_B_PHE36ALA	2.76	0.52	nonloop	toALA	toSmall	cpx69
2G2U_B_TYR50ALA	-2.07	0.53	loop	toALA	toSmall	cpx69
2G2U_B_TRP162ALA	0.53	1.44	nonloop	toALA	toSmall	cpx69
2G2U_B_SER35ALA	-0.95	0.24	nonloop	toALA	neutral	cpx69
2G2U_B_GLY141ALA	-0.41	0.42	loop	toALA	toLarge	cpx69
2G2U_B_SER113ALA	-0.61	0.28	nonloop	toALA	neutral	cpx69
2G2U_B_TYR51ALA	-0.63	1.03	nonloop	toALA	toSmall	cpx69
2G2U_B_SER71ALA	-0.51	0.13	nonloop	toALA	neutral	cpx69
2G2U_B_TYR53ALA	2.30	0.67	nonloop	toALA	toSmall	cpx69
2G2U_B_ARG144ALA	-0.34	0.16	loop	toALA	toSmall	cpx69
2G2U_B_TRP150ALA	1.78	1.66	nonloop	toALA	toSmall	cpx69
2G2U_B_GLU73ALA	-1.98	-0.62	nonloop	toALA	toSmall	cpx69
2G2W_A_LYS79ASP	0.45	0.13	loop	toNonALA	toSmall	cpx69

2GYK_A_ALA49ASP	-5.92	-3.41	nonloop	toNonALA	toLarge	cpx26
2HLE_A_LYS141GLN	-0.41	0.59	nonloop	toNonALA	toSmall	cpx32
2HLE_A_LEU87ARG	2.29	0.18	loop	toNonALA	toLarge	cpx32
2HRK_A_THR108VAL	0.72	1.54	loop	toNonALA	toLarge	cpx36
2HRK_A_LYS140ALA	0.95	1.20	nonloop	toALA	toSmall	cpx36
2HRK_B_THR55VAL	0.62	1.27	loop	toNonALA	toLarge	cpx36
2I26_A_ALA29VAL	0.03	0.97	loop	toNonALA	toLarge	cpx83
2I9B_B_ARG129ALA	-0.29	0.07	loop	toALA	toSmall	cpx85
2I9B_B_LYS131ALA	0.67	0.21	loop	toALA	toSmall	cpx85
2J0T_B_SER68ALA	2.11	1.74	nonloop	toALA	neutral	cpx59
2J0T_B_VAL69ILE	0.81	1.23	nonloop	toNonALA	toLarge	cpx59
2J0T_B_SER68ARG	2.84	2.17	nonloop	toNonALA	toLarge	cpx59
2J0T_B_SER68TYR	2.98	2.02	nonloop	toNonALA	toLarge	cpx59
2J0T_B_VAL4LYS	1.82	0.73	loop	toNonALA	toLarge	cpx59
2J0T_B_THR2ALA	4.39	2.51	nonloop	toALA	toSmall	cpx59
2J0T_B_CYS70SER	4.41	2.17	nonloop	toNonALA	neutral	cpx59
2J0T_B_VAL4ILE	1.64	1.11	loop	toNonALA	toLarge	cpx59
2J0T_B_THR2LEU	2.68	2.84	nonloop	toNonALA	toLarge	cpx59
2J0T_B_SER68GLU	2.18	2.40	nonloop	toNonALA	toLarge	cpx59
2J0T_B_VAL4ALA	0.00	0.55	loop	toALA	toSmall	cpx59
2J0T_B_MET66ALA	1.68	1.38	loop	toALA	toSmall	cpx59
2J0T_B_VAL4SER	0.98	0.82	loop	toNonALA	toSmall	cpx59
2J0T_B_VAL69THR	1.32	1.05	nonloop	toNonALA	toSmall	cpx59
2J0T_B_THR2ARG	5.04	2.09	nonloop	toNonALA	toLarge	cpx59
2J0T_B_THR2SER	1.59	2.36	nonloop	toNonALA	toSmall	cpx59
2J1K_A_GLY10ASP	0.18	-2.03	loop	toNonALA	toLarge	cpx21
2J1K_A_ARG24ALA	0.77	1.22	nonloop	toALA	toSmall	cpx21
2NU0_B_TRP13LEU	-1.84	-2.50	loop	toNonALA	toSmall	cpx70
2NU1_B_HIS13LEU	-1.69	-1.65	loop	toNonALA	neutral	cpx70
2NU2_B_ARG13LEU	-3.32	-0.34	loop	toNonALA	toSmall	cpx70
2NU4_B_LYS13LEU	-3.14	-1.07	loop	toNonALA	neutral	cpx70
2O3B_B_ASP75ASN	5.90	2.41	nonloop	toNonALA	toLarge	cpx61
2O3B_B_GLU24ALA	5.47	2.79	loop	toALA	toSmall	cpx61
2O3B_B_GLU24GLN	5.40	2.22	loop	toNonALA	neutral	cpx61
2O3B_B_GLU24ASP	0.60	3.40	loop	toNonALA	toSmall	cpx61
2O3B_B_ASP75GLU	5.44	1.96	nonloop	toNonALA	toLarge	cpx61
2O3B_B_GLN74ALA	3.23	0.55	loop	toALA	toSmall	cpx61
2O3B_B_TRP76ALA	4.07	3.41	nonloop	toALA	toSmall	cpx61
2OOB_A_GLY13SER	0.24	0.99	nonloop	toNonALA	toLarge	cpx22
2PCB_A_GLU35GLN	0.68	1.55	loop	toNonALA	neutral	cpx31
2PCB_A_ALA193PHE	0.73	-0.46	loop	toNonALA	toLarge	cpx31
2PCB_A_GLU290ASN	0.87	2.15	nonloop	toNonALA	toSmall	cpx31
2PCB_A_ASP34ASN	0.82	0.81	loop	toNonALA	toLarge	cpx31
2PCB_A_GLU32GLN	0.61	0.99	nonloop	toNonALA	neutral	cpx31
2PCC_A_GLU290ALA	6.20	1.20	nonloop	toALA	toSmall	cpx30
2PCC_A_ASP34ALA	-0.90	1.14	nonloop	toALA	toSmall	cpx30
2PCC_A_VAL197ALA	2.10	1.13	loop	toALA	toSmall	cpx30
2PCC_B_ALA86GLY	1.90	1.43	loop	toNonALA	toSmall	cpx30
2PCC_B_LYS92ALA	0.90	1.57	loop	toALA	toSmall	cpx30
2PCC_B_LYS77ALA	0.30	1.22	nonloop	toALA	toSmall	cpx30
2SGP_B_PRO13LEU	-8.33	-3.49	loop	toNonALA	toLarge	cpx70
2SGQ_B_GLN13LEU	-2.57	-2.63	loop	toNonALA	toLarge	cpx70
2SIC_B_MET67LYS	0.00	0.50	loop	toNonALA	neutral	cpx73
2SIC_B_MET67LEU	-0.24	0.53	loop	toNonALA	neutral	cpx73
2SIC_B_MET67VAL	0.71	0.43	loop	toNonALA	toSmall	cpx73
2SIC_B_MET67GLY	0.15	1.23	loop	toNonALA	toSmall	cpx73
2SIC_B_MET67GLU	0.80	0.56	loop	toNonALA	toSmall	cpx73
2SIC_B_MET67ILE	1.60	0.41	loop	toNonALA	neutral	cpx73
2SIC_B_MET67ALA	0.22	0.60	loop	toALA	toSmall	cpx73
2SIC_B_MET67HIS	0.22	0.74	loop	toNonALA	neutral	cpx73
2SIC_B_MET67ASP	0.75	0.51	loop	toNonALA	toSmall	cpx73
2SIC_B_MET67ARG	0.00	0.73	loop	toNonALA	toLarge	cpx73
2VLN_B_ALA75ASN	-2.33	-2.72	nonloop	toNonALA	toLarge	cpx26
2VLO_B_ALA95LYS	-1.96	0.07	loop	toNonALA	toLarge	cpx26
2VLQ_B_ALA86PHE	-3.88	-0.03	loop	toNonALA	toLarge	cpx26
2WPT_A_VAL34ALA	3.81	1.00	nonloop	toALA	toSmall	cpx25
2WPT_A_ARG35THR	-1.04	0.19	nonloop	toNonALA	toSmall	cpx25
2WPT_A_SER47ALA	2.42	1.98	nonloop	toALA	neutral	cpx25
2WPT_A_PRO53ALA	2.93	2.16	loop	toALA	toSmall	cpx25

2WPT_A_ASN31ALA	-0.38	0.39	nonloop	toALA	toSmall	cpx25
2WPT_A_ASN31VAL	-0.90	0.58	nonloop	toNonALA	toLarge	cpx25
2WPT_A_GLU27ALA	1.73	2.82	nonloop	toALA	toSmall	cpx25
2WPT_A_ASP30LEU	-3.40	0.65	nonloop	toNonALA	toLarge	cpx25
2WPT_A_GLU38ALA	4.50	1.20	nonloop	toALA	toSmall	cpx25
2WPT_A_ASP30ALA	-0.13	0.00	nonloop	toALA	toSmall	cpx25
2WPT_A_ARG35ALA	-1.11	-0.05	nonloop	toALA	toSmall	cpx25
3BK3_B_LEU2ARG	0.03	0.70	loop	toNonALA	toLarge	cpx09
3BK3_B_ILE22ARG	2.12	1.03	nonloop	toNonALA	toLarge	cpx09
3BK3_B_THR6PRO	1.74	0.99	nonloop	toNonALA	neutral	cpx09
3BK3_B_LEU2ALA	0.00	1.05	loop	toALA	toSmall	cpx09
3BK3_B_ILE28ARG	1.17	1.18	nonloop	toNonALA	toLarge	cpx09
3BK3_B_ILE28ALA	1.26	1.22	nonloop	toALA	toSmall	cpx09
3BK3_B_ILE19ARG	0.42	0.87	loop	toNonALA	toLarge	cpx09
3BK3_B_ILE3ALA	1.04	1.40	loop	toALA	toSmall	cpx09
3BK3_B_ILE3ARG	0.65	1.74	loop	toNonALA	toLarge	cpx09
3BK3_B_ALA37ARG	1.38	1.17	nonloop	toNonALA	toLarge	cpx09
3BK3_B_ILE19ALA	0.49	0.87	loop	toALA	toSmall	cpx09
3BK3_B_THR4PRO	0.49	0.66	loop	toNonALA	neutral	cpx09
3BK3_B_ILE22ALA	1.31	1.36	nonloop	toALA	toSmall	cpx09
3BP8_A_PHE115ALA	0.71	2.33	nonloop	toALA	toSmall	cpx58
3BP8_B_ALA51PHE	0.62	0.61	nonloop	toNonALA	toLarge	cpx58
3BTD_B_ASP13LYS	-11.40	-8.53	loop	toNonALA	toLarge	cpx17
3BTE_B_GLU13LYS	-9.32	-8.29	loop	toNonALA	toLarge	cpx17
3BTF_B_PHE13LYS	-6.95	-8.17	loop	toNonALA	toSmall	cpx17
3BTG_B_GLY13LYS	-12.20	-7.91	loop	toNonALA	toLarge	cpx17
3BTH_B_HIS13LYS	-8.69	-8.07	loop	toNonALA	toLarge	cpx17
3BTM_B_MET13LYS	-7.61	-0.02	loop	toNonALA	neutral	cpx17
3BTQ_B_GLN13LYS	-9.27	-7.85	loop	toNonALA	toLarge	cpx17
3BTT_B_THR13LYS	-10.50	-7.85	loop	toNonALA	toLarge	cpx17
3BTW_B_TRP13LYS	-8.57	-7.54	loop	toNonALA	toSmall	cpx17
3SGB_B_ASN30THR	0.01	0.46	nonloop	toNonALA	neutral	cpx70
3SGB_B_TYR14PHE	0.17	1.93	loop	toNonALA	neutral	cpx70
3SGB_B_LEU12HIS	1.69	3.15	loop	toNonALA	neutral	cpx70
3SGB_B_ASN30SER	0.40	0.39	nonloop	toNonALA	toSmall	cpx70
3SGB_B_ASN30GLU	0.95	0.20	nonloop	toNonALA	toLarge	cpx70
3SGB_B_GLY26THR	3.00	2.57	loop	toNonALA	toLarge	cpx70
3SGB_B_ALA9GLU	0.66	2.09	loop	toNonALA	toLarge	cpx70
3SGB_B_THR11GLN	2.90	2.60	nonloop	toNonALA	toLarge	cpx70
3SGB_B_LEU12GLY	4.93	3.52	loop	toNonALA	toSmall	cpx70
3SGB_B_GLY26GLN	2.92	2.52	loop	toNonALA	toLarge	cpx70
3SGB_B_TYR14ARG	2.72	2.28	loop	toNonALA	neutral	cpx70
3SGB_B_LEU12LYS	3.14	2.87	loop	toNonALA	neutral	cpx70
3SGB_B_ALA9TYR	-1.62	-0.59	loop	toNonALA	toLarge	cpx70
3SGB_B_ASN30ILE	0.20	0.21	nonloop	toNonALA	toLarge	cpx70
3SGB_B_THR11ASN	3.21	2.68	nonloop	toNonALA	neutral	cpx70
3SGB_B_TYR14LYS	3.39	3.15	loop	toNonALA	toSmall	cpx70
3SGB_B_LEU12VAL	3.00	3.06	loop	toNonALA	toSmall	cpx70
3SGB_B_GLU13SER	1.92	1.02	loop	toNonALA	toSmall	cpx70
3SGB_B_ARG15TRP	0.31	0.40	loop	toNonALA	toLarge	cpx70
3SGB_B_TYR14GLN	3.24	3.13	loop	toNonALA	toSmall	cpx70
3SGB_B_ALA9LEU	0.17	0.55	loop	toNonALA	toLarge	cpx70
3SGB_B_LEU12ARG	3.32	2.00	loop	toNonALA	toLarge	cpx70
3SGB_B_LYS7THR	-1.92	-1.03	loop	toNonALA	toSmall	cpx70
3SGB_B_THR11LYS	2.01	2.51	nonloop	toNonALA	toLarge	cpx70
3SGB_B_LEU12ILE	4.42	2.35	loop	toNonALA	neutral	cpx70
3SGB_B_TYR14SER	2.01	3.33	loop	toNonALA	toSmall	cpx70
3SGB_B_ARG15LEU	0.23	0.30	loop	toNonALA	toSmall	cpx70
3SGB_B_ALA9PHE	-1.16	-0.20	loop	toNonALA	toLarge	cpx70
3SGB_B_TYR14THR	4.80	3.30	loop	toNonALA	toSmall	cpx70
3SGB_B_GLU13PRO	2.24	1.33	loop	toNonALA	toSmall	cpx70
3SGB_B_LEU12PRO	8.33	3.73	loop	toNonALA	toSmall	cpx70
3SGB_B_PRO8MET	-0.49	-0.32	loop	toNonALA	toLarge	cpx70
3SGB_B_LYS7GLN	-0.62	-0.64	loop	toNonALA	toSmall	cpx70
3SGB_B_TYR14PRO	6.19	3.37	loop	toNonALA	toSmall	cpx70
3SGB_B_GLU13ASP	0.55	0.72	loop	toNonALA	toSmall	cpx70
3SGB_B_ASN30LYS	0.57	0.50	nonloop	toNonALA	toLarge	cpx70
3SGB_B_GLY26TRP	3.86	2.88	loop	toNonALA	toLarge	cpx70
3SGB_B_PRO8LYS	0.11	-0.24	loop	toNonALA	toLarge	cpx70

3SGB_B_LYS7HIS	-0.40	-0.68	loop	toNonALA	toSmall	cpx70
3SGB_B_LYS7CYS	-0.58	-1.15	loop	toNonALA	toSmall	cpx70
3SGB_B_ALA9ILE	-0.45	-0.04	loop	toNonALA	toLarge	cpx70
3SGB_B_ASN30MET	0.14	0.26	nonloop	toNonALA	toLarge	cpx70
3SGB_B_LYS7PHE	-0.72	-0.76	loop	toNonALA	toLarge	cpx70
3SGB_B_LEU12PHE	1.35	2.61	loop	toNonALA	toLarge	cpx70
3SGB_B_GLU13ALA	1.01	1.46	loop	toALA	toSmall	cpx70
3SGB_B_ARG15THR	0.45	1.23	loop	toNonALA	toSmall	cpx70
3SGB_B_GLY26SER	1.59	1.87	loop	toNonALA	toLarge	cpx70
3SGB_B_GLU13MET	-0.19	1.01	loop	toNonALA	toLarge	cpx70
3SGB_B_GLU13LEU	0.77	0.90	loop	toNonALA	toLarge	cpx70
3SGB_B_LYS7VAL	-0.94	-0.86	loop	toNonALA	toSmall	cpx70
3SGB_B_PRO8VAL	-0.31	-0.06	loop	toNonALA	toLarge	cpx70
3SGB_B_ALA9PRO	0.55	0.56	loop	toNonALA	toLarge	cpx70
3SGB_B_ALA9GLN	0.42	0.55	loop	toNonALA	toLarge	cpx70
3SGB_B_GLU13ARG	1.26	0.90	loop	toNonALA	toLarge	cpx70
3SGB_B_GLY26ASN	2.24	2.20	loop	toNonALA	toLarge	cpx70
3SGB_B_LYS7ILE	-1.33	-1.05	loop	toNonALA	neutral	cpx70
3SGB_B_TYR14GLY	2.80	3.46	loop	toNonALA	toSmall	cpx70
3SGB_B_TYR14ALA	1.92	3.73	loop	toALA	toSmall	cpx70
3SGB_B_ALA9ASP	0.47	0.52	loop	toNonALA	toLarge	cpx70
3SGB_B_ARG15ALA	0.05	1.12	loop	toALA	toSmall	cpx70
3SGB_B_ARG15SER	0.27	0.35	loop	toNonALA	toSmall	cpx70
3SGB_B_ASN30ASP	0.90	0.39	nonloop	toNonALA	toSmall	cpx70
3SGB_B_ARG15VAL	-0.02	0.37	loop	toNonALA	toSmall	cpx70
3SGB_B_PRO8ASP	-1.02	-0.09	loop	toNonALA	neutral	cpx70
3SGB_B_ALA9TRP	-1.53	0.51	loop	toNonALA	toLarge	cpx70
3SGB_B_PRO8ASN	-0.12	-0.23	loop	toNonALA	neutral	cpx70
3SGB_B_TYR14CYS	1.67	3.42	loop	toNonALA	toSmall	cpx70
3SGB_B_PRO8LEU	-0.14	-0.28	loop	toNonALA	toLarge	cpx70
3SGB_B_GLY26PRO	1.08	2.26	loop	toNonALA	toLarge	cpx70
3SGB_B_GLU13VAL	0.13	0.98	loop	toNonALA	neutral	cpx70
3SGB_B_TYR14LEU	1.55	2.67	loop	toNonALA	toSmall	cpx70
3SGB_B_LYS7ARG	-0.68	-0.81	loop	toNonALA	toLarge	cpx70
3SGB_B_LYS7LEU	-1.79	-0.95	loop	toNonALA	neutral	cpx70
3SGB_B_THR11PRO	3.14	2.80	nonloop	toNonALA	neutral	cpx70
3SGB_B_TYR14ASN	3.11	2.14	loop	toNonALA	toSmall	cpx70
3SGB_B_GLU13ILE	-0.62	0.77	loop	toNonALA	toLarge	cpx70
3SGB_B_LEU12THR	3.16	3.77	loop	toNonALA	toSmall	cpx70
3SGB_B_LEU12ASN	3.35	3.36	loop	toNonALA	toSmall	cpx70
3SGB_B_GLY26LYS	2.49	2.55	loop	toNonALA	toLarge	cpx70
3SGB_B_GLY26ILE	4.04	2.62	loop	toNonALA	toLarge	cpx70
3SGB_B_GLY26TYR	3.05	2.83	loop	toNonALA	toLarge	cpx70
3SGB_B_ALA9LYS	2.46	0.44	loop	toNonALA	toLarge	cpx70
3SGB_B_PRO8ILE	-0.02	-0.14	loop	toNonALA	toLarge	cpx70
3SGB_B_GLU13TRP	1.53	1.18	loop	toNonALA	toLarge	cpx70
3SGB_B_ALA9MET	0.09	-0.39	loop	toNonALA	toLarge	cpx70
3SGB_B_ARG15HIS	0.45	0.38	loop	toNonALA	toSmall	cpx70
3SGB_B_ARG15TYR	0.29	0.39	loop	toNonALA	neutral	cpx70
3SGB_B_ARG15ASP	0.63	0.27	loop	toNonALA	toSmall	cpx70
3SGB_B_THR11HIS	3.46	2.57	nonloop	toNonALA	toLarge	cpx70
3SGB_B_ASN30HIS	-0.12	0.13	nonloop	toNonALA	toLarge	cpx70
3SGB_B_ARG15CYS	0.55	1.46	loop	toNonALA	toSmall	cpx70
3SGB_B_ASN30PRO	0.57	0.40	nonloop	toNonALA	neutral	cpx70
3SGB_B_THR11ILE	1.73	2.80	nonloop	toNonALA	toLarge	cpx70
3SGB_B_THR11ASP	4.89	2.48	nonloop	toNonALA	neutral	cpx70
3SGB_B_TYR14ILE	3.54	2.71	loop	toNonALA	toSmall	cpx70
3SGB_B_ASN30VAL	-0.24	0.48	nonloop	toNonALA	toLarge	cpx70
3SGB_B_GLU13GLY	2.08	1.46	loop	toNonALA	toSmall	cpx70
3SGB_B_PRO8SER	0.07	-0.17	loop	toNonALA	toSmall	cpx70
3SGB_B_LYS7SER	-2.55	-0.85	loop	toNonALA	toSmall	cpx70
3SGB_B_ARG15PRO	7.58	0.58	loop	toNonALA	toSmall	cpx70
3SGB_B_THR11CYS	2.89	3.27	nonloop	toNonALA	toSmall	cpx70
3SGB_B_PRO8TYR	-0.40	-0.14	loop	toNonALA	toLarge	cpx70
3SGB_B_THR11ARG	1.95	3.00	nonloop	toNonALA	toLarge	cpx70
3SGB_B_ARG15GLU	0.66	0.29	loop	toNonALA	toSmall	cpx70
3SGB_B_ASN30LEU	0.73	0.36	nonloop	toNonALA	toLarge	cpx70
3SGB_B_ARG15GLY	1.09	2.42	loop	toNonALA	toSmall	cpx70
3SGB_B_PRO8THR	-0.11	-0.05	loop	toNonALA	neutral	cpx70

3SGB_B_PRO8GLN	-0.31	-0.22	loop	toNonALA	toLarge	cpx70
3SGB_B_LYS7ASN	-0.65	-1.01	loop	toNonALA	toSmall	cpx70
3SGB_B_GLY26CYS	2.58	2.13	loop	toNonALA	toLarge	cpx70
3SGB_B_ALA9GLY	2.45	0.48	loop	toNonALA	toSmall	cpx70
3SGB_B_ALA9THR	0.33	0.61	loop	toNonALA	toLarge	cpx70
3SGB_B_GLY26MET	2.77	2.84	loop	toNonALA	toLarge	cpx70
3SGB_B_ALA9HIS	-0.45	0.44	loop	toNonALA	toLarge	cpx70
3SGB_B_GLY26PHE	2.98	2.57	loop	toNonALA	toLarge	cpx70
3SGB_B_ALA9SER	0.90	0.52	loop	toNonALA	neutral	cpx70
3SGB_B_ARG15PHE	0.23	0.36	loop	toNonALA	neutral	cpx70
3SGB_B_PRO8CYS	-0.32	-0.22	loop	toNonALA	toSmall	cpx70
3SGB_B_THR11TYR	3.32	2.54	nonloop	toNonALA	toLarge	cpx70
3SGB_B_ASN30PHE	-0.14	0.09	nonloop	toNonALA	toLarge	cpx70
3SGB_B_GLU13ASN	1.09	1.06	loop	toNonALA	toSmall	cpx70
3SGB_B_LEU12ASP	5.59	3.28	loop	toNonALA	toSmall	cpx70
3SGB_B_LYS7ASP	-0.62	-1.34	loop	toNonALA	toSmall	cpx70
3SGB_B_THR11LEU	2.44	2.98	nonloop	toNonALA	toLarge	cpx70
3SGB_B_LYS7TYR	-0.58	-1.16	loop	toNonALA	toLarge	cpx70
3SGB_B_LYS7GLY	-0.72	-0.72	loop	toNonALA	toSmall	cpx70
3SGB_B_PRO8GLU	-0.62	-0.28	loop	toNonALA	toLarge	cpx70
3SGB_B_PRO8PHE	-0.34	-0.32	loop	toNonALA	toLarge	cpx70
3SGB_B_ARG15ASN	0.33	0.33	loop	toNonALA	toSmall	cpx70
3SGB_B_PRO8HIS	0.27	-0.08	loop	toNonALA	toLarge	cpx70
3SGB_B_ALA9CYS	0.04	0.69	loop	toNonALA	toLarge	cpx70
3SGB_B_ARG15LYS	-0.27	0.34	loop	toNonALA	toSmall	cpx70
3SGB_B_GLY26ASP	1.60	2.80	loop	toNonALA	toLarge	cpx70
3SGB_B_THR11TRP	3.00	2.42	nonloop	toNonALA	toLarge	cpx70
3SGB_B_ASN30ARG	0.57	0.61	nonloop	toNonALA	toLarge	cpx70
3SGB_B_PRO8TRP	-0.49	-0.31	loop	toNonALA	toLarge	cpx70
3SGB_B_LYS7ALA	-2.54	-0.84	loop	toALA	toSmall	cpx70
3SGB_B_GLY26ARG	3.46	2.61	loop	toNonALA	toLarge	cpx70
3SGB_B_TYR14TRP	0.38	1.36	loop	toNonALA	toLarge	cpx70
3SGB_B_LYS7TRP	-0.01	-0.72	loop	toNonALA	toLarge	cpx70
3SGB_B_GLY26LEU	2.62	3.03	loop	toNonALA	toLarge	cpx70
3SGB_B_LEU12TYR	1.65	2.53	loop	toNonALA	toLarge	cpx70
3SGB_B_ASN30ALA	0.33	0.20	nonloop	toALA	toSmall	cpx70
3SGB_B_PRO8ALA	-0.19	-0.20	loop	toALA	toSmall	cpx70
3SGB_B_THR11GLY	5.51	2.92	nonloop	toNonALA	toSmall	cpx70
3SGB_B_TYR14MET	1.98	2.43	loop	toNonALA	toSmall	cpx70
3SGB_B_ASN30TYR	-0.11	0.34	nonloop	toNonALA	toLarge	cpx70
3SGB_B_GLY26GLU	1.95	2.72	loop	toNonALA	toLarge	cpx70
3SGB_B_THR11MET	2.01	2.83	nonloop	toNonALA	toLarge	cpx70
3SGB_B_ARG15MET	0.13	0.35	loop	toNonALA	toSmall	cpx70
3SGB_B_GLU13TYR	0.77	1.37	loop	toNonALA	toLarge	cpx70
3SGB_B_LEU12SER	4.10	3.70	loop	toNonALA	toSmall	cpx70
3SGB_B_ARG15GLN	0.04	1.00	loop	toNonALA	toSmall	cpx70
3SGB_B_THR11PHE	3.59	2.86	nonloop	toNonALA	toLarge	cpx70
3SGB_B_ALA9ASN	-0.09	1.03	loop	toNonALA	toLarge	cpx70
3SGB_B_GLU13THR	2.11	0.63	loop	toNonALA	toSmall	cpx70
3SGB_B_ARG15ILE	0.24	0.40	loop	toNonALA	toSmall	cpx70
3SGB_B_PRO8GLY	0.05	-0.29	loop	toNonALA	toSmall	cpx70
3SGB_B_GLU13GLN	0.18	0.86	loop	toNonALA	neutral	cpx70
3SGB_B_TYR14GLU	2.01	2.90	loop	toNonALA	toSmall	cpx70
3SGB_B_GLU13PHE	1.92	1.10	loop	toNonALA	toLarge	cpx70
3SGB_B_GLU13HIS	0.52	1.19	loop	toNonALA	toLarge	cpx70
3SGB_B_LYS7GLU	0.03	-0.92	loop	toNonALA	toSmall	cpx70
3SGB_B_ALA9ARG	2.01	1.65	loop	toNonALA	toLarge	cpx70
3SGB_B_GLY26HIS	2.70	2.28	loop	toNonALA	toLarge	cpx70
3SGB_B_ASN30CYS	0.35	0.53	nonloop	toNonALA	toSmall	cpx70
3SGB_B_LEU12TRP	1.84	2.16	loop	toNonALA	toLarge	cpx70
3SGB_B_ASN30GLN	0.24	0.23	nonloop	toNonALA	toLarge	cpx70
3SGB_B_TYR14VAL	4.36	3.78	loop	toNonALA	toSmall	cpx70
3SGB_B_ASN30TRP	0.52	0.31	nonloop	toNonALA	toLarge	cpx70
3SGB_B_PRO8ARG	0.31	-0.18	loop	toNonALA	toLarge	cpx70
3SGB_B_GLU13CYS	1.16	1.25	loop	toNonALA	toSmall	cpx70
3SGB_B_LYS7PRO	0.00	-0.83	loop	toNonALA	toSmall	cpx70
3SGB_B_GLU13LYS	0.17	1.05	loop	toNonALA	toLarge	cpx70
3SGB_B_LYS7MET	-1.15	-0.88	loop	toNonALA	neutral	cpx70
3SGB_B_ASN30GLY	0.31	0.52	nonloop	toNonALA	toSmall	cpx70

3SGB_B_LEU12CYS	-0.01	3.70	loop	toNonALA	toSmall	cpx70
4CPA_B_TYR36GLY	0.50	1.55	loop	toNonALA	toSmall	cpx20
4CPA_B_VAL37ILE	0.20	1.11	loop	toNonALA	toLarge	cpx20
4CPA_B_PRO35GLY	2.59	1.28	loop	toNonALA	toSmall	cpx20
4CPA_B_VAL37ALA	2.32	0.98	loop	toALA	toSmall	cpx20
4CPA_B_TYR36PHE	0.00	0.95	loop	toNonALA	neutral	cpx20
4CPA_B_VAL37PHE	0.00	1.11	loop	toNonALA	toLarge	cpx20
4CPA_B_VAL37LEU	1.28	1.15	loop	toNonALA	toLarge	cpx20
4CPA_B_VAL37GLY	3.73	1.31	loop	toNonALA	toSmall	cpx20

Table S4. NM test dataset with experimental ΔΔG and predictions of different methods. ΔΔG unit is kcal mol^{-1}.

mutationID	ΔΔGexp	iSEE	pred1	pred2	CCPBSA	BeAtMuSiC	FoldX	mCSM	ZeMu	BindProfX
1IAR_B_ASN122ALA	0.68	0.93	0.91	0.87	0.47	0.64	0.03	0.37	-0.20	0.01
1IAR_B_ASP121ALA	0.80	0.75	2.41	2.81	0.49	1.87	1.59	0.52	2.18	0.99
1IAR_B_ASP66ALA	0.73	0.55	1.32	1.22	1.70	0.33	1.07	0.06	1.06	0.87
1IAR_B_ASP67ALA	2.36	0.78	4.85	4.64	2.08	1.42	3.12	0.73	5.08	2.34
1IAR_B_ASP72ALA	4.35	1.01	2.05	2.19	1.76	0.23	3.08	1.82	3.64	2.49
1IAR_B_LEU39ALA	2.77	0.78	1.29	1.60	1.36	1.36	0.93	-0.28	0.92	1.70
1IAR_B_LEU42ALA	0.00	0.14	0.92	0.53	1.55	-0.09	0.14	0.33	0.15	0.05
1IAR_B_LEU43ALA	0.33	0.04	1.12	1.21	0.33	0.59	1.51	0.66	1.47	0.94
1IAR_B_PHE41ALA	2.26	1.25	2.59	3.26	2.26	2.81	3.19	2.17	4.28	2.17
1IAR_B_SER70ALA	-0.24	0.16	0.96	1.22	0.62	1.41	-0.46	1.14	-1.26	0.82
1IAR_B_SER93ALA	-0.18	0.71	1.00	0.97	0.37	0.33	0.83	0.57	-0.06	0.45
1IAR_B_TYR123ALA	2.17	1.50	3.24	3.99	2.91	3.38	3.01	2.44	2.91	2.23
1IAR_B_TYR123PHE	-0.18	0.78	1.74	1.50	0.78	1.12	-1.23	1.48	-0.57	1.08
1IAR_B_TYR13ALA	5.22	2.38	1.69	2.22	1.66	1.53	2.26	0.20	3.43	2.10
1IAR_B_TYR13PHE	1.91	2.10	1.42	1.37	1.56	0.29	1.37	0.74	2.14	1.61
1IAR_B_TYR174ALA	3.68	2.09	2.42	3.03	2.16	1.89	3.25	1.29	2.71	2.40
1IAR_B_TYR174PHE	3.16	1.51	1.71	1.67	1.73	0.35	1.40	0.64	1.02	1.59
1IAR_B_VAL68ALA	0.84	1.23	0.92	1.03	0.54	0.92	0.19	0.26	-0.19	0.34
1IAR_B_VAL69ALA	2.10	1.19	1.95	2.24	0.78	1.81	1.52	1.98	1.60	1.46

Table S5. S540 test dataset with experimental ΔΔG and predictions of different methods. ΔΔG units are kcal mol^{-1}.

mutationID	ΔΔGexp	iSEE	BindProfX	FoldX	mCSM	combined
1A22_A_LYS157ALA	0.05	0.66	1.67	1.20	1.06	1.15
1A22_A_ASP160ALA	1.16	1.53	1.75	1.70	1.81	1.70
1A22_A_LYS161ALA	1.54	1.02	1.89	0.86	3.35	1.78
1A22_A_GLU163ALA	-0.90	0.59	1.20	-0.90	0.38	0.32
1A22_A_THR164SER	1.69	1.07	1.86	1.58	1.18	1.42
1A22_A_PHE165ALA	1.64	1.31	1.58	0.68	1.19	1.19
1A22_A_PHE165TYR	1.27	0.70	0.41	-0.02	1.44	0.63
1A22_A_ARG167ASN	1.27	1.00	1.61	-0.15	-0.10	0.59
1A22_A_ARG167LYS	0.95	0.87	1.00	-0.34	0.09	0.41
1A22_A_ILE168ALA	0.59	1.08	1.71	0.29	1.12	1.05
1A22_A_CYS171ALA	1.02	1.54	2.40	-0.07	0.86	1.18
1A22_A_ARG172ALA	0.44	1.31	0.02	0.06	0.29	0.42
1A22_A_PHE180ALA	0.19	1.02	-0.01	0.00	0.18	0.30
1A22_A_HIS18ALA	-0.21	0.65	1.59	-2.34	0.44	0.09
1A22_A_PHE25ALA	-0.39	0.91	0.78	0.66	1.53	0.97
1A22_A_GLU56ALA	0.84	0.53	0.59	1.00	0.66	0.70
1A22_A_ASN63ALA	0.71	1.01	1.05	-0.24	1.18	0.75
1A22_A_ARG64ALA	1.80	1.26	2.07	2.66	2.72	2.18
1A22_A_ARG64LYS	-0.31	0.97	0.66	1.03	2.22	1.22
1A22_A_GLU65ALA	-0.31	0.33	0.84	-0.07	0.48	0.40
1A22_A_GLN68ALA	0.99	0.69	1.47	0.04	0.24	0.61
1BP3_A_TYR160ALA	0.45	0.54	1.37	0.80	0.29	0.75
1BP3_A_ARG163ALA	3.02	0.76	2.04	1.50	1.25	1.39
1BP3_A_LYS164ALA	1.73	0.80	1.03	-0.02	1.10	0.73
1BP3_A_LYS168ALA	2.61	1.93	1.43	0.88	3.63	1.97
1BP3_A_GLU170ALA	1.83	1.15	1.09	-0.72	0.61	0.53
1BP3_A_THR171SER	0.49	1.60	1.01	0.21	0.54	0.84
1BP3_A_PHE172ALA	1.93	1.93	1.40	0.63	1.24	1.30
1BP3_A_ARG174ALA	1.15	1.29	1.43	1.82	0.32	1.22
1BP3_A_ILE175ALA	0.35	1.06	1.05	0.62	0.88	0.90
1BP3_A_ILE175MET	-0.16	1.61	0.79	0.30	0.81	0.88
1BP3_A_ARG179ALA	0.57	1.18	0.74	1.25	0.10	0.82
1BP3_A_SER184ALA	-0.30	1.43	0.20	0.04	-0.16	0.38
1BP3_A_HIS18ALA	1.55	0.83	1.47	0.20	0.26	0.69
1BP3_A_HIS21ALA	1.25	0.99	0.67	-0.96	0.86	0.39
1BP3_A_PHE25ALA	1.15	0.79	0.66	1.64	1.95	1.26
1BP3_A_ASN63ALA	0.86	0.65	0.83	-0.43	0.25	0.33
1BP3_A_ARG64ALA	0.35	1.02	1.27	-0.11	3.24	1.36
1BP3_A_GLU65ALA	0.55	0.50	0.77	-0.08	0.50	0.42
1BP3_A_GLN68ALA	0.11	0.85	0.73	0.33	-0.01	0.48
1C1Y_B_ASN10ALA	0.50	0.91	0.92	0.10	1.22	0.79
1C1Y_B_ASN10ASP	1.48	0.66	0.75	-0.13	2.02	0.83
1C1Y_B_LYS11ALA	1.11	0.69	0.63	0.07	1.53	0.73
1C1Y_B_LYS11GLU	0.89	0.95	0.10	-1.33	1.47	0.30
1C1Y_B_LYS11MET	0.71	0.76	0.66	0.16	0.51	0.52
1C1Y_B_GLN12ALA	1.58	1.17	0.87	0.84	2.72	1.40
1C1Y_B_ARG13ALA	1.45	1.53	1.30	1.17	1.36	1.34
1C1Y_B_LYS30ALA	1.31	1.17	0.61	0.38	0.49	0.66
1C1Y_B_LYS30GLU	2.23	1.18	0.32	0.20	0.17	0.47
1C1Y_B_ARG5ALA	1.91	1.26	1.43	2.37	1.37	1.61
1E50_A_VAL101ALA	-0.04	0.93	1.47	2.34	0.91	1.41
1E50_A_THR103ALA	2.18	0.59	1.34	1.40	0.98	1.08
1E50_A_ASN11ALA	0.68	1.26	0.45	-1.61	0.85	0.24

1E50_A_MET48ALA	1.32	1.16	0.99	1.11	0.85	1.03
1E50_A_ASN51ALA	1.92	1.09	1.10	0.37	2.17	1.18
1E50_A_TYR55ALA	0.91	1.39	1.93	1.85	2.69	1.97
1E50_A_SER56ALA	0.98	1.00	0.96	0.36	0.85	0.79
1E50_A_ASP8ALA	-0.32	1.13	1.46	-0.29	1.27	0.89
1E50_A_THR91ALA	1.28	0.93	0.84	0.50	0.62	0.72
1E50_B_ARG32ALA	1.77	1.11	1.59	0.48	2.31	1.37
1E50_B_VAL57ALA	0.00	1.56	1.09	0.71	1.22	1.15
1E50_B_ASN62ALA	0.96	0.67	1.20	-0.06	1.43	0.81
1E50_B_SER64ALA	0.11	0.57	0.78	-0.84	0.82	0.33
1E50_B_ASN99ALA	1.41	0.59	1.31	1.12	2.23	1.31
1FC2_C_TYR10PHE	1.03	0.88	1.12	-0.42	1.79	0.84
1FC2_C_PHE1MET	0.91	1.43	1.42	-0.84	0.74	0.69
1FC2_C_ASN24PHE	0.85	1.20	0.85	-1.48	0.76	0.33
1FC2_C_GLN28LEU	0.46	0.61	0.09	-0.11	0.12	0.18
1FC2_C_GLN28LYS	0.17	0.76	0.11	-0.21	0.67	0.33
1FC2_C_ASN2GLN	0.00	1.12	0.60	0.01	-0.14	0.40
1FC2_C_ASN2PHE	-0.11	0.91	0.54	0.01	0.53	0.50
1FC2_C_ASN7PHE	0.09	1.16	0.56	-0.32	1.13	0.63
1FFW_A_ALA102VAL	1.36	0.95	1.40	1.42	1.07	1.21
1GUA_A_GLU37ALA	1.30	1.72	1.82	0.57	1.76	1.47
1GUA_A_SER39ALA	1.40	1.49	0.83	-0.24	1.09	0.79
1GUA_B_LYS10ALA	-0.40	0.60	0.93	-0.31	2.13	0.84
1GUA_B_GLN11ALA	0.10	1.34	1.25	0.83	2.13	1.39
1GUA_B_THR13ALA	0.70	1.11	1.38	1.67	0.47	1.16
1GUA_B_VAL14ALA	0.10	1.39	1.37	1.68	0.79	1.31
1GUA_B_LYS29ALA	2.00	0.98	0.99	0.09	0.92	0.75
1GUA_B_LYS32ALA	0.80	1.05	0.88	0.60	0.39	0.73
1GUA_B_VAL33ALA	0.20	1.19	1.32	1.54	1.76	1.45
1GUA_B_ARG4ALA	1.00	1.37	1.82	1.58	1.48	1.56
1GUA_B_ASN9ALA	-0.40	1.16	1.17	1.73	1.77	1.46
1JCK_B_PHE176ALA	1.79	1.45	1.92	0.74	1.41	1.38
1JCK_B_THR20ALA	1.32	0.97	0.75	-0.04	0.83	0.63
1JCK_B_TYR26ALA	1.75	1.36	0.89	1.26	1.51	1.26
1JCK_B_ASN60ALA	1.02	1.13	1.19	-0.31	0.38	0.60
1JCK_B_VAL91ALA	1.93	0.72	0.63	0.20	1.08	0.66
1JTD_A_MET103ALA	2.52	0.99	0.62	1.29	1.15	1.01
1JTD_A_VAL190ALA	0.04	1.10	0.73	0.03	0.78	0.66
1JTD_A_MET244ALA	0.28	1.05	0.41	0.42	0.85	0.68
1JTD_A_GLN73ALA	0.52	0.69	0.91	1.58	0.52	0.93
1JTD_A_ASN74ALA	0.80	0.36	0.70	0.44	-0.20	0.33
1JTD_A_LEU76ALA	1.73	1.02	1.77	0.82	1.58	1.30
1JTD_A_GLU78ALA	0.84	1.13	0.68	-0.52	1.34	0.66
1JTD_A_TYR79ALA	2.25	0.43	1.76	1.58	1.57	1.34
1JTD_A_PRO81ALA	1.73	0.87	2.14	1.02	1.63	1.42
1JTD_A_LYS85ALA	2.14	0.81	1.21	0.60	2.89	1.38
1JTD_B_TRP114ALA	3.25	0.91	2.28	1.38	2.69	1.82
1JTD_B_ASP129ALA	0.96	0.83	0.01	-0.29	-0.08	0.12
1JTD_B_ASN12ALA	1.30	2.24	1.05	0.35	0.84	1.12
1JTD_B_SER131ALA	0.15	0.96	0.44	-0.11	0.16	0.36
1JTD_B_ASP132ALA	-0.55	0.65	-0.17	-0.11	-0.06	0.08
1JTD_B_ASP14ALA	1.51	0.77	1.29	-0.49	1.27	0.71
1JTD_B_TYR153ALA	3.30	0.77	2.14	1.74	0.80	1.36
1JTD_B_TRP15ALA	1.39	1.14	2.30	2.24	2.74	2.11
1JTD_B_ASP168ALA	-1.06	1.02	1.81	0.66	0.35	0.96
1JTD_B_TYR170ALA	2.03	0.55	1.89	1.96	1.56	1.49
1JTD_B_PHE171ALA	2.20	1.01	1.70	0.52	0.41	0.91
1JTD_B_ILE191ALA	2.89	-0.06	1.09	0.42	0.51	0.49

1JTD_B_PHE192ALA	3.96	0.93	1.69	1.11	-0.16	0.89
1JTD_B_THR19ALA	0.30	0.90	0.69	0.69	0.59	0.72
1JTD_B_TYR210ALA	0.82	0.83	1.59	0.12	0.72	0.82
1JTD_B_GLU230ALA	1.85	0.58	0.76	-3.19	0.94	-0.23
1JTD_B_TRP231ALA	5.81	0.74	2.02	-0.82	1.48	0.86
1JTD_B_ARG248ALA	0.89	0.97	1.51	1.77	1.01	1.32
1JTD_B_ASN266ALA	2.67	0.25	0.98	-0.04	0.69	0.47
1JTD_B_TYR35ALA	3.15	0.78	1.72	0.53	1.84	1.22
1JTD_B_PHE36ALA	2.55	0.87	1.63	1.08	0.20	0.95
1JTD_B_LEU53ALA	0.67	0.16	1.64	0.22	0.44	0.62
1JTD_B_ASN74ALA	1.21	0.83	1.14	1.53	1.21	1.18
1JTD_B_TYR75ALA	0.48	1.02	1.63	0.09	0.67	0.85
1JTD_B_ASP93ALA	1.99	1.08	1.43	-0.40	0.37	0.62
1JTG_A_MET104ALA	1.51	1.44	1.06	1.57	0.98	1.26
1JTG_A_GLU143GLY	-0.17	0.91	1.61	0.08	0.88	0.87
1JTG_A_GLU146LYS	-0.61	0.84	-0.05	0.17	0.39	0.34
1JTG_A_VAL190ALA	-0.58	1.25	1.03	0.91	0.24	0.86
1JTG_A_GLU213LYS	-0.41	0.78	1.06	-0.04	0.53	0.58
1JTG_A_ARG214TYR	-0.14	0.88	0.31	-0.01	0.12	0.33
1JTG_A_MET244ALA	-0.05	1.43	0.69	0.30	0.77	0.80
1JTG_A_GLN74ALA	0.59	1.31	0.88	0.16	1.23	0.90
1JTG_A_ASN75ALA	-1.48	0.84	0.93	-0.22	-0.01	0.39
1JTG_A_LEU77ALA	0.87	2.10	2.01	0.80	1.29	1.55
1JTG_A_GLU79ALA	2.30	1.01	1.53	2.84	2.15	1.88
1JTG_A_GLU79ASP	3.64	1.12	1.06	2.62	1.99	1.70
1JTG_A_GLU79LYS	2.24	1.30	1.55	2.65	3.06	2.14
1JTG_A_TYR80ALA	-0.09	1.56	2.21	3.39	2.15	2.33
1JTG_A_PRO82ALA	0.24	1.33	2.39	0.96	2.14	1.71
1JTG_A_PRO82GLN	0.46	0.56	2.71	0.99	1.45	1.43
1JTG_A_GLU85ALA	-1.31	0.72	1.58	0.12	1.43	0.96
1JTG_A_GLU85GLY	-0.91	1.16	1.81	0.52	1.61	1.28
1JTG_A_GLU85VAL	-0.67	0.91	1.35	-0.64	1.04	0.67
1JTG_A_LYS86ALA	-0.86	0.80	1.23	0.01	1.10	0.79
1JTG_A_LYS86ASN	0.18	0.88	1.10	-1.01	0.87	0.46
1JTG_B_SER113ALA	-0.70	1.29	0.79	0.00	0.48	0.64
1JTG_B_GLY141ALA	1.31	0.67	2.12	-0.02	0.28	0.76
1JTG_B_PHE142ALA	3.00	0.04	2.58	3.62	2.87	2.28
1JTG_B_TYR143ALA	0.85	0.83	2.30	1.68	1.59	1.60
1JTG_B_ARG144ALA	0.65	0.11	0.77	1.28	0.80	0.74
1JTG_B_HIS148ALA	3.04	1.61	1.73	0.19	1.13	1.17
1JTG_B_TRP150ALA	4.51	1.22	2.42	1.06	3.24	1.99
1JTG_B_ARG160ALA	2.99	1.16	1.84	2.21	1.26	1.62
1JTG_B_GLU31ALA	0.82	0.36	1.51	0.17	0.59	0.66
1JTG_B_SER35ALA	0.00	0.74	1.11	-0.42	0.25	0.42
1JTG_B_PHE36ALA	3.26	0.95	2.31	2.22	2.58	2.02
1JTG_B_SER39ALA	0.02	0.10	1.24	0.34	0.37	0.51
1JTG_B_HIS41ALA	3.44	1.68	1.93	-0.12	1.62	1.28
1JTG_B_GLY48ALA	1.15	0.30	3.12	4.47	1.11	2.25
1JTG_B_ASP49ALA	2.85	0.59	2.58	3.92	1.33	2.11
1JTG_B_TYR50ALA	-2.15	0.27	2.63	3.25	0.85	1.75
1JTG_B_TYR51ALA	0.81	1.27	1.83	0.73	0.52	1.09
1JTG_B_TYR53ALA	3.16	0.95	2.27	1.83	1.68	1.68
1JTG_B_SER71ALA	0.02	0.62	1.47	0.60	0.87	0.89
1JTG_B_GLU73ALA	0.43	0.66	1.33	1.63	0.64	1.07
1JTG_B_GLU73MET	0.50	0.55	0.93	1.23	-1.01	0.43
1JTG_B_LYS74ALA	3.62	0.46	2.03	3.29	1.47	1.81
1K8R_A_ASP38ALA	1.71	1.60	1.97	2.13	2.26	1.99
1K8R_A_ASP38ASN	1.90	1.57	1.84	2.76	1.49	1.92

1K8R_A_ASP38GLU	3.44	1.45	1.47	1.12	1.14	1.30
1K8R_A_SER39ALA	0.71	1.25	0.68	-0.21	2.68	1.10
1K8R_A_TYR40CYS	3.44	2.08	1.75	0.38	1.91	1.53
1K8R_A_TYR40PHE	1.49	1.27	1.19	-0.10	1.11	0.87
1K8R_A_ARG41ALA	1.18	1.18	0.91	-0.95	1.15	0.57
1K8R_B_GLN11ALA	1.80	0.66	0.29	-0.23	3.17	0.97
1K8R_B_ARG13ALA	2.80	1.04	0.65	0.78	1.74	1.05
1K8R_B_LYS31ALA	2.73	0.83	1.13	1.85	0.86	1.17
1K8R_B_ARG77ALA	1.44	0.61	0.89	1.21	1.35	1.02
1LFD_A_ASN14ALA	0.93	0.65	0.90	0.05	0.32	0.48
1LFD_A_ASN14LYS	0.40	0.71	0.94	-0.05	0.51	0.53
1LFD_A_ASN16ALA	0.49	0.94	1.11	1.09	1.08	1.06
1LFD_A_MET17LYS	-0.92	0.90	0.88	0.76	0.11	0.66
1LFD_A_TYR18ALA	3.46	1.74	1.78	2.11	3.23	2.22
1LFD_A_TYR18PHE	1.32	0.80	1.36	1.55	1.62	1.33
1LFD_A_LYS19ALA	2.07	1.23	0.97	1.62	1.00	1.21
1LFD_A_SER20ALA	0.93	1.18	0.81	0.20	0.69	0.72
1LFD_A_ASP38ALA	-0.39	0.76	0.97	0.11	0.54	0.60
1LFD_A_ASP38LYS	-1.09	0.61	0.93	-1.35	-0.28	-0.02
1LFD_A_LYS39ALA	2.22	1.33	1.50	0.55	0.84	1.06
1LFD_A_ASN41LYS	-1.17	0.39	0.75	-0.09	0.10	0.29
1LFD_A_ILE5ALA	1.41	1.36	1.43	2.47	0.44	1.43
1LFD_A_ARG7ALA	1.88	1.70	1.00	0.87	1.24	1.20
1LFD_B_GLN25ALA	0.90	0.94	1.35	0.08	0.89	0.82
1LFD_B_VAL29ALA	0.48	1.28	0.01	0.00	0.46	0.44
1LFD_B_ASP33ALA	1.10	1.71	1.69	-0.38	0.82	0.96
1LFD_B_GLU37ALA	1.15	1.52	1.78	1.17	1.58	1.51
1LFD_B_ASP38ALA	3.75	1.70	1.82	0.07	2.74	1.58
1LFD_B_TYR40ALA	3.55	2.80	2.38	2.41	3.06	2.66
1LFD_B_TYR40PHE	2.11	1.34	1.50	-0.25	1.12	0.93
1LFD_B_ARG41ALA	0.83	1.49	1.65	0.53	1.21	1.22
1SBB_B_LEU20THR	-0.11	0.73	1.37	1.94	0.64	1.17
1SBB_B_VAL26TYR	-0.91	0.17	0.84	-1.66	0.12	-0.13
1SBB_B_TYR91VAL	0.09	1.45	1.51	0.36	0.43	0.94
1WQJ_I_ARG20ALA	0.68	1.17	0.36	-0.34	0.83	0.51
1YCS_A_ARG177HIS	-0.12	1.09	0.07	-0.13	0.78	0.45
2AW2_B_PRO16ALA	2.57	1.50	1.86	1.09	1.06	1.38
2AW2_B_TYR22ALA	1.88	0.92	1.68	1.81	1.75	1.54
2AW2_B_VAL35ALA	1.10	0.69	0.94	1.16	0.87	0.92
2C5D_C_VAL66ALA	-0.60	1.15	0.75	0.32	0.65	0.72
2DVW_A_LYS114ALA	0.03	3.41	2.00	3.39	0.27	2.27
2DVW_A_GLU180ALA	0.44	1.60	2.43	3.68	2.71	2.61
2DVW_A_ARG39ALA	0.91	2.52	2.23	3.52	1.38	2.41
2DVW_B_LYS62GLU	0.21	0.88	1.06	2.31	1.29	1.39
2DVW_B_ARG7ALA	0.69	1.11	2.73	5.18	1.47	2.62
2G2U_A_ASP79ALA	-1.54	0.23	1.02	-0.56	1.18	0.47
2G2U_A_ASP79GLU	-4.38	0.11	0.87	-0.63	0.68	0.26
2G2U_A_ASP79LYS	-0.67	0.36	1.08	0.37	1.24	0.76
2G2U_B_GLU73MET	-2.47	0.78	1.12	-0.56	-1.17	0.04
2KSO_A_LYS10ASP	0.33	1.40	1.66	4.49	1.32	2.22
2KSO_A_ARG43GLU	-0.66	1.35	0.78	0.19	0.59	0.73
2KSO_B_HIS20GLU	-0.16	-0.16	1.13	-0.07	2.23	0.78
2REX_A_LEU70TYR	0.56	0.79	3.29	6.13	-0.35	2.47
2REX_B_TYR97PHE	0.00	0.11	1.47	-0.30	0.33	0.40
2WPT_A_ASP30ALA	-1.42	0.59	1.07	0.24	0.21	0.53
2WPT_A_ASN31ALA	-0.14	0.87	0.53	-0.02	0.04	0.36
2WPT_B_SER77ALA	-0.09	0.78	0.79	-0.09	0.48	0.49
2WPT_B_PHE79ALA	2.67	1.45	2.21	2.90	2.31	2.22

3BT1_U_GLY10ALA	0.27	1.61	1.53	-0.28	0.52	0.85
3BT1_U_ASP11ALA	-0.03	1.51	1.14	-0.51	0.36	0.63
3BT1_U_VAL123ALA	0.79	1.25	0.12	0.60	0.60	0.64
3BT1_U_VAL124ALA	0.75	1.11	0.66	0.08	0.33	0.55
3BT1_U_THR125ALA	1.00	0.98	1.11	1.34	0.64	1.02
3BT1_U_GLU132ALA	-0.16	0.40	0.01	0.01	0.19	0.15
3BT1_U_GLU133ALA	-0.15	1.21	0.04	0.14	0.24	0.41
3BT1_U_PRO136ALA	0.34	0.73	1.60	0.12	1.18	0.91
3BT1_U_LYS137ALA	0.62	1.35	0.64	0.30	0.61	0.73
3BT1_U_ASP138ALA	1.30	0.52	1.50	1.20	1.61	1.21
3BT1_U_ASP139ALA	1.05	0.78	1.23	-0.07	0.93	0.72
3BT1_U_LEU142ALA	0.72	1.49	1.38	0.73	0.57	1.04
3BT1_U_LEU148ALA	1.66	1.06	1.49	1.06	1.25	1.22
3BT1_U_PRO149ALA	0.60	1.11	1.68	0.28	0.73	0.95
3BT1_U_ASN155ALA	0.60	-0.10	0.02	-1.08	-0.19	-0.34
3BT1_U_HIS164ALA	1.03	1.02	1.15	1.65	0.37	1.05
3BT1_U_PHE165ALA	0.13	0.66	0.01	0.02	0.68	0.34
3BT1_U_LEU166ALA	0.75	1.09	1.33	0.22	0.47	0.78
3BT1_U_GLU228ALA	0.18	0.75	0.00	-0.11	0.34	0.25
3BT1_U_HIS249ALA	0.28	0.64	0.00	0.13	0.32	0.27
3BT1_U_ASP252ALA	0.06	0.94	1.16	0.04	0.49	0.66
3BT1_U_ALA253SER	0.20	0.18	0.76	0.14	0.47	0.39
3BT1_U_SER255ALA	0.21	0.34	-0.06	-0.30	0.37	0.09
3BT1_U_ARG25ALA	1.02	1.47	0.82	0.57	1.25	1.03
3BT1_U_THR27ALA	0.91	1.03	0.74	0.51	0.18	0.62
3BT1_U_VAL29ALA	0.72	1.22	0.92	1.38	1.30	1.21
3BT1_U_LEU31ALA	0.31	1.02	1.42	0.66	0.43	0.88
3BT1_U_GLU33ALA	0.38	1.39	0.87	-0.26	0.71	0.68
3BT1_U_GLU36ALA	0.09	0.77	0.93	0.44	1.10	0.81
3BT1_U_LEU38ALA	0.52	1.31	1.46	0.82	0.51	1.03
3BT1_U_GLU39ALA	0.16	0.88	0.02	0.14	0.48	0.38
3BT1_U_LEU40ALA	0.87	1.35	1.52	0.73	0.56	1.04
3BT1_U_VAL41ALA	0.49	0.84	0.02	0.06	0.57	0.37
3BT1_U_GLU42ALA	-0.20	0.80	0.92	-0.02	1.06	0.69
3BT1_U_THR46ALA	0.46	0.93	0.23	1.15	-0.17	0.54
3BT1_U_LYS50ALA	0.64	0.87	0.97	1.63	0.29	0.94
3BT1_U_ARG53ALA	0.89	0.75	1.53	2.16	1.71	1.54
3BT1_U_THR54ALA	0.39	0.92	0.66	-0.06	0.78	0.58
3BT1_U_LEU55ALA	1.11	0.74	1.37	0.74	1.11	0.99
3BT1_U_TYR57ALA	1.20	0.97	1.27	0.14	0.29	0.67
3BT1_U_THR59ALA	0.55	0.71	-0.09	-0.04	-0.30	0.07
3BT1_U_LEU61ALA	-0.13	0.46	-0.05	-0.17	0.10	0.09
3BT1_U_LYS62ALA	0.42	0.48	0.51	-0.58	0.33	0.19
3BT1_U_THR64ALA	0.66	0.37	0.70	-0.01	-0.18	0.22
3BT1_U_LEU66ALA	1.38	0.90	1.76	1.58	1.27	1.38
3BT1_U_THR67ALA	0.19	0.51	0.67	0.03	0.80	0.50
3BT1_U_GLU68ALA	0.05	1.34	1.23	0.86	2.82	1.56
3BT1_U_THR8ALA	0.18	0.96	0.82	0.09	0.63	0.63
3BT1_U_SER99ALA	0.30	1.31	0.53	-0.18	0.25	0.48
3BT1_U_ASN9ALA	0.31	0.95	0.66	-0.17	0.20	0.41
3BX1_C_PHE84VAL	0.41	2.36	0.68	0.39	1.22	1.16
3BX1_C_ARG85GLY	0.36	-0.06	-0.62	-0.44	0.40	-0.18
3BX1_C_ALA86THR	1.84	0.60	0.50	1.91	0.97	1.00
3BX1_C_TYR87ALA	1.30	1.41	1.88	3.80	2.22	2.33
3BX1_C_TYR87ILE	1.78	1.49	0.91	2.33	2.11	1.71
3BX1_C_THR88VAL	2.84	1.19	-0.01	-0.02	0.40	0.39
3BX1_C_THR89ALA	0.17	0.80	0.88	-0.37	1.82	0.78
3EG5_A_HIS104PHE	-2.08	1.60	-0.19	0.82	0.52	0.69

3F1S_A_ASP200ALA	0.55	1.43	1.63	0.28	1.32	1.17
3F1S_A_LYS201ALA	-2.08	0.84	1.26	0.93	3.66	1.67
3F1S_A_LYS201CYS	-1.69	0.88	1.53	0.92	2.37	1.43
3F1S_A_TYR202ALA	2.99	1.08	2.39	3.19	3.49	2.54
3F1S_A_ASP255ALA	3.76	1.72	2.22	3.07	2.63	2.41
3F1S_A_MET33ALA	1.24	1.44	1.00	1.60	0.84	1.22
3F1S_A_ASP36ALA	2.18	1.14	2.11	2.01	0.66	1.48
3KUD_B_ASN16ARG	-0.80	0.78	-0.29	-1.44	0.08	-0.22
3KUD_B_LYS30ALA	1.95	-0.83	0.40	0.88	0.58	0.26
3LB6_A_LYS100ALA	5.81	1.28	1.27	1.67	1.64	1.47
3LB6_A_LYS101ALA	2.54	0.96	0.28	0.33	3.24	1.20
3LB6_A_PHE103ALA	5.12	1.79	1.66	1.96	4.26	2.42
3LB6_A_ILE10ALA	3.72	1.09	1.34	0.57	1.32	1.08
3MZG_A_HIS14ALA	-0.02	1.26	2.13	1.14	0.54	1.27
3MZG_A_HIS160ALA	0.92	1.49	0.00	-0.06	0.57	0.50
3MZG_A_HIS167ALA	1.49	1.43	1.32	1.66	2.69	1.78
3MZG_A_HIS17ALA	0.06	0.97	1.02	1.08	1.77	1.21
3MZG_B_HIS188ALA	1.78	1.55	1.96	1.52	2.08	1.78
3N06_A_ALA14HIS	0.02	-0.89	-1.05	0.34	1.55	-0.01
3N0P_A_ALA17HIS	-0.06	-2.05	0.78	7.87	1.52	2.03
3N4I_A_GLU79ASP	4.38	0.84	0.61	3.31	1.69	1.61
3NCB_A_ALA167HIS	-1.49	-2.27	0.13	0.75	1.41	0.01
3NCC_B_ALA188HIS	-1.78	-0.57	-0.98	-0.46	-0.38	-0.60
3NVN_A_ARG193GLU	2.49	0.68	1.42	3.76	-0.17	1.42
3NVN_B_ARG186SER	1.27	1.06	1.93	1.35	-0.06	1.07
3Q3J_B_TYR100PHE	0.21	0.29	1.01	-0.44	0.65	0.38
3QHY_B_ASN10ALA	2.25	2.32	1.00	0.59	0.82	1.18
3QHY_B_TRP112ALA	3.79	0.97	2.26	1.62	2.90	1.94
3QHY_B_ASP127ALA	0.38	0.98	0.84	0.88	0.45	0.79
3QHY_B_SER129ALA	-0.08	0.47	-0.01	0.07	0.13	0.17
3QHY_B_ASP12ALA	2.25	1.36	1.50	0.06	1.90	1.21
3QHY_B_ASP130ALA	0.96	0.88	0.62	0.93	0.82	0.81
3QHY_B_TRP13ALA	2.86	1.18	2.40	2.44	2.71	2.18
3QHY_B_TYR151ALA	3.42	0.79	2.39	2.81	2.00	2.00
3QHY_B_ASP166ALA	3.50	1.22	1.57	0.19	0.90	0.97
3QHY_B_TYR168ALA	1.74	1.07	1.97	1.79	1.40	1.56
3QHY_B_PHE169ALA	2.06	1.18	1.50	0.44	0.32	0.86
3QHY_B_THR17ALA	0.06	1.28	0.03	-0.10	0.16	0.34
3QHY_B_ILE189ALA	3.07	-0.10	0.90	0.02	0.45	0.32
3QHY_B_PHE190ALA	3.07	0.66	1.72	0.74	-0.10	0.76
3QHY_B_TYR208ALA	0.24	1.27	1.51	0.11	0.64	0.88
3QHY_B_GLU228ALA	3.01	0.81	0.61	-1.91	1.06	0.14
3QHY_B_TRP229ALA	5.43	1.21	2.04	0.58	2.16	1.50
3QHY_B_ARG246ALA	0.53	1.01	1.82	0.34	1.09	1.07
3QHY_B_ASN264ALA	2.69	0.71	0.95	0.09	0.74	0.62
3QHY_B_TYR33ALA	2.90	0.68	1.89	1.33	2.74	1.66
3QHY_B_PHE34ALA	3.98	0.99	1.83	1.51	0.60	1.23
3QHY_B_LEU51ALA	0.82	0.04	1.73	0.92	0.52	0.80
3QHY_B_ASN72ALA	1.61	0.77	0.86	0.84	1.36	0.96
3QHY_B_TYR73ALA	0.80	1.10	1.62	-0.52	0.71	0.73
3QHY_B_ASP91ALA	1.89	1.02	1.68	1.68	0.45	1.21
3RF3_C_ALA8LYS	1.73	0.80	2.05	-0.04	2.54	1.34
3S9D_A_ARG115ALA	2.15	1.57	0.13	0.40	1.36	0.87
3S9D_A_ALA116GLY	2.10	0.90	0.76	0.69	0.93	0.82
3S9D_A_ALA116MET	1.07	1.31	0.21	-0.57	1.08	0.51
3S9D_A_MET119ALA	2.25	1.36	1.13	1.86	1.54	1.47
3S9D_A_ARG120ALA	3.02	2.19	0.93	1.32	1.88	1.58
3S9D_A_SER123ALA	1.12	1.59	0.56	-0.44	1.19	0.73

3S9D_A_LEU124ALA	1.45	0.87	1.69	0.78	0.79	1.03
3S9D_A_ASN127ALA	-0.04	1.06	0.31	-0.14	0.18	0.35
3S9D_A_ALA12TRP	-0.18	1.06	0.60	-0.44	0.49	0.43
3S9D_A_ARG15ALA	0.20	1.05	1.16	-0.24	0.42	0.60
3S9D_A_SER18ALA	-0.10	2.23	0.90	-0.03	0.13	0.81
3S9D_A_LEU19ALA	1.10	0.52	1.15	1.55	1.32	1.14
3S9D_A_PHE20ALA	0.71	1.43	1.92	1.93	-0.09	1.30
3S9D_A_LEU23ALA	3.81	2.22	2.21	2.41	0.70	1.89
3S9D_A_LEU23VAL	2.44	1.67	1.89	1.64	0.72	1.48
3S9D_A_ARG26ALA	5.12	2.07	1.85	2.46	0.78	1.79
3S9D_A_ARG26GLN	6.08	1.56	2.31	2.51	0.61	1.75
3S9D_A_ARG26LYS	4.59	1.51	1.14	0.69	1.03	1.09
3S9D_A_HIS27ALA	0.54	0.93	0.75	0.01	1.25	0.74
3S9D_A_ASP28ALA	0.30	2.41	1.56	-0.10	0.55	1.11
3S9D_A_ARG5ALA	0.62	1.16	1.19	0.16	1.57	1.02
3S9D_A_LEU8ALA	1.54	1.76	1.87	1.13	1.83	1.65
3S9D_A_MET9ALA	0.06	1.42	0.39	0.44	1.09	0.84
3S9D_B_ASP121ARG	-0.08	0.41	-0.15	-0.48	0.21	0.00
3S9D_B_HIS166ALA	0.00	0.98	1.39	-0.45	1.55	0.87
3S9D_B_THR33ALA	1.73	0.60	1.20	0.70	0.06	0.64
3S9D_B_ILE34ALA	1.85	1.25	0.88	0.10	0.93	0.79
3S9D_B_MET35ALA	3.00	1.69	1.50	3.20	1.01	1.85
3S9D_B_MET35VAL	2.37	1.55	1.03	1.87	0.79	1.31
3S9D_B_SER36ALA	0.50	1.45	0.81	-0.47	0.85	0.66
3S9D_B_LYS37ALA	0.50	0.80	1.06	0.85	0.57	0.82
3S9D_B_GLU39ALA	0.21	1.27	1.29	0.39	1.29	1.06
3S9D_B_GLU39ARG	0.65	1.09	1.17	0.10	1.23	0.90
3S9D_B_ASP40ALA	0.00	0.95	0.15	0.58	0.10	0.45
3S9D_B_THR64ALA	0.26	1.13	0.00	0.03	0.71	0.47
3S9D_B_HIS65ALA	0.82	1.35	1.61	0.07	1.90	1.23
3S9D_B_GLU66ALA	2.41	1.65	0.91	0.37	1.53	1.12
3S9D_B_ALA67MET	-0.17	0.41	0.72	-1.99	0.62	-0.06
3S9D_B_VAL69ALA	2.32	1.36	1.36	1.88	1.16	1.44
3S9D_B_HIS84ALA	0.04	0.06	0.03	0.12	1.71	0.48
3S9D_B_ASN85ALA	-0.17	1.29	0.82	-0.60	0.98	0.62
3S9D_B_TRP87ALA	1.11	1.15	2.80	3.70	2.48	2.53
3S9D_B_ILE90ALA	1.62	0.88	1.32	2.24	0.70	1.29
3SE3_A_LEU116ALA	0.00	1.93	2.04	1.93	1.40	1.83
3SE3_A_ASP117ALA	0.54	0.75	2.54	3.69	0.46	1.86
3SE3_A_SER120ALA	0.54	1.26	0.80	-0.46	0.34	0.49
3SE3_A_ASN140THR	0.13	0.53	0.97	0.13	0.29	0.48
3SE3_A_THR166ALA	-0.16	0.82	1.27	1.18	0.54	0.95
3SE3_A_SER167ALA	-0.24	0.23	0.87	-0.08	0.41	0.36
3SE3_A_PHE223ALA	1.50	1.54	1.50	3.61	1.82	2.12
3SE3_A_ARG226ALA	0.41	0.54	1.86	1.96	1.18	1.39
3SE3_A_ASN230ALA	0.21	0.89	0.34	-0.03	-0.31	0.22
3SE3_A_TYR55ALA	1.50	2.07	1.85	0.17	3.79	1.97
3SE3_A_PHE81ALA	0.41	1.48	1.74	-0.73	1.21	0.93
3SF4_A_ARG202GLU	2.36	1.68	2.05	2.90	-0.37	1.57
3SF4_A_ASN264ARG	1.23	0.82	1.20	0.21	2.29	1.13
3SF4_D_GLU19ARG	1.93	2.10	2.33	5.25	2.41	3.02
3SF4_D_LYS27ASP	0.41	1.13	1.96	4.56	2.14	2.45
3SF4_D_TRP8ALA	3.07	3.39	2.65	3.45	3.29	3.20
3U82_B_ILE45ALA	2.60	1.30	1.16	0.51	1.03	1.00
3WWN_A_ARG221GLU	-0.34	1.49	1.56	3.53	1.59	2.04
3WWN_A_ARG224GLU	1.29	0.09	0.05	0.27	-0.27	0.04
3WWN_A_LYS225GLU	0.16	3.61	0.34	0.70	0.71	1.34
4BFI_B_LEU29LYS	2.08	2.08	1.52	1.05	0.04	1.17

4BFI_B_ASN43ALA	2.32	3.04	1.08	1.55	1.54	1.80
4BFI_B_ASN43ASP	2.73	2.82	1.20	1.73	2.35	2.03
4BFI_B_LEU91ALA	1.31	1.90	1.34	0.41	1.00	1.16
4BFI_B_ASN93LYS	2.73	2.65	0.97	1.09	1.45	1.54
4BFI_B_PHE95ALA	2.08	3.42	1.95	2.85	-0.02	2.05
4BFI_B_PHE95ASP	2.73	2.72	2.19	3.64	1.41	2.49
4BFI_B_LYS99GLU	2.32	1.50	0.86	-0.09	1.04	0.83
4EKD_A_CYS147ARG	-0.06	-3.27	-0.06	-0.10	0.70	-0.68
4FZA_A_PHE168GLU	0.54	2.64	2.34	3.08	1.29	2.34
4FZA_A_TYR213ALA	1.27	3.25	2.00	1.26	1.68	2.05
4FZA_A_ARG217ALA	1.03	3.25	1.96	2.92	1.32	2.36
4FZA_B_GLU122ALA	0.43	1.27	0.50	0.04	0.73	0.64
4G0N_A_ILE21ALA	0.87	1.85	0.88	1.09	1.44	1.32
4G0N_A_HIS27ALA	-0.29	2.02	0.00	-0.17	0.54	0.60
4G0N_A_GLU31ALA	0.94	1.36	0.50	0.30	0.88	0.76
4G0N_A_ASP33ALA	0.88	2.06	1.57	0.44	0.23	1.08
4G0N_A_ILE36ALA	1.74	1.56	1.23	1.29	0.26	1.09
4G0N_A_GLU37ALA	1.74	1.49	1.50	0.53	2.01	1.38
4G0N_A_ASP38ALA	2.86	1.35	2.25	2.51	2.78	2.22
4G0N_A_SER39ALA	0.29	1.42	0.80	-0.54	2.69	1.09
4G0N_A_ARG41ALA	-0.34	1.31	1.56	1.38	0.31	1.14
4G0N_B_ASN11ALA	0.68	0.72	1.00	0.09	0.12	0.48
4G0N_B_ASN11ASP	1.81	0.56	0.93	-0.44	0.13	0.30
4G0N_B_LYS12ALA	1.83	0.50	0.89	0.22	0.95	0.64
4G0N_B_LYS12GLU	1.92	0.46	0.23	-1.69	0.94	-0.02
4G0N_B_LYS12MET	1.32	0.51	0.96	0.12	-0.04	0.39
4G0N_B_GLN13ALA	2.21	1.13	1.30	1.22	2.47	1.53
4G0N_B_ARG14ALA	1.92	1.89	1.60	1.31	1.66	1.62
4G0N_B_THR15ALA	1.80	1.40	1.32	1.38	0.74	1.21
4G0N_B_VAL16ALA	1.15	1.48	1.31	1.43	0.69	1.23
4G0N_B_ASN18ARG	-0.70	0.68	-0.25	-1.00	0.47	-0.03
4G0N_B_LYS31ALA	2.58	1.15	0.95	0.36	0.61	0.77
4G0N_B_LYS31GLU	5.06	1.49	0.75	1.21	0.29	0.94
4G0N_B_ALA32LYS	-1.11	1.02	-0.57	-2.38	2.10	0.04
4G0N_B_VAL35ALA	-0.01	1.24	1.32	1.39	1.27	1.31
4G0N_B_VAL35ILE	0.55	1.43	0.59	-0.56	1.09	0.64
4G0N_B_ARG6ALA	2.14	1.36	1.59	1.76	0.77	1.37
4G2V_A_ARG198GLU	2.24	1.35	1.96	2.97	-0.46	1.46
4HRN_D_LEU17ALA	2.60	1.18	1.74	1.96	0.51	1.35
4HRN_D_SER43ALA	0.80	1.42	0.60	-0.11	0.87	0.70
4HRN_D_VAL44ALA	2.81	0.86	1.06	1.85	0.55	1.08
4HRN_D_PHE47ALA	2.46	1.36	1.86	2.54	1.16	1.73
4L0P_A_GLU27LYS	2.66	1.84	1.66	2.22	2.55	2.07
4L0P_A_THR76GLN	1.47	1.78	2.72	2.12	0.95	1.89
4MYW_B_ILE48ALA	2.57	1.35	1.53	2.05	1.09	1.51
4NZW_A_LYS77ALA	0.08	2.04	0.68	0.50	0.36	0.90
4NZW_B_GLU124ALA	0.36	1.05	0.92	-0.42	0.79	0.59
4NZW_B_GLU49ALA	0.33	1.65	0.97	0.58	0.77	0.99
4O27_A_TYR215ALA	1.19	2.05	2.23	3.19	1.28	2.19
4O27_A_LYS88ALA	1.02	2.03	0.32	2.29	0.10	1.19
4O27_B_GLU122ALA	0.30	1.03	-0.11	0.19	0.40	0.38
4O27_B_GLU42ALA	0.37	1.15	1.76	3.52	2.44	2.22
4OFY_A_GLN34ALA	1.18	1.26	0.60	-0.05	0.75	0.64
4OFY_A_MET36ALA	0.08	1.34	0.72	0.79	1.44	1.07
4OFY_A_ASP38ALA	0.55	2.04	1.33	0.53	0.86	1.19
4OFY_A_GLN85ALA	1.73	1.77	0.54	0.49	0.86	0.92
4OFY_D_GLN34ALA	2.87	1.89	0.93	1.55	0.16	1.13
4OFY_D_LEU42ALA	2.57	1.60	1.62	3.42	1.30	1.99

4OFY_D_GLN86ALA	4.64	1.68	1.55	2.55	1.51	1.82
4OFY_D_ARG96ALA	3.42	1.66	1.80	3.90	1.22	2.15
4RA0_C_ALA66VAL	0.93	0.97	0.09	0.64	1.29	0.75
4RS1_A_ARG10ASP	0.18	1.34	0.88	-0.33	-0.39	0.38
4RS1_A_ARG11ASP	0.19	0.85	-0.02	-0.15	-0.28	0.10
4RS1_A_GLU25ALA	1.50	0.65	0.97	-0.42	1.14	0.59
4RS1_A_GLU25LYS	2.14	0.70	0.70	0.10	1.26	0.69
4RS1_A_ASP28ALA	2.59	1.50	1.56	1.50	1.67	1.56
4RS1_A_ASP28LYS	3.62	1.81	1.20	0.37	1.52	1.23
4RS1_A_ILE6GLY	0.86	1.59	0.14	0.46	0.69	0.72
4RS1_A_GLN79ALA	0.47	1.09	0.61	0.07	1.44	0.80
4RS1_A_GLN79GLU	1.21	0.84	0.31	0.20	1.64	0.75
4RS1_A_GLU88ALA	0.48	0.85	-0.02	-0.14	0.18	0.22
4RS1_A_GLU88GLN	0.92	0.84	0.00	0.02	0.59	0.36
4RS1_A_GLU88LYS	0.34	0.76	0.00	-0.40	-0.13	0.06
4RS1_A_ASN89ALA	1.29	0.79	0.01	-0.07	0.23	0.24
4RS1_A_ASN89ASP	0.30	0.61	-0.01	-0.01	0.27	0.22
4RS1_A_ASN89LYS	0.91	0.86	-0.03	-0.13	0.69	0.35
4RS1_A_LYS91ALA	-0.11	0.69	-0.04	-0.27	0.48	0.22
4RS1_A_LYS91GLN	0.27	0.56	-0.04	-0.03	0.36	0.21
4RS1_A_LYS91GLU	0.13	0.72	-0.07	-0.32	0.12	0.11
4RS1_A_ASP92ALA	1.93	0.57	1.34	0.39	1.15	0.86
4RS1_A_ASP92ARG	3.13	0.74	1.36	0.82	0.70	0.91
4RS1_A_ASP92ASN	1.43	0.73	1.16	0.02	1.32	0.81
4RS1_A_ASP92LYS	3.62	0.54	1.40	0.84	0.89	0.92
4RS1_A_LEU95ALA	2.36	0.88	1.65	1.39	1.68	1.40
4RS1_A_PHE99ALA	3.62	1.81	1.68	3.06	1.97	2.13
4RS1_B_LYS174ALA	0.87	0.37	0.77	0.86	0.83	0.71
4RS1_B_LYS203ALA	0.28	0.65	0.58	0.49	0.10	0.46
4RS1_B_LEU204ALA	0.07	0.84	1.20	0.14	0.51	0.67
4RS1_B_SER205ALA	0.62	0.30	0.57	0.48	0.85	0.55
4WND_A_ARG201GLU	2.79	1.62	2.14	4.12	-0.41	1.87
4WND_A_ASN263ARG	-0.02	1.18	1.19	0.81	1.29	1.12
4Y61_A_TYR246ALA	-0.08	0.68	1.99	3.10	3.31	2.27
4Y61_B_ARG86ALA	-0.19	1.67	1.57	0.16	1.28	1.17
4YEB_B_PHE131ALA	2.42	1.52	1.43	-0.05	0.46	0.84
4YFD_A_ARG169ALA	0.16	1.13	1.12	0.71	2.09	1.26
4YFD_A_GLU259ALA	1.22	2.49	1.98	4.10	1.04	2.40
4YFD_B_TRP4ALA	1.13	2.85	2.40	4.09	2.38	2.93
4YFD_B_LYS71ALA	1.47	1.99	1.61	3.09	0.55	1.81
4YFD_B_ASP7ALA	-0.05	1.68	1.48	1.28	0.65	1.27
5CXB_B_GLU49ASP	0.36	1.74	1.44	2.19	1.08	1.61
5CXB_B_THR52GLN	0.06	1.11	1.15	1.80	1.63	1.42
5CXB_B_ARG54ALA	0.56	2.75	1.70	2.85	1.27	2.14
5CXB_B_ARG54GLU	2.68	2.86	1.82	4.16	2.23	2.77
5CYK_B_GLU52ALA	-2.12	-0.76	0.45	-1.17	1.11	-0.09
5CYK_B_GLU52ARG	-2.68	-3.91	-0.02	-3.21	1.99	-1.29
5F4E_A_HIS136ALA	2.02	1.02	1.42	0.49	1.11	1.01
5F4E_A_ARG139ALA	1.49	1.33	1.40	0.85	1.63	1.30
5F4E_A_ARG139GLU	2.14	1.54	1.15	1.70	2.31	1.68
5F4E_A_GLU50ALA	0.29	0.92	0.87	-0.14	0.57	0.56
5F4E_A_GLU50LYS	0.42	0.46	0.71	-0.02	0.41	0.39
5F4E_B_LYS139ALA	0.29	0.81	0.59	0.15	0.36	0.48
5F4E_B_LYS139GLU	0.49	0.40	0.33	0.57	0.01	0.33
5F4E_B_GLU26ALA	1.45	0.83	1.01	-0.79	0.99	0.51
5F4E_B_GLU26LYS	2.29	1.24	0.55	1.66	0.65	1.03
5F4E_B_TRP43ALA	1.07	1.16	2.27	2.06	2.91	2.10
5F4E_B_LEU62ALA	2.98	0.61	1.89	2.58	1.94	1.76

5K39_B_MET108ALA	-0.48	1.51	0.30	0.80	0.94	0.89
5K39_B_MET112ALA	-0.23	1.28	-0.07	0.16	1.03	0.60
5K39_B_SER115ALA	0.45	0.39	-0.06	-0.23	0.18	0.07
5K39_B_PHE142ALA	2.72	0.59	0.67	2.16	0.47	0.97
5K39_B_ILE148ALA	2.05	-0.71	0.40	1.91	1.82	0.86
5M2O_A_HIS117ALA	0.88	1.04	2.06	2.92	0.71	1.68
5M2O_A_ASN120ALA	0.45	0.93	0.86	0.68	0.47	0.74
5M2O_A_ASN64ALA	0.04	1.12	0.93	0.95	0.66	0.92
5M2O_A_ASN71ALA	0.15	0.98	1.37	2.82	1.63	1.70
5M2O_A_LYS73ALA	-0.76	0.85	0.76	0.64	1.48	0.93
5M2O_A_LEU75ALA	1.63	0.75	1.86	2.50	0.43	1.39
5M2O_A_GLU80ALA	0.70	0.99	1.20	1.12	0.97	1.07
5M2O_B_ILE17ALA	2.03	1.53	1.09	1.87	1.83	1.58
5M2O_B_SER18ALA	0.05	1.83	1.03	1.58	2.35	1.70
5M2O_B_VAL21ALA	2.44	1.57	1.21	2.21	1.85	1.71
5M2O_B_GLN25ALA	1.14	2.51	1.08	2.02	1.92	1.88
5M2O_B_LYS32ALA	1.06	2.38	0.75	0.46	1.72	1.33
5M2O_B_GLN61ALA	-0.16	2.99	0.89	1.24	1.55	1.67
5M2O_B_LEU65ALA	0.85	1.94	1.96	2.85	1.51	2.07
5TAR_B_GLN114ALA	0.16	0.60	0.63	0.04	0.25	0.38
5TAR_B_GLU86ALA	1.13	1.09	0.86	-0.47	1.04	0.63
5TAR_B_TRP88ALA	0.38	2.98	1.99	1.84	0.76	1.89
5UFE_B_GLN25ARG	0.29	0.32	0.51	-0.21	-0.06	0.14

References

[1] I.H. Moal, J. Fernández-Recio, SKEMPI: a Structural Kinetic and Energetic database of Mutant Protein Interactions and its use in empirical models, Bioinformatics. 28 (2012) 2600–2607. doi:10.1093/bioinformatics/bts489.